NTNU

Norwegian University of
Science and Technology

# Lipid accumulation in docohexaenoic acid producing *Aurantiochytrium* sp. strain T66

Simen Liberg Tronsaune

Chemical Engineering and Biotechnology
Submission date: June 2018
Supervisor: Per Bruheim, IBT
Co-supervisor: Inga Marie Aasen, SINTEF materialer og kjemi

Norwegian University of Science and Technology
Department of Biotechnology and Food Science

# Acknowledgements

This MSc Thesis was performed at the Department of Biotechnology and Food Science at NTNU in Trondheim between February and June 2018, as a part of the NFR Digital Life/Biotek2021 research project "AurOmega - Microbial production of omega-3 fatty acids - a model-based approach".

I would like to thank the following people:

My supervisor Professor Per Bruheim for introducing me to biochemical engineering and exposing me to the powerful microbial world, igniting my interest and enthusiasm for biochemical engineering. Per has shown great passion for my work, as well as guiding and supporting me through the trial in an admirable manner. His knowledge on strain development, biochemical engineering, metabolics, and experimental work, is substantial and he is more than glad to share his thoughts and expertise.

A special thanks to Marit Halvarsdotter Stafnes for patiently explaining and helping me through the entire work. Marit instructed me during most of the laboratory work and result analysis, and responded to all my questions in a warm and welcoming way.

Inga Marie Aasen, Silje Malene Olsen, Lisa Marie Røst, Lilja Brekke Thorfinnsdottir, Kanhaiya Kumar, Katsuya Fuchino, Kåre Kristiansen, Janne Øiaas, and Zdenka Bartosova, all deserve the best in return for their support and counseling regarding analysis methods, bioreactor techniques and interpreting results.

My family and friends showed me support and love during my entire education, with encouraging words and talks during compressed working hours of the MSc Thesis - thank you.

# Abstract

Docohexaenoic acid (DHA), one of the omega-3 fatty acids, is an essential nutrient for human, animal and fish health. The DHA production from fish oil resources is associated with several negative features, and microbial DHA production has emerged as a sustainable and promising alternative. Extensive screening of thraustochytrids, including the genus *Aurantiochytrium*, has yielded strains producing more than 70% lipids of dry cell weight, and DHA comprising more than 50% of the total fatty acids (TFA).

*Aurantiochytrium* sp. strain T66 was grown in a bioreactor and shake-flask cultures with glutamate-glucose as carbon sources. Profiling of intracellular lipids, fatty acids, and central metabolites was performed to develop the knowledge regarding T66 as a potential DHA producer. Sampling protocol development was a central part of this work, and was performed to establish robust and reproducible protocols for qualitative analyses of intracellular metabolites (IM). The analyses of IM provided important remarks on proposed limiting factors of lipid biosynthesis.

Exponentially growing cells in the bioreactor culture, showed a lipid content of 20% of dry cell weight, increasing to 69% during the lipid accumulation phase, initiated by N-limitation at 92 hours. The dry biomass concentration was 27 g/l after 161 hours, with an overall DHA productivity of 16 mg DHA/l·h. Neutral (NL) and polar lipids (PL) were the two major lipid groups of total lipids (TL), with TAGs constituting more than 90% of TL during the lipid accumulation phase. In contrast, only 5% of the TL was phospholipids, but this class remained stable at 5% throughout the lipid accumulation phase. The NL and PL were separated by solid phase extraction, and the FA profiles of the two lipid groups were determined and compared. The concentrations of all fatty acids (FA) increased throughout the cultivation, showing a decreased fraction of saturated FA (SFA), and developing portions of monounsaturated FAs (MUFAs) and polyunsaturated FAs (PUFAs) of TFA.

A shake-flask pilot study was performed to test if shake-flasks was a relevant model system, and could be used as an alternative to bioreactor cultivations for expensive $^{13}$C-label experimentation. The results indicated minor differences in metabolic fluxes in the upper glycolysis and the pentose phosphate pathway during growth and the lipid accumulation phase, i.e. glutamate carbon did not entering the glycolytic pathway via anaplerotic reactions during the growth phase with glutamate still present.

Additionally, the life-cycle of *Aurantiochytrium* sp. strain T66 was explored to observe the co-existence of zoospores and vegetative cells. Zoospore-release from a mature

zoosporangium was caught on film, and staining provided information demonstrating high metabolic activity during zoospores settlement.

This MSc project contributed with improving experimental protocols, generated new biological data, that collectively will be important for future work towards optimizing DHA production in thraustochytrids.

# Sammendrag

I løpet av de siste tiårene har matvarer som inneholder de essensielle omega-3-fettsyrene mottatt større oppmerksomhet. Omega-3-fettsyrene, og da spesielt docohexaensyre (DHA), er sentral for utviklingen av normal hjerne- og øyefunksjon hos mennesker. Laks, ørret, makrell, krill og tran er alle kjente omega-3-kilder, og har en sentral rolle i mange norske kosthold. Oppdrettsnæringen er en av de største eksportnæringene i Norge, med ønske om produksjonsøkning for kommende år. Denne produksjonsøkningen vil øke etterspørselen etter fiskefôr, som igjen øker etterspørselen etter gode omega-3-kilder for fiskefôrproduksjon. I dag er fiskeolje hovedkilden for omega-3 og DHA, men nedstrømsprosessen for DHA-produksjon fra fiskeolje er kostbar. Videre er det påvist høyt innhold av toksiske forbindelser og andre marine forurensninger i fiskeoljen. Med økende etterspørsel etter DHA, har fiskeoljeproduksjonen medført overfiske og populasjonsreduksjoner for enkelte fiskearter. Disse negative sidene ved fiskjeoljeproduksjon, har introdusert etterspørselen etter bærekraftige DHA-kilder som kan erstatte dagens fiskeolje.

En rekke mikroorganismer er undersøkt som potensielle produksjonskilder for DHA og andre flerumettede fettsyrer. Thraustochytrider er marine protister, som er observert med høyt innhold av DHA i sitt rike fettinnhold. Flere arter er observert med produksjon over 70% fett av tørrvekt, og DHA utgjør over 50% av fettsyrene hos enkelte arter. *Aurantiochytrium* sp. T66 tilhører thraustochytridene, og ble undersøkt som DHA produsent i denne masteroppgaven. T66, dyrket i bioreaktor med glukose og glutamat som N- og C-kilde, ble observert med et fettinnhold på 20-30% under eksponensiell vekst. Fettinnholdet økte fra 30% til 69% i løpet av fettakkumuleringsfasen. Total biomass ble målt til 27 g/l etter 161 timer, med en volumetriske produktivitet av DHA på 16 mg/l·t. Sluttkonsentrasjonen av DHA ble målt til 2.6 g/l i bioreaktorkulturen. De to største fettklassene ble bestemt til å være nøytrale og polare lipider. De polare lipidene ble redusert fra 20% av fettinnholdet, til 5%, ved overgangen fra vekst til fettakkumulering. Triacylglycerolene utgjorde over 90% av lipidene i under fettakkumuleringen. Nøytrale og polare lipider ble separert, og fettsyreprofilene ble sammenlignet. Konsentrasjonen av alle fettsyrer var økende. Prosentdelen av mettede fettsyrer var synkende, mot at fraksjonen av umettede- og flerumettede fettsyrer var økende gjennom hele fettakkumuleringen.

Et pilot-prosjekt med $^{13}$C-merket glucose i rysteflasker ble gjennomført for å validere hvorvidt rysteflasker var et relevant og billigere modelsystem enn bioreaktorer. Resultatene tydet på små forskjeller mellom den øvre delen av glykolysen og pentosefosfatveien i vekst- og fettakkumuleringsfasen. Resultatene indikerte at C fra glutamat ikke ble inlemmet i glykolysen via anaplerotiske reaksjoner. Utvikling av prøveuttak

og protokoller for sentrale metabolitter ble gjennomført for å etablere robuste og reproduserbare thraustochytridedyrkninger. Intracellulære metabolittkonsentrasjoner ble kvantifisert med CapIC-MS, fra både bioreaktoren og rysteflasker. Konsentrasjonene ble sammenliknet for prøveuttak fra vekst- og fettakkumuleringsfasen, og begrensende faktorer for lipidsyntesen ble foreslått.

I tillegg, ble livssyklussen til *Aurantiochytrium* sp. T66 undersøkt for å studere kulturer med zoosporer og vegetative celler. Zoosporer og løslatelsen av zoosporer fra en zoosporangium ble observert. Farging av vegetative celler og zoosporangium viste høyt metabolsk aktivitet for zoosporene.

Denne masteroppgaven har bidratt til utviklingen av eksperimentelle protokoller, og samlet inn viktig biologisk data, som sammen vil være viktig for arbeidet med å optimalisere DHA produksjon i thraustochytrider.

# Contents

# List of Figures

# List of Tables

# Acronyms

| | |
|---|---|
| **AcCoA** | **A**cetyl-**C**oA |
| **ACC** | **A**cetyl-**C**oA **C**arboxylase |
| **ACL** | **A**TP-**c**itrate **Lyase** |
| **ACN** | **AC**eto **N**itril |
| **CapIC** | **C**apillary **I**on **C**hromatography |
| **DHA** | **D**ocosa**h**exaenoic **A**cid |
| **DGAT** | **D**iacyl**g**lycerol **A**cyl**t**ransferase |
| **DO** | **D**issolved **O**xygen |
| **DPA** | **D**ocosapentaenoic **A**cid |
| **EPA** | **E**icosa**p**entaenoic **A**cid |
| **ESTD** | **E**stablished **S**tandard |
| **FAD** | **F**lavin **A**denine **D**inucleotide |
| **FAS** | **F**atty **A**cid **S**ynthetase |
| **GPAT** | **G**lycerol-3-**p**hosphate **A**cyl**t**ransferase |
| **HPLC** | **H**igh **P**erformance **L**iquid **C**hromatography |
| **ISTD** | **I**nternal **S**tandard |
| **LC-MS** | **L**iquid **C**hromatography - **M**ass **S**pectrometry |
| **LPAAT** | **L**yso**p**hosphatidic **A**cid **A**cyl**t**ransferase |
| **MalCoA** | **M**alonyl-**C**o**A** |
| **ME** | **M**alic **E**nzyme |
| **MS** | **M**ass **S**pectrometry |
| **MUFA** | **M**ono **U**nsaturated **F**atty **A**cids |
| **NAD/NADH** | **N**icotinamide **A**denine **D**inucleotide |
| **NADPH** | **N**icotinamide **A**denine **D**inucleotide **P**hosphate |
| **NL** | **N**eutral **L**ipid |
| **OA** | **O**rganic **A**cids |
| **OD** | **O**ptical **D**ensity |
| **PAP** | **P**hosph**a**tidate **P**hosphatase |
| **PKS** | **P**oly**k**etide **S**ynthetase |
| **PL** | **P**olar **L**ipid |
| **PUFA** | **P**oly **U**nsaturated **F**atty **A**cids |
| **SF** | **S**hake-**F**lask |
| **SFA** | **S**aturated **F**atty **A**cids |
| **SPE** | **S**olid **P**hase **E**xtraction |
| **TAG** | **T**ri**acylg**lyceride |
| **UPLC-MS** | **U**ltra **P**erformance **L**iquid |
| **VVM** | **V**olume air per **V**olume broth per **M**inute |

# 1

# Background

The traditional source of omega-3 fatty acids for human consumption, aquaculture industry and animal feed is fish oil from wild-caught fish [1]. The annual global production of about 1 million tonnes are today directly produced from wild-caught fish. Currently, about 30% of the fish oil are used for human consumption, while the remaining 70% are used for marine aquaculture and animal feed [1]. From data (2005-2015) provided by Finco *et al.* [2], a future projection for the consumption of fish oil indicates that the largest increase will be direct human consumption (80% increase), while the aquaculture industry was projected to increase with 17% by 2025. The sustainability scheme of aquaculture is today precarious. The salmon feed must be rich in omega-3 fatty acids in order to maintain high levels in the fish [2]. Due to expanding demands of fish feed, fishing production is forced to its limits. During the last few decades, the increase in fish production by capture has been insignificant, indicating that the carrying capacity of fish capture is met. The wild catch fish peaked early in the 1990s, and has been constant ever since [2]. The aquaculture has grown exponentially since the 1990s, and in 2012 almost equalled the wild catch sector. The fish oil market will increase from USD 1.7 billion to USD 5 billion by 2025. Fish farming, especially salmon aquaculture, is an important industry for the Norwegian economy, and is growing. The aquaculture industry represented more than 60 billion NOK in 2016 from export alone [3].

Omega-3 is vital for salmon health and essential to the status of salmon as a healthy food. The aquaculture industry requires more omega-3 fatty acids from sustainable resources, as a consequence of the developing economy. Furthermore, the amount of wild-caught fish cannot be increased without harming the marine biodiversity. The indiscriminate fishing could lead to unpredicted imbalances, and it is therefore imperative to search for alternative resources of omega-3.

During this MSc thesis, *Aurantiochytrium* sp. strain T66 was investigated as a microbial host for production of docohexaenoic acid (DHA), one of the omega-3 fatty acids. This MSc thesis is a part of the AurOmega project, associated with NFR Digital Life/Biotek2021 [4]. The aim of this study was to increase the basic understanding of the fatty acid synthesis and other important metabolic pathways involved in lipid accumulation in thraustochytrids.

# 2

# Theory

## 2.1 Omega-3 fatty acids

There are two major groups of polyunsaturated fatty acids (PUFAs), n-3 (omega-3) and n-6 (omega-6), which are distinguished by the position of the terminal double bond. They were named by the methyl terminus in n-3, located three carbon atoms away from the terminal double bond, and n-6 for the located six carbons away from the methyl terminus. Among the PUFAs, docohexaenoic acid (DHA), with 22 carbons and six double bonds (written 22:6) has received most attention due to its many associated benefits [5]. Figure 2.1 show the molecular structure of DHA (22:6).

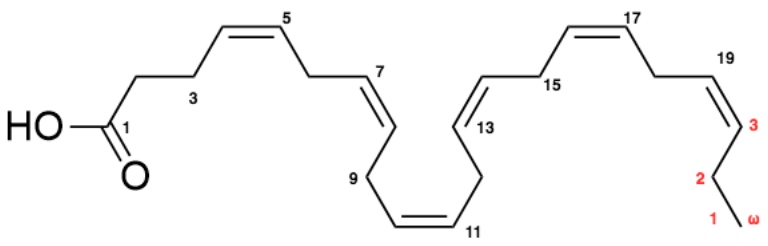


FIGURE 2.1: Molecular structure of docohexaenoic acid (DHA, 22:6).

An ongoing debate about the appropriate consumption level of long-chain fatty acids has led to confusion among consumers [6]. Today, the consumption of PUFAs from plants are larger than from fish. This has caused a larger ratio of omega-6 PUFAs relative to omega-3 PUFAs, which has been linked to increased risk of cancer, diabetes and cardiovascular diseases [7]. The health benefits of eicosapentaenoic acid (EPA, 20:5), docosapentaenoic acid (DPA, 22:5), and DHA (22:6), have been extensively studied, showing that omega-3 fatty acids help prevent heart attack and decrease the risk of cardiovascular disease [8]. DHA is stated to be physiological essential for brain and eye development, particularly in infants [9]. According to Meyer *et al.* [10], several other health benefits have been proven, which states the importance of increased availability of health-benefitting omega-3 to the world population. Humans can acquire a minor fraction of the required DHA through conversion of EPA to DHA, but the main part is supplied through our diets. Many western diets have been recognized to be deficit in omega-3 PUFAs. A large source of the omega-3 acid in human diets originate from salmon, trout, mackerel, and other crustaceans. The omega-3 level in these stocks are vital to maintain their prestige as a healthy food.

## 2.2 Alternative sources of omega-3 and high lipid-containing biomass

The existing alternatives to produce polyunsaturated fatty acids are fatty fish, genetically modified (GM) plant species, and a range of microbial production organisms [2]. Potential omega-3 production from one ton of fish, GM plant (*Camelina Sativa*) and thraustochytrids is shown in Figure 2.2 [2].

Several different microorganisms (yeast, fungi, algae and bacteria) produce PUFAs as a part of their lipid synthesis [11]. Several of the microorganisms produce higher levels of omega-3, show relatively simple fatty acid profiles [5], and are of special interest as hosts for DHA-production. High lipid-containing biomass from heterotrophic fermentations is one sustainable alternative to fish oils [5], [2], [12], [11].

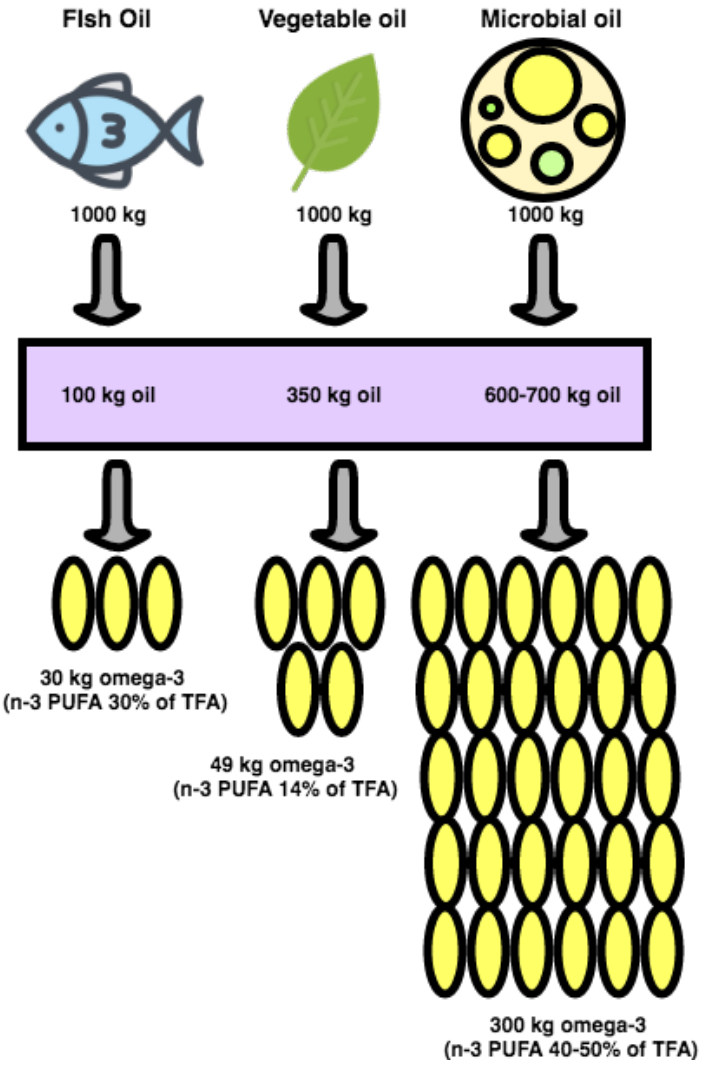


FIGURE 2.2: Production of omega-3 (n-3) by three different pathways, and its yields. The following are example of sources; Fish oil: *Peruvian Anchovy*, Vegetable oil: *Camelina Sativa GM* and Microbial oil: *Schizochytrium*, *Aurantiochytrium* and *Thraustochytrium*.

### 2.2.1 High lipid-containing biomass from heterotrophic fermentations as alternative to fish oil

According to Ratledge [13], about 5 tons of fish oil is needed to mature one ton of fish to maturity. The production cost of fatty oils from heterotrophic fermentations is still higher than the cost of fish oil [12]. Nevertheless, biomass from heterotrophic fermentations is a sustainable source of DHA, a range of other fatty acids, astaxanthin, squalene and other nutrients crucial for fish health. To ensure that heterotrophic fermentations can substitute fish oils, the overall costs of microbial production needs to be reduced. The carbon source is responsible for more than 60% of the total cost associated with heterotrophic fermentations [2].

Agricultural residues do not compete with foods, and are potential alternative carbon sources. Choosing adequate residues requires evaluation of several economical aspects: availability, transport, usefulness to society and restriction of use. According to Finco *et al.* [2], four main classes of low-cost substrates are to this day used for production of microbial oils: (1) monosaccharide and disaccharide rich sources (molasses, sugarcane juice, brewing residues and industrial sugars), (2) starchy feedstocks - important fraction of agro-industrial residues (cereal and tuber processings), (3) glycerol, an increasingly available byproduct from biofuel production and other industries, and (4) the lignocellulosic substrates (sugarcane bagasse, rice and wheat straw). The first class is directly used by most microorganisms with good yields, the second class is usually hydrolyzed to monosaccharides before use, the third class show promising results as a substrate for a vast number of microbial species (yeasts [14], thraustochytrids [15],[16] and bacteria [17], [18]). The latter shows encouraging results considering yeasts and fungi as production organisms, because they are able to synthesize cellulases and accumulate lipids simultaneously. Crude glycerol needs to be processed before use because the methanol and soap residues showed negative influence on DHA production [15]. Selection of substrate source from purified sources or agro-industrial byproducts are ultimately dependent on the availability, supply chain, pre-treatment cost and transportation costs [2].

Earlier reported results indicate that the biomass yield on glucose is slightly higher than on pure glycerol [19]. Shene *et al.* [20] have tested chitin, cellulose, starch, coconut water, and several lipid substrates for heterotrophic fermentation with thraustochytrids. Both Yokochi *et al.* [19] and Bajpai *et al.* [21] report that glucose and glycerol yield higher amounts of total lipids than other carbon sources. The dry cell weight (DCW) was similar for glycerol and glucose as carbon sources [19]. The same result was observed by Tronsaune [22], during the specialization project of the fall 2017. Glucose and glycerol showed very similar growth and dry cell weight profiles.

Biomass grown under heterotrophic fermentations is generally free from contaminants such as heavy metals, dioxins and polychlorinated biphenyls [23], [13]. The standard marine fish oil diet contains higher levels of these undesirables, making the heterotrophic fermentation biomass a better alternative to reduce toxic compounds in feed and filet flesh of aquacultured fish. Pesticides are found in fish oil due to polluted waters and oceans. Already in 2005, the content of toxic compounds was too high to allow the fish oil to be given as a dietary supplement to infants [13].

### 2.2.2 Alternative microbial producers of high lipid-containing biomass

A large number of microorganisms is suggested as novel production organisms for high lipid-containing biomass and lipid associated products like DHA. Table 2.1 shows a selection of potential production organisms. A more complete list is given in Liang and Jiangs work [24].

TABLE 2.1: Lipid content of selected microorganisms. The total lipid content is listed as %w/w of dry cell weight (DCW).

| Species | Culture conditions | Lipids % | Reference |
|---|---|---|---|
| **Microalgae** | | | |
| *Crypthecodinium cohnii* | Heterotrophic | 25 | [25] |
| *Chloralla* sp. | Phototrophic | 33-66 | [26] |
| **Mold** | | | |
| *Morterella isabellina* | Xylose | 55-60 | [14] |
| **Yeast** | | | |
| *Rhodosporidium toruloides* | Glucose (fed-batch) | >65 | [27] |
| **Bacteria** | | | |
| *Rhodococcus opacus* | Glucose/molasses | 38-50 | [28] |
| *Streptomyces coelicolor* | Glucose | 64-83 | [29] |
| **Thraustochytrids** | | | |
| *Schizohytrium* sp. HX-308 | Glucose | 69 | [30] |
| *S. limacinum* SR 21 | Gycerol/Glucose | 70 | [31] |
| *Aurantiochytrium* sp. T66 | Glycerol | 63 | [16] |

Adapted from Liang and Jiang [24]

The biflaggelated algae *Crypthecodinium cohnii* produces no significant amount of other PUFAs than DHA. Martek (DSM, [25]) report that their *C. cohnii* produce lipids accounting for 25%w/w of DCW, with a DHA content ranging from 30-50%w/w of the lipids. Mendes *et al.* [18] showed that *C. cohnii* species could produce DHA with ethanol, and acetic acid as carbon source. Both carbon sources gave a large increase in biomass and productivity of DHA compared to cultivations with glucose as substrate. However, acetic acid as carbon source in large-scale fermentations requires careful handling, and spillage could cause severe damage to workers [18].

Fakas *et al.* [14] present the use of the mold *Morterella isabellina*, with lipid content ranging from 55-60%w/w of DCW when grown on xylose, a five-carbon substrate with high abundance in wood, agriculture residues and energy crops [32]. The yeast, *Rhodosporidium toruloides* Y4 (Li *et al.* [27]), shows lipid contents above 65% when utilized in fed-batch glucose fermentation. Numerous bacteria are currently investigated as production organisms for DHA, where *Rhodococcus opacus* [28] and *Streptomyces coelicolor* [29] are two examples of hosts with high lipid production capacities. Arabolaza *et al.*

reported *Streptomyces coelicolor* with productions as high as 64 and 83%w/w of DCW [29].

Another host for lipid production is phototrophic microalgae, like *Choralla* sp. [26], which could potentially be an excellent low-cost producer. The microalgae utilize carbon dioxide and solar energy to produce biomass and intracellular products [33]. Today, several challenges concerning phototropic production are present: distribution of sunlight through the fermentation broth is difficult, and enormous areas are needed to produce low levels of biomass in algal ponds. A large number of cultivation methods are investigated for increased lipid and biomass production, high light intensity [34], low temperature [35], nitrogen deprivation [36], and high salt concentrations [37]. Under these stress conditions, many microalgae responded by significantly increasing their lipid content, ranging from 30-60%w/w of DCW [26]. Further studies are needed to develop phototrophic microalgae as lipid producers, but it is undoubtedly a potentially excellent low-cost producer of lipids.

Several species within thraustochytrids are described as great alternatives for production of microbial oil. *Schizochytrium*, *Thraustochytrium*, and *Aurantiochytrium* are of special interest because of their high lipid contents and DHA-enriched fatty acid profiles [38]. Algamac® (*Schizochytrium* sp.) is currently available as a resource to enrich aquaculture feed (Aquafauna Bio-Marine, USA). *Schizochytrium* strains are reported with lipid contents close to 70%w/w of DCW grown on glucose, glycerol or a combination of the two [30], [31]. The *Aurantiochytrium* sp. strain T66, investigated during this MSc Thesis, was reported to reach 63%w/w lipids of DCW by Jakobsen *et al.* [16].

## 2.3 Thraustochytrids

Thraustochytrids are unicellar, eukaryote, heterotrophic, obligate marine protists [6]. Thraustochytrids consist of several genera, *Schizochytrium*, *Thraustochytrium*, *Ulkenia*, and *Aurantiochytrium*. The thraustochytrids are normally found in seawater and sediments, and have the ability to accumulate high levels of lipids. Lipid contents of more than 77% of dry cellular weight (DCW) have been reported [39]. In addition to the high lipid content, Li *et al.* [40] and Bajpai *et al.* [21] observed DHA contents above 50% of the total fatty acids (TFA). However, reported results of lipid content of 77%(w/w of DCW) and 50%(w/w of TFA) DHA are not reported simultaneously. The thraustochytrids are investigated as novel production organisms for high lipid-containing biomass, DHA, and other high value products [5].

### 2.3.1 Life-cycle of thraustochytrids

Marchan *et al.* [41] and Bennett *et al.* [42] described a co-existence of two modes of cell division for thraustochytrids. Figure 2.3 shows the life-cycle of selected thraustochytrids.

The first mode, is described as the formation of a zoosporangia (4-6), whereas the second mode is the more familiar binary cellular division (2-4). Observations suggest that media composition, temperature, pH, and other stress factors [43], [42], [44] strictly affect the life-cycle, and by optimizing these influentors it is possible to achieve cultures where the second cellular mode is favored.

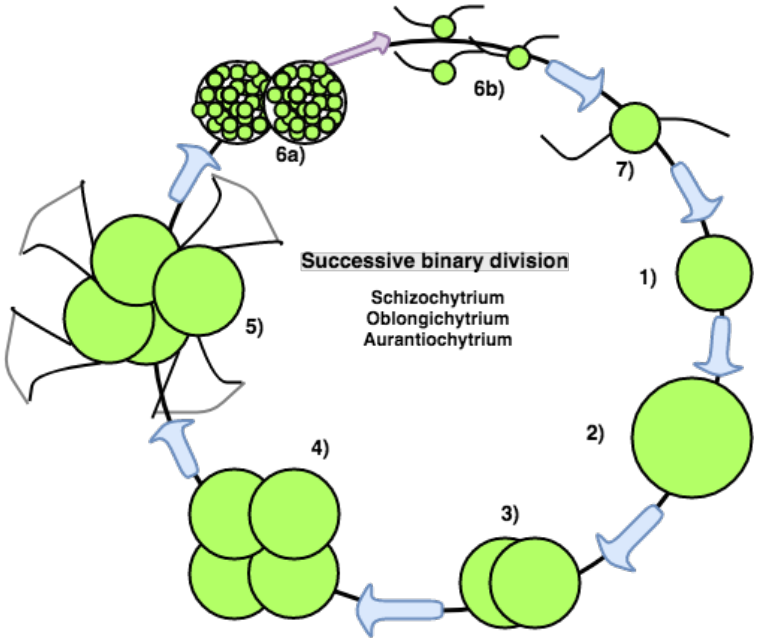


FIGURE 2.3: Life cycles of thraustochytrids *Schizochytrium*, *Aurantiochytrium*, and *Oblongichytrium*. Explanation: see text below. Adapted from Bennett *et al.* [42].

Figure 2.3 shows the differentiation from vegetative cell (1) to zoospores (6b and 7), via the formation of zoosporangium thallus (6a). Starting from the vegetative cell (1), the cells accumulate biomass (2), before they undergo binary cellular division ((3) and (4)). After a certain number of cellular divisions, the cells develop a cup-like invagination with endoplasmic nets, called the brothosome (attached to cells in 5) [43]. The brothosome plays a central role in substrate uptake during the transition from vegetative cells to formation of a zoosporangium, but the mechanism is not yet understood [43]. In the transition from vegetative cell, with brothosome, to zoosporangia, the entire cytoplasm differenciates into biflaggelated zoospores (6a). The initial release of zoospores occurs by a small tear in the outer membrane, before the whole zoosporangium disintegrates [42].

The formation of zoosporangium (6a) is an asexual mean of propogation. The zoosporangium commonly have a size range between 15-35 µm, and somewhere between 10-75 biflaggelated zoospores (2-3x5-8 µm) are formed [44]. Bongiorni *et al.* [45] observed the disintegration of zoospores (6b) from the zoosporangium (6a), showing rapid movement for 5-10 seconds inside the zoosporangium prior to liberation, with the cell wall totally disintegrated after 3-5 minutes. During this work, the release of zoospores was observed by light microscopy for several shake-flask cultures, and internal zoosporangial movement was caught on film.

The understanding of the thraustochytrid life-cycle is still limited [42], and further investigation is needed to fully unravel the mechanisms controlling the formation of zoosporangium (first cell mode) or maintaining regular cellular division to accumulate high biomass levels (favoring second cell mode).

### 2.3.2 Lipid accumulation and composition of thraustochytrids

The distribution of the lipid classes varies among the thraustochytrid strains, but some general features are shared among them [5]. In general, the major lipid class are the neutral lipids, making up 50-95% of the total lipids. The glycolipids and the phospholipids (the polar lipids) are minor constituents, ranging from 0-27 % and 9-28%, respectively [5]. Figure 2.4 shows the lipid classes in some selected thraustochytrids [5].

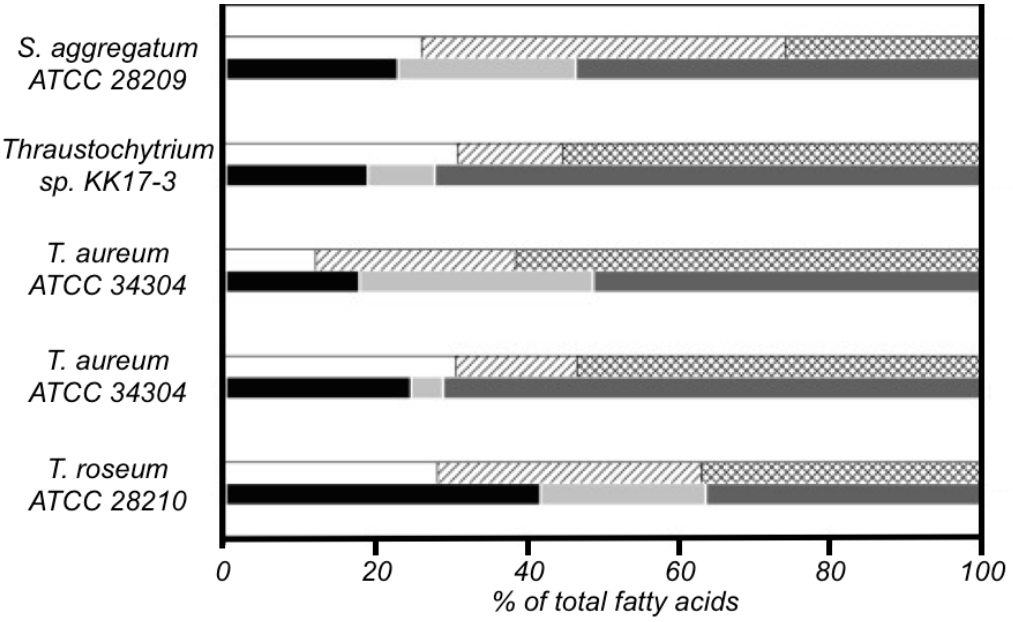


FIGURE 2.4: Percentage of saturated (SFA), monounsaturated (MUFA), and polyunsaturated (PUFA) fatty acids in neutral (NL) and polar (PL) lipid classes in thraustochytrids. White: NL-SFA, white with slash: NL-MUFA, white with cross: NL-PUFA, black: PL-SFA, light grey: PL-MUFA and grey: PL-PUFA. The figure is reproduced from Fan and Chen; Figure 4, page 302, [5]

Triacylglycerols (TAGs/TGs) constitute the major fraction in neutral lipids, followed by smaller portions of diacylglycerols (DGs) and monoacylglycerols (MGs) [46], [47]. Phospholipids were the major class present in the polar lipids [47]. Furthermore, Kendrick and Ratledge [47] reported that phosphatidylcholine and phosphatidylethanolamine were the major components of the polar phospholipids. PUFAs comprise a large fraction of both the neutral (NL) and the polar lipids (PL) [46]. Fan and Chen [5] summarized data of NL and PL content in thraustochytrids, and reported that PUFAs make up a larger fraction of the polar lipids (37-72%), than in the neutral lipids (26-61%). Huang *et al.* [48] explained this by the role of PUFAs in regulation of fluidity of cellular membranes. DHA is the dominant PUFA in both NL and PL of several thraustochytrids, with evidence of the TAGs C16/C16/22:6 (Palmitic acid/palmitic acid/DHA) and C16/C22:6/C22:6 (palmitic acid/DHA/DHA) being the two most abundant TAGs [46], [49].

### 2.3.3 Fatty acid synthesis in thraustochytrids

The lipid profiles in several thraustochytrid species show a high fraction of DHA of total fatty acids, constituting more than 50% for several strains [5]. In thraustochytrids the DHA synthesis is shown to be controlled by the enzyme complex poleketide synthase (PKS), using malonyl-CoA (MalCoA) as precursor, and not the regular fatty acid synthase (FAS) [50], [51]. The FAS synthesize saturated FAs up to C16-C18, and FAS is working in combination with desaturases and elongases, creating MUFAs and PUFAs [50], [13]. Lippmeier *et al.* [52] demonstrated that PKS was necessary for DHA production in thraustochytrids. The regular FAS pathway and PKS pathway are operating in parallel, but the regulation of carbon flow or relative activity is not known. A more extensive study of these pathways could lead to a greater understanding of the complex interactions between them, and provide information about how DHA productivity can be improved [12], [53]. An overview of the glycolysis, TCA-cycle, pentose phosphate pathway (PPP), and fatty acid biosynthesis in thraustochytrids, is shown in Figure 2.5.

The accumulation of triacylglycerols (TAGs) typically occur when one of the essential nutrients, often nitrogen, are limited or depleted [16]. Protein and nucleic acid biosynthesis stops, as a consequence of the nutrient limitation (N or P), and cell division ceases. The excess of available carbon source is channeled towards lipid synthesis. The surplus of carbon leads to increased ATP and acetyl-CoA (AcCoA) concentrations, and citrate is transported to the cytosol [54], [55]. ATP-citrate lyase (ACL) splits the citrate into AcCoA and oxaloacetate (OAA). AcCoA is converted to malonyl-CoA (MalCoA) by acetyl-CoA carboxylase (ACC), the rate limiting step of lipid biosynthesis [55], [56]. The

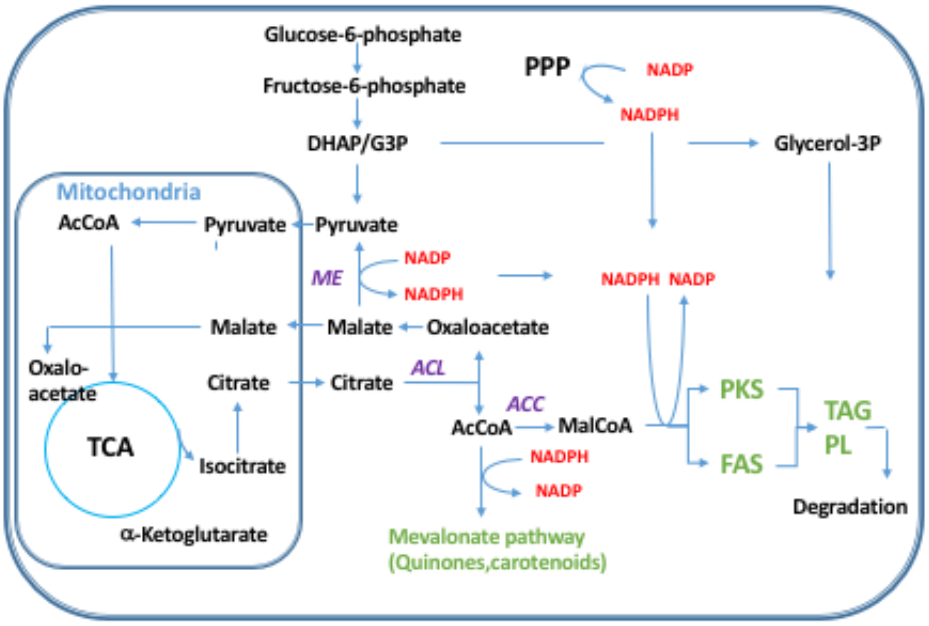


FIGURE 2.5: Overview of the metabolic pathway for DHA biosynthesis, incoroporation in lipids and degradation. Abbreviations: AcCoA: Acetyl-CoA, MalCoA: Malonyl-CoA, ACC: AsCoA carboxylase, DHAP: dihydroacetone phosphate, G3P: Glyceraldehyde 3-phosphate, PPP: Pentose phosphate pathway, TCA: Tricarboxylic acid cycle, PL: phoshpolipid

high ATP and AcCoA levels down-regulate the isocitrate dehydrogenase activity (convert isocitrate to $\alpha$-ketoglutarate), which is partly responsible for maintaining elevated citrate levels during surplus of carbon [55].

DHA is released from PKS as free fatty acids, and needs to be coupled to CoA by ketoacyl synthase (KS), before they can be integrated into TAGs [50]. The FAS pathway generate fatty acids (FA) linked to CoA, and ready for incorporation to TAGs, DGs, MGs, or other lipids. TAGs are composed of three FAs linked together by a glycerol-3-phosphate backbone. Glycerol-3-phosphate acyltransferases (GPAT), lysophosphatidic acid acyltransferases (LPAAT), phosphatidate phosphatase (PAP), and diacylglycerol acyltransferases (DGAT) are needed to produce TAGs from free fatty acids and the glycerol-3-phosphate backbone. It is currently not known if the different enzymes have specific affinities for certain FA substrates. Changes in cultivation conditions have shown a larger decrease in the FAS than PKS, but not an increased DHA-production rate [12].

Ratledge reported a decrease in lipid accumulation 30-70 hours after nitrogen depletion, in both yeasts and thraustochytrids [54]. Inactivation of enzymes needed to produce NADPH or enzymes directly involved in the FA synthesis are proposed reasons [54]. Other potential bottlenecks could be assembly of the fatty acids into lipids, and the degradation of fatty acids for energy consumption [57]. Regulation of lipid accumulation,

preformed in yeast, suggest post-translational modifications and metabolite overflow as possible bottleneck mechanisms [58].

### 2.3.4 NADPH requirements for biosynthesis of fatty acids

Both PKS and FAS consumes reducing power in the form of NADPH. The PKS pathway consume 14 NADPH, while the FAS pathway consume 26 NADPH [12]. Figure 2.6 shows the consumption of reducing power for DHA synthesis.

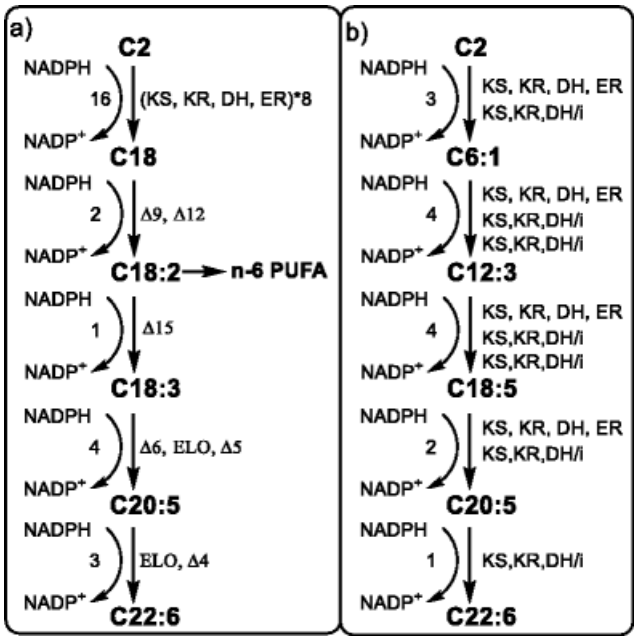


FIGURE 2.6: Alternative pathways for DHA (22:6) biosynthesis. a) The FAS pathway followed by elongation and desaturation. Only the n-3 pathway to DHA is depicted, while the branching point to the n-6 pathway is indicated. b) The PKS pathway ([51] and [50]). The number of NADPH needed at each step, or sequence of steps, is displayed to the left of the arrows, while the enzyme activities involved are indicated to the right. KS ketoacyl synthase; KR ketoreductase; DH dehydratase; DH/i bifunctional dehydratase and trans-cis isomerase, the isomerase may also move the double bond; ER enoyl reductase; $\delta$-desaturase, the number indicates which bond (counted from the carboxyl end) is desaturated; and ELO elongase, a multifunctional enzyme with KS, KR, DH, and ER activities. Reproduced from [12].

The NADPH consumption shown in Figure 2.6 (a) shows that the assimilation of one mol C18 chain of fatty acid requires 16 mol of NADPH. The theoretical amount of glucose needed to provide 16 mol NADPH is 4.5 mol, involving malic enzyme for NADPH generation [54]. However, ME can only provide 9 mol NADPH per 4.5 mol glucose, leaving 7 mol which is proposed to be generated by the Pentose Phosphate Pathway (PPP) [54]. This leads to slightly higher theoretical consumption of glucose, becoming 5.1 mol per mol of C18-fatty acyl-CoA. The assembly of TAGs require 3 mol fatty acyl-CoA in addition to 1 mol glycerol-3-phosphate (0.5 mol glucose), requiring a total of

15.7 mol glucose per mol TAG (containing only C18 fatty acids). From this information, a theoretical yield of 31.6 g of TAGs are potentially produced from 100 g of glucose [54].

## 2.4 Cultivation of *Aurantiochytrium* sp. T66

*Aurantiochytrium* sp. T66 accumulates lipids intracellulary during N- or P-starvation [59], [16]. Figure 2.7 shows an experimental curve of $CO_2$-evolution for a bioreactor cultivation of *Aurantiochytrium* sp. T66 with glucose and glutamate as carbon source [22]. Commonly, the cultivation is separated into three distinct phases; the lag phase, growth phase, and the lipid accumulation phase. The transition from the growth phase to the lipid accumulation phase (shown in the black circle) was initiated by the limiting concentration of N. The depletion is observed as the definite drop in $CO_2$-content [60].

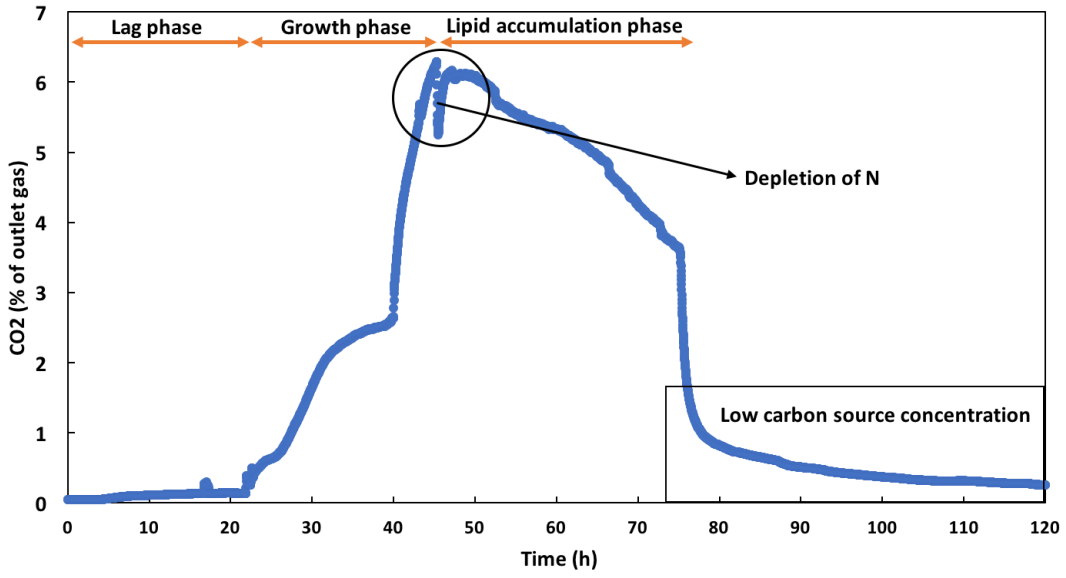


FIGURE 2.7: Example of $CO_2$-evolution during a fermentation of *Aurantiochytrium* sp. T66 with glucose as carbon source*. The lag phase, growth phase and lipid accumulation phase is shown. Nitrogen depletion are shown by the characteristic drop in $CO_2$-content enclosed in a circle. *The data is collected from Tronsaune [22].

The lag phase is the most poorly understood stage of cellular growth. The lag phase is characterized by limited growth, where the cells synthesize RNA, enzymes, proteins and other molecules necessary for growth [61]. The lag phase shows metabolic activity, and is not a dormant stage [62].

During the growth phase, all nutrients are present and the main flow of carbon and other nutrients is spent on generation of new cells. When deprivation of a key nutrient takes place, they enter the lipid accumulation phase if excess carbon is present in the medium [59]. The intracellular lipids are vital for thraustochytrids, and function as

energy reserves for starvation. The lipid accumulation phase continues until the available carbon source is spent. The exhaustion of the carbon source shown in Figure 2.7 from 80-120h showed decreasing lipid content, suggesting lipid catabolism during starvation [22]. The same result was reported by, Ruchi *et al.* [57], whom extended the starvation period, resulting in decreasing lipid content.

### 2.4.1 Formulation of carbon and nitrogen for lipid accumulation

The growth medium needs to be formulated with a high C:N ratio, to ensure that carbon and other nutrients are kept in excess when nitrogen is exhausted [12], [5]. A high C:N ratio is generally preferred for lipid accumulation. By lowering the amount of available N, the cellular dry weight (g/l) decreases, and the overall volumetric productivity of the desired products declines.

In other words, there is a trade-off between the carbon and nitrogen ratio. A C:N ratio larger than 24 was reported to be optimal according to data provided by Fan and Chen [5] from 1991-2003. Ugalde *et al.* [63] reported that the highest C:N ratio was not necessarily the most optimal for lipid production and fatty acid profile. An optimal C:N ratio for one species may induce no growth in another species, and the C:N ratio should therefore be optimized for each production organism.

### 2.4.2 Maximizing DHA production

Two possible changes to improve DHA production from thraustochytrids are: (1) increasing the biological productivity (g DHA/g dry cell weight), or (2) increase the growth rate (g dry cell weight/h). The increase of biological productivity, or the specific productivity, requires improvements regarding the anabolism of fatty acids, and especially DHA. Medium optimization is the first step towards increasing the DHA production of the cells [64], [59]. Secondly, genetic modification can improve strain productivity by increasing enzyme-substrate interaction or conversion rates [12].

In contrast to increasing the growth rate for improved DHA production, changing the specific productivity does not necessarily increase the substrate consumption relative to the increased DHA production. Increasing the growth rate, makes it possible to generate higher biomass yields per day, but a direct consequence of increased biomass yields is elevated substrate consumption. The overall volumetric productivity is improved, because of higher biomass yields, but the costs increase accordingly.

Thraustochytrids are promizing producers of sustainable DHA, but strain improvement by utilizing available genetic tools, optimizing medium, temperature, pH, and oxygen supply, are required to embrace a production host with high lipid content, rich in DHA.

### 2.4.3 Production of other high-value products

Several thraustochytrids species are pigmented and have been found to synthesize carotenoids [59]. The carotenoids are commonly divided into xantophylls and carotens [12]. Astaxanthin, cantaxanthin, lutein, β-carotene, and lycopene, are commercially the most important carotenoids, with their main application as a colorant in food and feed, and additive in pharmaceuticals and cosmetics [12]. Astaxanthin ($C_{40}H_{52}O_4$) is of special interest in marine feed for salmonids, because the salmonids lack the ability to synthesize astaxanthin *de novo*, thus having to supply the pigment through their diets [38]. Astaxanthin is a superior antioxidant, and Burja *et al.* [59] suggest that the astaxanthin production is a part of the system preventing oxidation of storage lipids. Observations by Quilodran *et al.* [65] and Tronsaune [22], suggest that the production of pigments are largest during high level of lipid biosynthesis, corresponding well with the proposed mechanism of pigments described by Burja *et al.* [59]. Figure 2.8 shows a bioreactor culture in the lipid accumulation phase, where lipids are the only generated products (intracellularly).

Squalene ($C_{30}H_{50}$) is another high-value product produced by several thraustochytrids, in particular species belonging to the genus *Aurantiochytrium* [12]. Squalene is an intermediate in sterol biosynthesis, normally obtained from deep-sea shark liver. Governmental regulations, and ruthless killing of the sharks, demonstrate the need of alternative sources. Squalene is used in pharmaceuticals, vaccine and drug delivery, and several medical substances [12]. Furthermore, numerous health benefits are associated with squalene, anti-carcinogenic activity, strong antioxidant, protection of lipid oxidation. Squalene is also an essential component of skin lipids in humans [66].

Non-pigmented *Aurantiochytrium* strains also exist, and were described to produce higher levels of DHA and other desired fatty acids than pigmented species [5]. This primary difference could be explained by the large energy demands for production of complex biological molecules like astaxanthin and other carotenoids.

Astaxanthin and squalene could potentially contribute to the economical aspects of using thraustochytrid biomass from heterotrophic cultivations to produce sustainable sources of DHA, astaxanthin and squalene, or for direct consumption, or additive in feed for industry. Addition of thraustochytrids could provide aquaculture feed with essential biomolecules to maintain fish health and their status as a healthy food. Utilization of

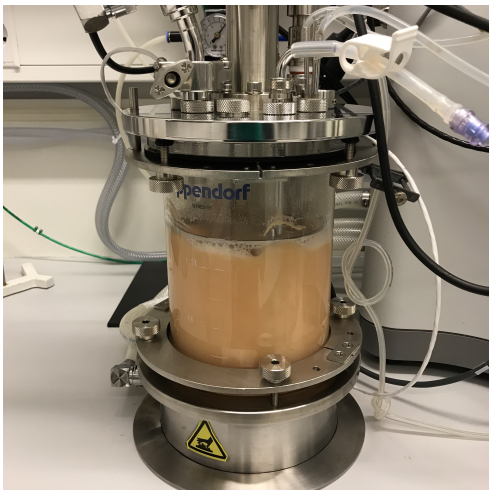


FIGURE 2.8: Bioreactor culture of *Aurantiochytrium sp.* T66. The characteristic orange color induced by astaxanthin and carotenoid production become very clear during lipid accumulation.

the entire thraustochytrid biomass could replace the costly process of purification to isolate DHA, astaxanthin and squalene, improving the economics related to heterotrophic cultivations of thraustochytrids [12].

## 2.5 Intracellular mapping

Cellular metabolism is an extremely complex and intertwined network of biochemical reactions [55]. The different pathways are regulated through a complicated set of signal molecules, enzymes and interactions between metabolic pathways. To understand the reaction pathways, mapping and quantifying the metabolites is required [67], [68], [69]. A simple overview of the main metabolic pathways of thraustochytrids were shown earlier in Figure 2.5. To map the metabolism of the thraustochytrid used during this work, a combination of the Black-box model and metabolic analysis was used.

### 2.5.1 Black-box model

The Black-Box model is a tool used to investigate the relation between the input and output of a system [70]. In biochemistry, the cell is considered as the system. The chemical reactions taking place inside the cell are not directly considered, only the overall mass balance of the system. An illustration of the Black-Box model is shown in Figure 2.9. The main constituents of a cell is C, N, O and H, constituting more than 90-95% of the cellular dry weight (DCW) for most microorganisms. P, Fe, S, Mg, K, Na, Ca, Cl, and a few more trace elements, make up the remaining 5-10% of DCW

[71],[55]. The microorganisms have adapted their cell life-cycles to their environmental conditions, and some organisms utilize $O_2$ for energy generation and metabolism. These microorganisms are called aerobic, while microorganisms not dependent on $O_2$ for growth are called anaerobic [72].

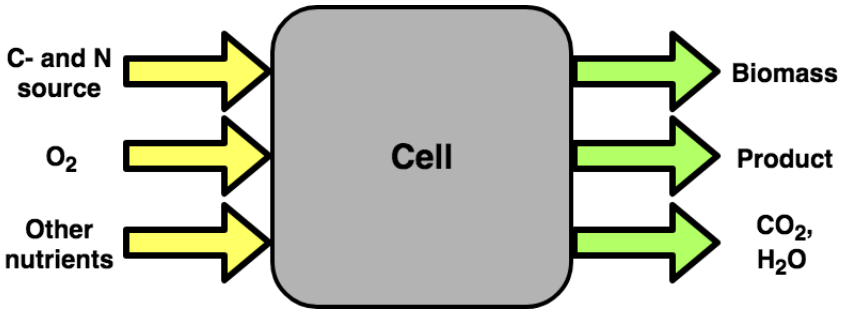


FIGURE 2.9: Black-Box model of a cell using oxygen ($O_2$), C, N and other nutrients for growth and production. Other nutrients are trace metals, minerals, phosphor and sulfur.

Carbon (C), nitrogen (N), sulfur (S) and phosphor (P) are directly coupled to cellular division [72]. The carbon source is directly coupled to all biochemical reactions, and understanding the flow of carbon through the central metabolism of a cellular system is very important to interpret the connection between all the anabolic and catabolic reactions [55]. The carbon is often linked to both cellular growth and product formation. The product(s) can be intra- or intercellular, depending on the nature of the organism and the growth conditions [72].

The thraustochytrids investigated here produce intracellular lipids as a consequence of nutrient limitation. Both nitrogen and phosphor limitation has shown increased lipid synthesis with surplus of carbon present [16]. A depletion of nitrogen initiates the lipid accumulation phase, and the cellular growth (biomass increase because of cell division) ceases because N is needed for biosynthesis of proteins and nucleic acids [59]. With all necessary nutrients available, carbon is mainly spent on synthesis of metabolites required for cellular division. However, when the thraustochytrids detect depletion of N or P, they channel their main carbon flow towards lipogenesis [16], [12]. A large set of enzymes participate in the synthesis of intracellular lipid droplets surrounded by a protein-rich membrane [73]. The cells increase their survival rate by accumulating energy reserves, which they can spend for energy generation when encountering undesirable growth conditions.

Complex analytic tools have during the last few decades developed rapidly, and are utilized to map the reactions taking place inside the Black-box model. Quantification of selected metabolites by CapIC-MS/MS, LC-MS/MS were used to recognize the metabolites of *Aurantiochytrium* sp. T66.

### 2.5.2 Metabolite profiling of phosphometabolome, organic acids and amino acids

Metabolites comprise less than 3% of the dry cellular weight, but play a crucial part in energy generation and as building blocks for macromolecules [69]. The analysis of these metabolites, metabolomics, can provide quantitative and qualitative information on several different metabolite groups [67]. Phosphometabolome (e.g sugar phosphates, nucleotides, phospho-carboxylic acid), organic acids and amino acids are intermediates in the glycolysis, tricarboxylic acid cycle (TCA), pentose phosphate pathway (PPP) and other pathways, and are essential in all life processes [68]. Determining the concentration of these intracellular metabolites is a key to understanding biological processes. Primary and secondary metabolism, energy states, signal-tranducing pathways, cell cycles and stress responses are core-processes where metabolomics are essential [74], [75]. The relationship between the metabolic pathways are vital during optimization of production organisms. In the thraustochytrids, two competing pathways are involved in fatty acid synthesis (FAS and PKS) [12]. The regulation of carbon flow through these pathways are poorly understood, and the interaction between fatty acid synthesis pathway, PPP, TCA and glycolysis needs further investigation.

Energy charge of the cell is used as a tool to recognize the cells energy status. The cell requires energy to convert substrates to wanted products for metabolism. The energy status of a cell changes rapidly, and well-established protocols are required to gather valuable results from the sampling of intracellular metabolites.

### 2.5.3 Energy charge (EC)

Interaction between pathways consuming and generating adenosin triphosphate (ATP) are regulated in a complex way. This regulation must be determined by the energy balance of the cell [76]. The energy balance is equal to the ratio between the energy carriers ATP, ADP and AMP. The energy charge equation is shown in Equation 2.1 [76].

$$\text{Energy Charge} = \frac{[\text{ATP}] + \frac{1}{2}[\text{ADP}]}{[\text{ATP}] + [\text{ADP}] + [\text{AMP}]} \tag{2.1}$$

A "fully charged" cell has an energy charge equal to 1.0. If the cell has an energy charge of 0.0, only adenosin monophosphate (AMP) molecules are present. The energy charge of most metabolic active cells range between 0.8 and 0.95 [70].

## 2.6 $^{13}$C-labeled substrates in metabolic profiling

Metabolic profiling can provide quantitative and qualitative information about in vivo metabolism [77], [78]. A combination of metabolite balances and isotopic labeling experiments, is according to Christensen *et al.* [79], the best way to extract information about the metabolic network. Metabolic flux analysis (MFA) is a preferred technique for collecting qualitative information about the cell metabolism, and the information can be used to optimize medium, identify targets for biochemical engineering, and validate metabolic pathways [78]. MFA is commonly divided into two categories: methods on balancing fluxes with the assumption of stoichiometry within the network; and methods using isotopic tracers (e.g. $^{13}$C) to examine fluxes [80], [77]. The sole use of steady state metabolic balancing, is according to Buescher *et al.* [80] a limitation, because increased metabolite concentration could be a result of upturn in enzymatic activity of producing enzymes, or down-regulated activity of consuming enzymes. The latter methodology, $^{13}$C-tracers, can elucidate fluxes of parallel pathways, like glycolysis vs. pentose phosphate pathway, reversible reactions, and cyclic pathways [78], [81]. $^{13}$C-tracer exploration of cell metabolism, is according to Ratledge [53], the only reliable method to determine carbon flux distribution between FAS and PKS of thraustochytrids.

In practice, resolving metabolic fluxes from experimental data can be time- and data-intensive. In many cases, direct interpretation of $^{13}$C labeling patterns (mass distribution vector, MDV) is sufficient to provide information on relative pathway activities. The $^{13}$C-tracer analysis is one of the first steps to generate a complete MFA of the organism, and quantification of the metabolites, analysis of the fluxes, and statistical models are required to generate a complete $^{13}$C-MFA map.

During this MSc Thesis, $^{13}$C-glucose was used as a tracer in shake-flask cultivations. This was performed to establish an understanding of the carbon flux distribution. The system investigated here is not in metabolic pseudo-steady state, but the tracer experiments can still provide qualitative and quantitative information about the metabolic pathway fluxes. 1-$^{13}C_1$-glucose, 1,2-$^{13}C_2$-glucose, and U-$^{13}C_6$-glucose were utilized in $^{13}$C tracer analysis. The substrates are shown in Figure 2.10.

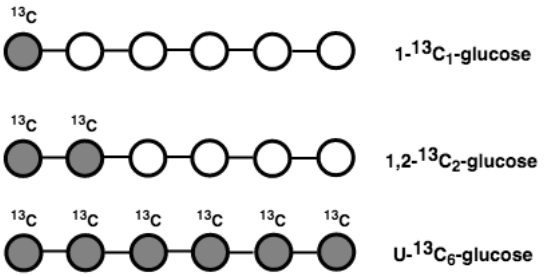


FIGURE 2.10: $^{13}$C-glucose (6C) substrates with number of isotope labeled carbon atoms (grey) and position. The white C atoms are regular $^{12}$C.

The three substrates are $^{13}$C-labeled with one, two and six carbon atoms, respectively. Cultivations with these substrates will therefore give different fractions of labeling of intracellular metabolites [70]. One out of six C-atoms (about 17%), in central carbon metabolism, should theoretically be labeled for 1-$^{13}C_1$-glucose, while 2/6 (33%) and 6/6 (100%) for 1,2-$^{13}C_2$-glucose and U-$^{13}C_6$-glucose, respectively. The conversion of the $^{13}$C-glucose substrates to acetyl-CoA, via pyruvate, is shown in Figure 2.11 with theoretically sum fractional label. This yield a theoretical labeling of 25, 50, and 100% for the three $^{13}$C-labeled glucose substrates.

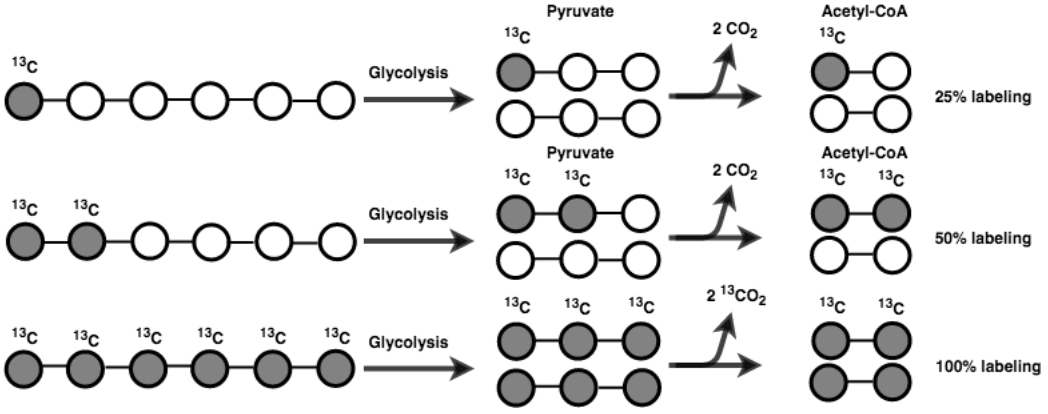


FIGURE 2.11: Labeling pattern of pyruvate and acetyl-CoA from $^{13}$C-labeled glucose substrates. Glycolysis is represented by one arrow, but consist of numerous reations. Dark grey represent $^{13}$C atoms, while white represent regular $^{12}$C carbon.

### 2.6.1 Labeling patterns and pathway activities of $^{13}$C-glucose cultivations

Change in metabolite mass occurs due to incorporation of isotopes during flux analysis with $^{13}$C-containing substrates (or other isotope substrates of other chemical elements). Metabolites that only differ in isotope composition are called isotopologues [77]. The mass distribution vectors (MDVs) describe the fractions of each isotopologue, normalized to the sum of all possible isotopologues. A metabolite with n carbons can have 0 to n $^{13}$C-atoms labeled, leading to isotopologues with masses (M) from M+0 (only $^{12}$C-atoms) to M+n (M+n has all carbons labeled with $^{13}$C). e.g. A six-carbon metabolite can range from M+0 to M+6 isotopologues. The sum of all fractions of MDVs is 100%, and is named sum fractional labels (SFL). SFL is calculated by equation 2.2 [77].

$$\mathrm{SFL} = \frac{\sum_{i=0}^{n} i \cdot m_i}{n \cdot \sum_{i=0}^{n} m_i} \tag{2.2}$$

Here n is the number of carbons in the metabolite, i denotes the isotopologues, and m the abundance of an isotopologue.

The $^{13}$C tracer analysis reveals the fraction of the metabolite being formed by all pathways from the labeled nutrient, and does not provide information about the activity of specific pathways, nor absolute fluxes [77]. The isotopologue patterns can indicate the relative pathway activities and qualitative changes in distributions to production of certain metabolites, and thus provide information about alternative metabolic routes [77]. Distinguishing the relative distribution between glycolysis, TCA-cycle, PPP, and lipid biosynthesis, is crucial during development of strategies for increased DHA production.

Evans and Ratledge [82] showed that the split ratio between glycolysis and PPP was 77/23% with glucose as carbon source. This split ratio changed to 89/11% when glutamate was utilized as N source, instead of $NH_4^+$. Glutamate functions as both a N- and C-source. Use of $^{13}$C-labeled substrates, 1-$^{13}C_1$- and 1,2$^{13}C_2$-glucose, could explain distribution between glycolysis and PPP. Furthemore, U-$^{13}C_6$-glucose, are used to distinguish carbon incorporation from glucose versus glutamate. Fully labeled $^{13}$C-glutamate, U-$^{13}C_6$-glutamate, could explain isotopic steady state for TCA intermediates, as shown by Ahn and Antoniewicz [78].

## 2.7 Principal component analysis (PCA)

Principal component analysis (PCA) is a multivariate data analysis tool for compressing large amounts of data into new variables called principal components (PCs) [83]. The new PCs account for the majority of the variability in the data. The first PC is the direction through the data that explains the most variability, and the second PC is orthogonal to the first PC and describes the maximum amount of remaining variability.

# 3

# Materials and methods

The thraustochytrids strain used in this Master Thesis, *Aurantiochytrium* sp. T66, was collected by SINTEF Industry outside the coast of Portugal (2003). Cryopreserved samples prepared during the fall 2017 were used for a bioreactor cultivation with natural glucose, and for $^{13}$C-labeled glucose experiments in shake-flask cultures.

## 3.1 Culture conditions, medium, and experimental set-up of the bioreactor cultivation

Ampules thawed on ice were added to separate 100 ml shake-flasks (SF) containing medium listed in Table 3.1. The SFs were incubated at 28°C and 200 rpm until measured optical density (OD) ranged between 6-8 (exponential growth phase - optimal for inoculation [60]). Microscopic studies, during the growth, were performed to ensure no growth of undesired microorganisms. The bench-top bioreactor cultivation medium was prepared as described in Table 3.2, and the procedure in Section 3.1.2 was followed. Two of three SFs were mixed, and a 5% inoculum was created by addition of 75 ml culture from the SF to the bioreactor.

All medium components, except the phosphate source, glucose, the vitamin mix (A.1) and the TMS-6 mix (A.2 for the bioreactor), were added prior to sterilization. The

TABLE 3.1: Medium components used for shake-flask cultures to generate biomass for inoculation of the bioreactor.

| **Nutrient** | **(g/l)** |
|---|---|
| Glycerol | 30 |
| Na-glutamate | 8 |
| Yeast extract | 5 |
| $Na_2SO_4$ | 18 |
| $MgSO_4 \cdot 7\,H_2O$ | 0.25 |
| KCl | 0.4 |
| Tris-base | 6.1 |
| Maleic acid | 5.8 |
| $KH_2PO_4$ | 0.3 |

TABLE 3.2: Medium components used for the bioreactor cultivation with glucose. The concentration of glucose is listed as the total concentration after addition and as start concentration.

| **Nutrient** | **(g/l)** |
|---|---|
| Glucose (total) | 125 |
| Glucose (start) | 50 |
| Yeast extract | 1 |
| Na-glutamate | 8 |
| $MgSO_4 \cdot 7\,H_2O$ | 1.2 |
| $Na_2SO_4$ | 18 |
| KCl | 0.4 |
| $CaCl_2 \cdot 2\,H_2O$ | 0.5 |
| $KH_2PO_4$ | 0.3 |

glucose solution (75g glucose, 95 ml deionized $H_2O$) and the phosphate solution (6g $KH_2PO_4$, 55 ml deionzed $H_2O$) were sterilized in separate containers, because of complex formation with other nutrients at high temperature and pressure.

The glucose-, $KH_2PO_4$-solutions, and 1.5 ml of sterile-filtered TMS-6 solution, vitamin mix, and antifoam 204 (Sigma-Aldrich, 10%v/v in MQ-$H_2O$), were added in a sterile bench before the shake-flask inoculum was added. pH was automatically adjusted to 7.0 during the bioreactor cultivation by addition of 3M NaOH and 1.5M $H_2SO_4$. The total glucose was distributed between two additions, in order to ensure that the biological system was not disturbed by osmotic stress due to high sugar concentration.

A picture of one of the shake-flask cultures and the bioreactor cultivation of *Aurantiochytrium* sp. T66 is shown in Figure 3.1. The picture of the shake-flask culture (b) was taken during the stationary phase (all carbon sources are depleted), while the bioreactor (a) was taken during the lipid accumulation phase (N-source exhausted with available C-source).

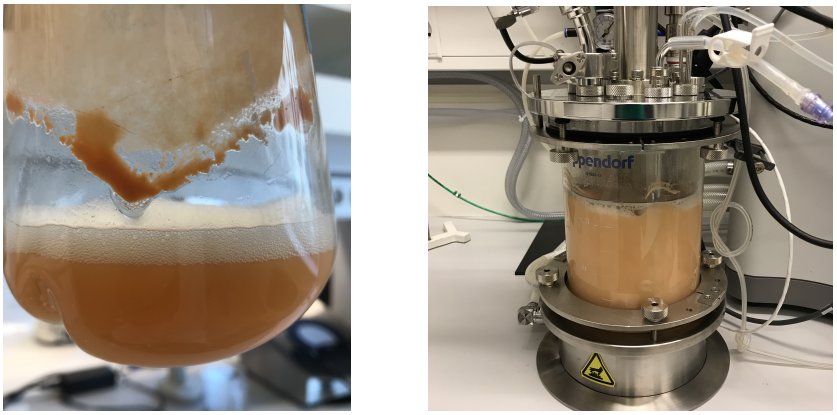


(a) (b)

FIGURE 3.1: Eppendorf BioFlo 320 bioreactor and shake-flask culture containing *Aurantiochytrium* sp. strain T66. The culture in the shake-flask: stationary phase, and the bioreactor culture: lipid accumulation phase.

### 3.1.1 Microscopic studies

During this work, problems with zoosporangium formation in the bioreactor and shake-flask cultures led to increased use of microscope to observe the thraustochytrids life-stages. Several inoculated bioreactor cultures failed to initiate growth, and the side-project with shake-flask cultivations was undertaken to characterize the development stages. The motivation was to improve the inoculum preparations to make robust and reproducible bioreactor cultivations. The microscopes used were light microscopy Zeiss Apotome Imager.Z2 with AxioCam ERc5s and Motic BA310.

#### 3.1.1.1 Staining of shake flask and bioreactor cultures

Staining of *Aurantiochytrium* sp. T66 was performed to observe differences associated with vegetative cells and zoospores, as well as differences associated with growth and lipid accumulation. Staining of cells with Live/Dead Assay L7012 (LIVE/DEAD BacLight Bacterial Viability Kits, from Molecular Probes [84]) was performed to observe the differences of metabolic activity between cultures with and without zoospores present.

### 3.1.2 Top-bench bioreactor set-up

Fermentation was conducted with Eppendorf Bioflo 320 bioprocess system, with Eppendorf Bioflo 320 Vessels. The dissolved oxygen (DO: 20%), pH adjusted to 7.0, temperature adjusted to 28°C, and agitation were controlled at all times. The content of

$CO_2$, $O_2$, pH, temperature, air flow, and agitation were monitored throughout the whole fermentation. The total fermentation time was 161h.

Before inoculation, the electrodes were calibrated, the reactor containing the growth medium sterilized, sterile filtered nutrients and antifoam were added, and the acid-base system for pH-control was prepared.

**Bioreactor set-up**

1. Eppendorf Bioflo 320 was assembled as described in Eppendorf Bioflo 320 installation manual.
2. The bioreactor contains 11 ports, where equipment such as pH-electrode, DO-electrode, sampler and sparger can be attached.
3. The 11 ports were sparger, exhaust, harvest, DO, pH, Tri-port (acid and base addition), addition port, thermowell, sampler (not used during this project), and two closed ports.
4. The exhaust port, as well as the water jacket, were connected to a cooling system with water at 4°C.

**Calibration of pH and dissolved oxygen (DO) electrode**

1. pH electrodes were calibrated by using standard solutions with known pH of 4.0, 7.0 and 11.0 (done in the listed order). Deviations corrected manually.
2. The DO electrode was calibrated by running air at 0.3 vvm (0.5 l/min) through the reactor.
3. Cascade between agitation and DO was set to 20% DO.

**Medium preparations**

1. Medium described in Table 3.2, was added to the bioreactor.
2. The phosphate source, TMS-6, antifoam 204, and vitamins, were added in the sterile bench.

**pH-control preparations**

1. 250 ml 1.5 M $H_2SO_4$ and 3.0 M NaOH were prepared.
2. The chemicals were added to sterilized graduated cylinders.

3. Both the base and acid was connected by a rubber tube to each reactor through an automatic pump (the pump was adjusted by a cascade in the software to maintain stable pH at 7.0).

**Inoculation**

1. 5% inoculum was created by addition of 75 ml culture to the reactor.

## 3.2 Analysis methods

Table 3.3 shows the analysis methods used in this MSc thesis, with a short summary of the analysis results.

TABLE 3.3: List of analysis methods used during investigation of *Aurantiochytrium* sp. T66.

| **Analysis** | **Instrument** | **Result** | **Section** |
|---|---|---|---|
| Dry cellular weight | Weight | Concentration of cells | 3.2.1 |
| Glucose consumption | HPLC | Concentration of glucose | 3.2.2 |
| Glutamate consumption | UPLC-MS | Concentration of glutamate | 3.2.2 |
| Bligh and Dyer (lipids) | Weight | Quantification of TL | 3.2.3 |
| Fatty acids (FAs) | LC-MS | Concentration of FAs | 3.2.4 |
| Separation of lipids | SPE | Separate PL and NL | 3.2.5 |
| Analysis of lipid classes | UPC$^2$-MS | FA profiles PL, NL | 3.2.5 |
| **Intracellular metabolites** | | | 3.2.6 |
| Phosphometabolites | CapIC-MS | Phospho-compounds | 3.2.6.1 |
| Amino acids (AAs) | LC-MS | Concentration of AAs | 3.2.6.2 |
| Organic acids (OAs) | LC-MS | Concentration of OAs | 3.2.6.3 |
| NADs and CoAs profiling | UPLC-TQS | NADs and CoAs | 3.2.6.4 |
| **$^{13}$C-tracer analysis** | | | |
| $^{13}$C-istopologues | CapIC-MS | Labeling pattern | 3.3 |
| $^{13}$C-labeling of metabolites | CapIC-MS | Labeling pattern | 3.3 |

### 3.2.1 Dry cell weight (DCW)

Determination of dry cell weight (DCW) is very important to develop a clear picture of how biomass is accumulated during growth. DCW was monitored throughout the fermentation, during the $^{13}$C-labeled glucose experiments in shake-flasks, and other cultivations in shake-flasks involving life-cycle investigations.

1. Two parallels of 10/20 ml of culture were added to 50 ml falcon tubes.
2. The tubes were centrifuged at 5000 rpm for 5 min.
3. About 1.5 ml of supernatant was added to Eppendorf tubes for HPLC analysis of the supernatant. The remaining supernatant was discarded.
4. The sediment was washed with 30 ml 1.5% NaCl-solution, and centrifuged at 5000 rpm for 5 min. Supernatant discarded.
5. The sediment was re-suspended in 20 ml of deionized water, before it was added to a pre-weighed aluminum tray.

6. The samples were dried at 120°C for over night.

7. The aluminum trays were weighed, and the dry weight was determined.

### 3.2.2 Glucose and glutamate consumption

**Glucose estimation:** The glucose concentration was monitored throughout the fermentation and the $^{13}$C-glucose experiments. The supernatant was removed from the DCW samples as described in Section 3.2.1. The samples were filtered with 0.2 µm membrane filters, and analyzed with HPLC in association with Silje Malene Olsen.

1. A standard mix of selected sugars, organic acids and EtOH was prepared to establish a standard curve. The standard mix is listed in Table E.1 in Appendix E.1.

2. All samples were diluted with HPLC grade $H_2O$ to an estimated concentration, within the interval 0-5 g/l of glucose.

3. The samples were run by HPLC with settings listed in Appendix E.1.

**Glutamate estimation:** Supernatant samples were filtered with 0.2 µm membrane filters, and diluted to 0-0.147 g/l glutamate. The glutamate concentration was determined for all samples of the fermentation, as well as for the shake-flasks from the $^{13}$C-glucose experiments. The glutamate samples were derivatizised with phenylisocyanate (PITC) by the method below, and then analyzed by UPLC-MS.

1. 10 µl internal standard was added to all wells except the blanks in the Waters well-plate.

2. 40 µl of water with known glutamate concentrations, 0.1, 1, 5, 100, 500 and 1000 µM, were added to separate wells. These measurements are used to generate the standard curve.

3. One blank sample (HPLC-grade $H_2O$) was added before and after the samples with known concentrations.

4. 40 µl of each sample was added to separate wells.

5. Another series of standard samples were run after the unknown samples.

6. 100 µl of a mixture of $\frac{19}{41}$ EtOH, $\frac{19}{41}$ pyridine and $\frac{3}{41}$ PITC was added to each well.

7. The well-plate was shaken for 20 min at 400 rpm.

8. The well-plate was evaporated in a speed vacuum at 800 rpm, 4 Torr and 45°C for 1.5h.
9. The well-plate was lidded, and stored at -80°C over night.
10. Each well was resuspended in 200 µl of ACN:$H_2O$ (30:70 v/v) with 0.38 mg/ml ammonium acetate.
11. The well-plate was shaken for 30 min at 400 rpm.
12. The well-plate was centrifuged for 5 min at 800 rpm, but no temperature or pressure requirements were applied.
13. The well-plate was analyzed by UPLC-MS with conditions described in Appendix E.2.

### 3.2.3 Bligh and Dyer method

Bligh and Dyer is a method used for lipid extraction, and quantification of total lipids present in a sample. The procedure uses extraction of lipids by addition of a non-polar solvent. A modified procedure of the protocol developed by Bligh and Dyer (1959) [85] was used. Samples of 20 ml were collected from the fermenter, and the following procedure was followed. Determination of lipid content was completed for the $^{13}C$-glucose experiments, but the volumes were reduced to 8-9 ml (depending on remaining volume after intracellular metabolite sampling (explained in Section 3.2.6)).

**Preparation of cell mass**

1. 20 ml culture centrifuged at 5000 rpm for 5 minutes, and the supernatant discarded.
2. The sediment was washed with 1.5% cold NaCl-solution, and centrifuged at 5000 rpm for 5 minutes. Supernatant discarded.
3. The samples were stored at -20°C before pre-treatment for the extraction.

The samples were freeze-dried for about 24 hours. The freeze-dried samples were homogenized by using the back-side of a spatula. The samples were prepared by the following procedure:

**Pre-treatment Bligh and Dyer**

1. About 28-32 mg freeze-dried cells (in a 13 ml plastic tube) were suspended in 0.7 ml 0.1M Tris-HCl (pH 7.5 heated to 50°C).

2. The solution was heated to 98°C for 10 min in a water bath.
3. The samples were cooled to 50°C in another water bath.
4. 0.1 ml freshly made protease solution containing 10 mg protease from Streptomyces griseus per ml buffer was added. The samples were incubated at 50°C for 1h.

The samples were cooled to ambient temperature before extraction:

**Extraction**

1. 2000 µl methanol and 1000 µl chloroform was added to the 13 ml plastic tube.
2. The sample was homogenized for 60 sec with Ultra Turrax at 25,000 rpm, while held on ice.
3. 1000 µl chloroform was added, Ultra Turrax for 20 sec.
4. 1000 µl deionized water was added, Ultra Turrax for 20 sec.
5. Centrifuged sample at 4000 rpm for 5 min at 15°C.
6. The chloroform phase, containing fat (the lower phase), was removed by penetrating the bottom of the plastic tube with a syringe tip. The sample was transferred to 1.5 ml Eppendorf tube.
7. Exact volumes (500-100 µl) were transferred to pre-weighed HPLC vials.
8. The chloroform was evaporated in a heating block at 60°C with $N_2$-flushing for 3-5 min.
9. The sample was kept in an exicator until the weight was determined.

### 3.2.4 Fatty acid analysis

Fatty acid concentrations and quantification was completed through direct hydrolysis of the fermentation broth (well-mixed), extraction with dichloromethane, and analysis with LC-MS. The LC-MS analysis was conducted in collaboration with Janne Øiaas from SINTEF Industry.

**Hydrolysis and extraction of fatty acids**

1. 100 µl well homogenized fermentation broth was transferred to 13 ml plastic tubes (round bottom). 400 µl 5M KOH was added.
2. All samples were flushed with $N_2$ for 10 sec and incubated in a water bath at 80°C for 120 min.
3. After 2 hours, 500 µl 4M $H_2SO_4$ was added, and the samples were flushed with $N_2$. The samples were placed in the freezer at -20°C. The last step is not needed if the procedure is continued directly.
4. The samples were thawed at room temperature, and 2000 µl dichloromethane (DCM) was added.
5. Samples were whirl-mixed for 60 sec and centrifuged at 4000 g for 10 min.
6. 200 µl of DCM (lower phase) was transferred to brown HPLC vials by penetrating the upper phase and gently extracting the desired volume of DCM.
7. The solvent was evaporated in a fume hood on a heat-block at 60°C flushing the samples with $N_2$.
8. The samples were analyzed by LC-MS as described in Appendix E.3.3.

### 3.2.5 Solid phase extraction (SPE) for separation of neutral and polar lipids

Solid phase extraction (SPE) was used to separate neutral and polar lipids. The protocol is a modified version of the protocol presented by Pernet *et al.* [86]. All samples were pre-treated by the Bligh and Dyer method, before divided into fractions of neutral (fraction A) and polar lipids (fraction B) by this method. Figure 3.2 shows the SPE separation of lipids into neutral and polar lipids. The two fractions, and the original lipid sample extracted by Bligh and Dyer, were hydrolyzed by the same protocol as described for the fatty acid analysis 3.2.4. Instead of 100 µl culture, 100 µl of fraction A and B (dissolved in chloroform and methanol, respectively) were used for the FA composition determined by LC-MS.

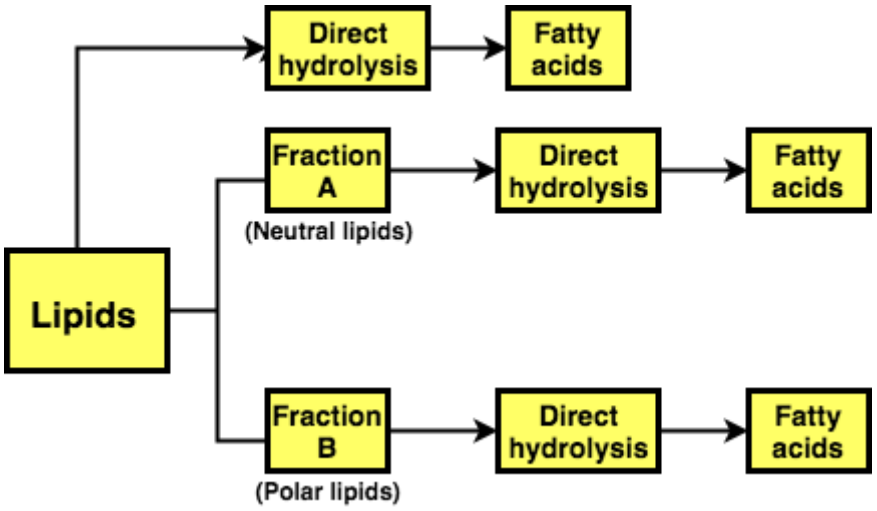


FIGURE 3.2: Solid phase extraction (SPE) scheme used for separation of neutral lipids (fraction A) and polar lipids (fraction B) from samples with extracted lipids by Bligh and Dyer (3.2.3). Direct hydrolysis of the fractions and the original sample with lipids were performed as described for fatty acid (FA) analysis in Section 3.2.4. The fatty acid profiles were determined.

All sample volumes were adapted to range between 2-3 mg of lipids per added volume to the column. The following procedure was used with vacuum pressure to extract the lipids.

**Description:** StrataO S1-1 Silica (55mm, 70Å), 100 mg/1 ml tubes (max. load 3 mg of lipids). **Sorbent Type:** Silica-based. **Format:** Tube. **Phase:** Silica.

**Procedure:**

1. For 100 mg columns, 1 ml methanol was added to wet the column. 1 ml of chloroform followed. Low vacuum pressure was applied to not exceed 1-3 drops/sec.

2. Samples (about 3 mg of lipids) were dissolved in 200 µl (or other volume to get a total lipid content of 2-3 mg) chloroform and gently added to the solid phase. Fraction A was collected. Simple lipids; like cholesterol esters and TAGs, were collected in fraction A by addition of 1 ml of chloroform:methanol mixture (98:2, v/v). vacuum pressure was applied, but was controlled to not exceed 1-2 drops/sec.

3. Polar lipids were collected in fraction B by addition of 4 ml of methanol to the column. Vacuum was used to get a drop rate of 1-2 drops/sec.

4. The fractions were evaporated under nitrogen atmosphere (methanol phase was heated in a heating-block at 60°C) and reconstituted in 200 µl (or other volume if another volume was used, see 2.)

5. The fractions (A and B), and the original lipid sample, were hydrolyzed by the procedure described in Section 3.2.4.

6. Samples were stored at -20°C prior to analysis with $UPC^2$-MS.

### 3.2.6 Profiling of intracellular metabolites

Metabolites comprise less than 3% of DCW, but serve critical functions in energy generation and as building blocks for macromolecules across all domains of life [69]. The studies of the metabolites, metabolomics, are therefore of great interest when investigating a microbial production-host. During this work, phosphorylated compounds, amino acids, and organic acids were investigated by different chromatography and mass spectrometric (MS) methods. Metabolite extracts were created first, and followed by the methods described below.

**Preparation of metabolite extract**

1. Volume based on OD (5 ml for sample 1-2, and 1 ml for sample 3-9) was added to 40 ml of cold 0.9% NaCl-solution (on ice) and centrifuged for 20 sec (centrifuge from 0-5000 rpm before stopping centrifuge manually). Supernatant discarded.
2. 30 ml cold deionized water (on ice) was added, and centrifuged for 20 sec (0-5000 rpm). Supernatant removed.
3. 20 ml of cold ACN-$H_2O$ (55:45, v/v) was added, and the tubes were frozen quickly in liquid $N_2$.
4. The samples were stored at -80°C with angle (between 20-45°) for at least 1h.
5. Three freeze-thaw cycles were performed by thawing the samples in liquid EtOH at 0°C, quickly freezing the samples in liquid $N_2$.
6. The samples were freeze-dried (-150°C and about 20 Pa) over night to evaporate the ACN:$H_2O$-solvent.
7. Re-suspended the samples in 500 µl cold $H_2O$.
8. The samples were centrifuged at 5000 rpm for 4 min at 4°C.
9. 450 µl was transferred to 3000 kDa spinfilters, and centrifuged at 5000 rpm for 10 min at 4°C.
10. The filters were discarded and the metabolite extract was ready for analysis.
11. The metabolite extracts were used for CapIC-MS, organic acids (LC-MS) and amino acids (LC-MS).

#### 3.2.6.1 Phosphorylated compounds

The original capillary ion chromatography (CapIC-MS) protocol was developed by Kvitvang *et al.* [68], but a modified method with $^{13}$C-interstandard correction was used during this work. The method was developed by Stafsnes, Røst and Bruheim [69], and are shown in Appendix E.4. The analysis was performed in association with Marit Stafsnes, and had to be optimized for the selected thraustochytrid strain (*Aurantiochytrium* sp. T66). 100 µl of metabolite extract was transferred to HPLC-vials for CapIC-MS. The settings are described by Stafsnes *et al.* [69], and are shown in Appendix E.4.

#### 3.2.6.2 Amino acid composition

Amino acid quantification was determined by LC-MS-analysis applying electrospray ionization in positive mode on the metabolite extracts. The metabolite extracts were derivatized by reaction of the amine (-$NH_2$) groups with phenylisochyanate (PITC) at alkaline pH, before separation by LC. Excess PITC is removed by evaporation, making it a suitable reagent for this analysis [87]. ESTD, ISTD and supplementary ESTD and ISTD is listed in Appendix E.3.1.

**96-well plate preparation:**

1. Prepared ESTD dilution series from 2.5 mM ESTD-mix stock and the supplementary ESTD (10 mM) to 300, 150, 75, 50, 25, 5, 0.5, 0.05 µM.
2. 10 µl of the complete $^{13}C^{15}N$ ISTD-mix was added to all wells of the well plate (Waters 350 µl), with exception of the blank well (position A1).
3. 200 µl of each ESTD was pipetted to their allocated wells (8 different concentrations), and a quality control (e.g. 25 µM ESTD) was included for every 20th sample.
4. 200 µL of the metabolite extract was transferred to their allocated wells. The blank well was empty at this point. All samples were kept on ice, to prevent potential enzymatic degradation.
5. Speedvacced plate for 1.5 h at 60°C, 4 Torr (plate without cover mat).

**Derivatization procedure:**

1. The derivatization solution was prepared for immediately use: (volume for one plate) Pre-mixed 1900 µl EtOH, 1900 µl $H_2O$, and 1900 µl pyridine (vortex about

10 sec). 300 µl of fresh PITC was added to the pre-mix (vortex until the solution is clear. The stability of the solution is reduced after adding PITC to the pre-mix).

2. 50 µl derivatization solution was pipetted to each well.
3. The well-plate was shaken carefully for 30 sec to include metabolites covered on the walls.
4. The well-plate was left in room temperature for 20 min to complete reaction.
5. Speedvacced plate for 1.5 h at 45°C, 4 Torr (plate without lid).
6. Extraction solvent was prepared in a volumetric flask: 5 mM ammonium acetate in 50:50 MeOH:H2O (v/v) was dissolved in a solution of 19 mg ammonium acetate in 50 mL 50:50 HPLC grade $H_2O$:MeOH (v/v).
7. Added 300 µl extraction solvent to each well.
8. The plate was covered with a plastic mat and shaken for 30 min at 400 rpm.
9. The plate was centrifuged using Speedvac (no temperature, turned off pump and cool trap) for 5 min, to ensure sedimentation of potential particles.
10. 100 µl transferred to a new well plate (700 µl) before analyzed by LC-MS.

#### 3.2.6.3 Organic acids analysis

Analysis of organic acids was performed in collaboration with Silje Malene Olsen. The method was adapted from Tan *et al.* [88], with LC-MS settings as shown in Appendix E.3.2. The purpose of the analysis is to investigate low molecular weight (LMW) organic acids (OA) from freeze-dried metabolite extracts. LMW OA were quantified by LC-MS with applied electrospray ionization in positive mode. A derivatization step was included prior to the chromatographic separation step. The derivatization links hydrophobic molecules to the organic acids, and their affinity to the hydrophobic column increases [88]. Ortho-benzylhydroxylamine (o-BHA) and N-(3-Dimethylaminopropyl)-N-ethylcarbodimide hydrochloride (EDAC) cause oxime formation in molecules with a keto group. The derivatization was carried out in 96-well plate format [89].

**96-well plate preparation:**

1. 80 µM ESTD-mix of Cit, Icit, Fum, Suc, Mal, 2HG, aKG, Lac, Pyr, OAA, Glx, and IA, was used to prepare a dilution series of 40, 20, 10, 5, 2.5, 1.25, 0.625, 0.3125, 0.1562 µM with MQ-water.

2. 10 µl of ISTD extract was added to each well of the well-plate. Blank samples were added between ESTD and samples, and were not added ISTD.
3. 10 µl of ISTD ($^{13}$C-mix of Lac and Pyr; 100 µM) was added to the same wells.
4. 80 µl of ESTD dilution was transferred to their allocated wells.
5. 80 µl of metabolite extract was added to their allocated wells.

**Derivatization procedure:**

1. 675 µl HCL (12M) was mixed with 1.1 ml pyridine and 11 ml MQ-water in the fume hood to create the o-BHA/EDAC solvent.
2. 1M o-BHA and 1M EDAC were created by dissolving 160 mg/ml (o-BHA) and 196 mg/ml (EDAC) the required volume of o-BHA/EDAC solvent (1).
3. 50 µl of o-BHA was added to each well, followed by 50 µl of EDAC (PS! important to add o-BHA first).
4. The well-plate (covered with a mat) was left shaking at room temperature for 1h.
5. 300 µl ethyl acetate was added to each well, and the plate was shaken for 10 min at room temperature.
6. 100 µl of the top-layer was transferred from each well to a new 96-well plate (700 µl).
7. The new plate was run in the Speedvac at 4 Torr, 60° for 1h to remove ethyl acetate. (Dried well-plates can be stored over night at -80° if covered with a mat).
8. All samples and ESTD were re-dissolved in 50 µl HPLC-water:MeOH (1:1, v/v) and shaken for 5 min. (Blank samples were filled with 500 µl HPLC-water:MeOH (1:1, v/v)).
9. The samples were analyzed with LC-MS and the settings listed in Appendix E.3.2.

#### 3.2.6.4 NADs and CoAs metabolite analysis

Profiling of NADs and CoAs metabolites were performed to supplement the mapping of intracellular metabolites involved in lipid accumulation of *Aurantiochytrium* sp. T66. This protocol is under development at NTNU, and was only tested for shake-flask cultivations during this work. The extraction procedure is very sensitive, and the optimal extraction procedure for each biological system needs to be established. The analysis

was not performed for bioreactor cultivations, but for a shake-flask cultivation with the focus of comparing growth and lipid accumulation. The following protocol was used, and the two extraction methods are described in 3a and 3b. The latter showed the best extraction for the biological system of *Aurantiochytrium*, and the results from this extraction method is included in the Results and Discussion 4.1.5.

1. 10 ml and 1 ml whole-culture were centrifuged at 5000 rpm for 60 sec.
2. The supernatant was discarded, and the samples were quick-freezed in liquid $N_2$, and stored at -80°C.
3. The samples were thawed on ice, and were tested by two different extraction methods:
   (a) The first extraction method was an established protocol for other biological model systems (*E.Coli*, *Streptomyces* and human cells [70]). The cells were boiled in ACN:$H_2O$ (90:10,v:v) pH 7 (pH adjusted by $NH_4OH$ at 80°C for 3 minutes using a shaking heater. The cells were centrifuged down (5000 rpm, 2 min) and the supernatant was transferred to vials for UPLC analysis.
   (b) The second extraction method was beating with Precellys homogenizator at 5500 rpm for two times 30 sec, with a 10 sec pause inbetween. The precellys 24 was equipped with temperature control Cryolys, Precellys tubes (2 ml), zirconium oxide beads with diameter 1.4 mm (all Bertin Technologies). The supernatant was transferred to vials for UPLC analysis after centrifugation at 5000 rpm for 2 min.
4. The samples were analyzed with UPLC-TQS with the settings described in Appendix E.5.

## 3.3 $^{13}$C-labeled glucose substrates in shake-flasks cultures

Utilization of $^{13}$C-labeled glucose substrates was performed to map the carbon flux through core metabolism, and to distinguish the flow-distribution between the different metabolic branch points. Three different $^{13}$C-labeled glucose substrates were used; 1-$^{13}C_1$-glucose, 1,2-$^{13}C_2$-glucose, and U-$^{13}C_6$-glucose. The substrates contain different numbers of $^{13}$C-labeled carbons, and can therefore support understanding of flow ditribution through glycolysis, the pentose phosphate pathway, TCA-cycle and into fatty acid synthesis. Fatty acid integration into neutral (NL) and polar lipids (PL) were investigated by SPE separation of the lipids.

Two 250 ml shake flasks (SF) (containing 50 ml of medium described in Table 3.1) were inoculated with 1 ml *Aurantiochytrium* sp. T66 cells from cryogenic preserved ampules. The SF was kept at 200 rpm and 28°C. The OD was measured for both SFs to monitor growth. 1.25 ml was collected at OD 8.0 (exponential growth phase), centrifuged at 4000 rpm for 1 min, and resuspended in 5 ml of fresh medium from each SF and added to six new SFs (50 ml liquid volume), with media composition described in Table 3.4.

TABLE 3.4: Medium composition used for shake-flask cultivations during the $^{13}$C-glucose analysis of *Aurantiochytrium* sp. T66. 100 µl of TMS-6 and vitamin mix was also added, see Appendix A.2 and A.1.*Natural glucose and $^{13}$C-labeled glucose were used (see Figure 3.3.

| **Component** | **(g/l)** |
|---|---|
| Glucose* | 10.0 |
| Yeast extract | 0.20 |
| Na-glutamate·$H_2O$ | 2.0 |
| $MgSO_4 \cdot 7H_2O$ | 0.24 |
| $Na_2SO_4$ | 3.60 |
| KCl | 0.08 |
| $CaCl_2 \cdot 2H_2O$ | 0.10 |
| $KH_2PO_4$ | 0.40 |

Figure 3.3 shows the six SFs with their correspondingly added glucose substrate.

The three first SFs were used as control shake-flask, only containing natural glucose. The different analysis methods performed for each SF are listed in Table 3.5. SF-1 was used for OD, DCW, SPE (with FAs), and consumption of glucose and glutamate (CC). SF-2 was used for intracellular metabolites (IM), and SPE (with FAs). SF-3 was used for establishing a OD-curve, and for profiling of NADs and CoAs, where two volumes and extraction protocols were tested. SF-1-$^{13}C_1$, SF-1,2-$^{13}C_2$ and SF-U-$^{13}C_6$, containing $^{13}$C-labeled glucose substrates, were used for profiling of intracellular metabolites (IM), and SPE (with FAs). The final glucose and glutamate concentration (FCC) and total

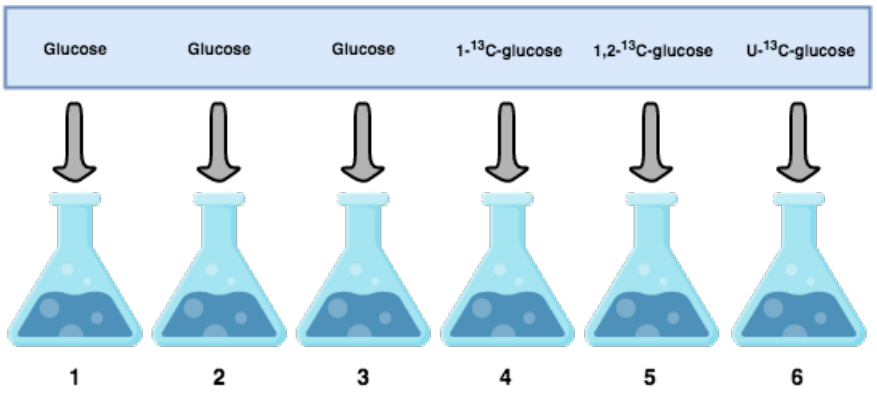


FIGURE 3.3: Shake-flasks (SF) with $^{13}$C-labeled glucose and natural glucose. SF 1-3 use natural glucose, while the remaining SFs were added different $^{13}$C-labeled glucose substrates.

lipids (TL) at the end of the experiment were measured for all SFs except SF-3. SF-1-$^{13}C_1$ contain glucose with $^{13}$C in $C_1$, SF-1,2-$^{13}C_2$ with glucose with $^{13}$C in position $C_1$ and $C_2$, and SF-U-$^{13}C_6$ with fully labeled glucose.

The shake-flasks were analyzed with equivalent methods as for the bioreactor cultivation. The following Table 3.5 shows the different analyses performed for the shake-flask cultures.

TABLE 3.5: Summarized analysis of each shake-flask (SF) cultivation. The glucose substrates for each SF is shown in Figure 3.3. The independent methods are described earlier during this chapter (Materials and Methods). Abbreviations: Intracellular metabolites (IM), solid phase extraction (SPE) and analysis of fatty acids (FAs), total lipids (TL), consumption of glucose and glutamate (CC), and final concentration of glucose and glutamate (FCC).

| **Shake flask** | **Analysis** |
|---|---|
| SF-1 | OD, DCW, CC, TL, and SPE with FAs |
| SF-2 | IM, TL, and SPE with FAs |
| SF-3 | OD, and profiling of NADs and CoAs |
| SF-1-$^{13}$C | IM, TL, FCC, and SPE with FAs |
| SF-1,2-$^{13}$C | IM, TL, FCC, and SPE with FAs |
| SF-U-$^{13}$C | IM, Tl, FCC, and SPE with FAs |

# 4

# Results and discussion

*Aurantiochytrium* sp. strain T66 cultivations were performed in shake-flasks and a bench-top bioreactor, to broaden the understanding of differences associated with growth, the lipid accumulation phase, and the transition between these phases.

Qualitative observations of strain T66 was performed throughout the entire work, to confirm culture purity, investigate the life-cycle, and to establish robust inoculum protocols.

Changes associated with lipid composition, fatty acid profiles, and metabolite concentrations, were investigated for both the bioreactor culture and in shake-flask cultivations.

A pilot study of shake-flask cultivations, with and without $^{13}$C-labeled glucose substrates, was performed to distinguish labeling patterns and central branch points for lipid biosynthesis, and to verify if shake-flasks is a proportionate model-system to $^{13}$C-label experiments in bioreactors.

## 4.1 Bioreactor cultivation of *Aurantiochytrium* sp. T66

Three distinct phases where identified during the cultivation of *Aurantiochytrium* sp. T66. The three phases were 1) lag phase, 2) growth phase and 3) lipid accumulation phase, and they are shown in Figure 4.1.

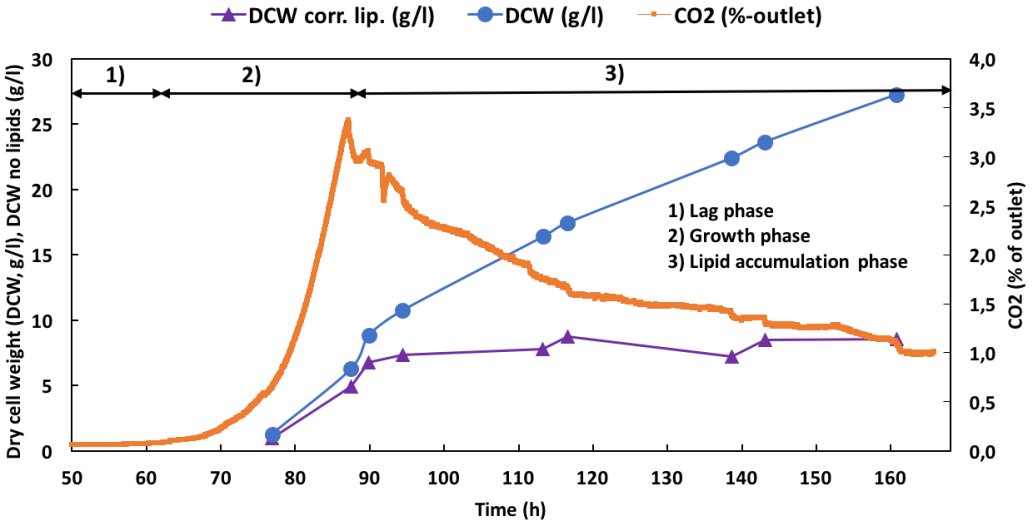


FIGURE 4.1: The three phases of *Aurantiochytrium* sp. strain T66, with evolution of cell dry weight (DCW, blue), DCW corrected for lipid content (DCW corr. lip, purple) and $CO_2$ (% of outlet gas, orange) for the bioreactor cultivation with glucose and glutamate as carbon sources. The lag phase lasted from 0-60 hours, but is only shown from 50-60h in the figure.

The lag phase lasted for around 60h, where a large content of zoospores was observed under the microscope. Earlier reported results, suggest that a normal lag phase lasts for about 20h [12], [16]. Maturation from zoospores to vegetative cells could be the reason for the extended lag phase. The produced $CO_2$ increased rapidly from 70-87h. The exponential growth phase ends at 87h, where glutamate (both N- and C-source) was depleted. However, smaller amounts of N was still present intracellularly as $NH_4^+$ until N-exhaustion occured at 92h, showing the characteristic drop in evolved $CO_2$. This rapid decline of produced $CO_2$ is shown more closely in Figure 4.2, a zoom of Figure 4.1. The depletion of N, with excess carbon source present, trigger the third phase; the lipid accumulation phase. Lipid synthesis occurs during the growth phase, but is controlled by requirements for cellular division (cell membrane and essential fatty acids), whereas the lipid accumulation phase is characterized by generation of only intracellular lipids, for energy storage.

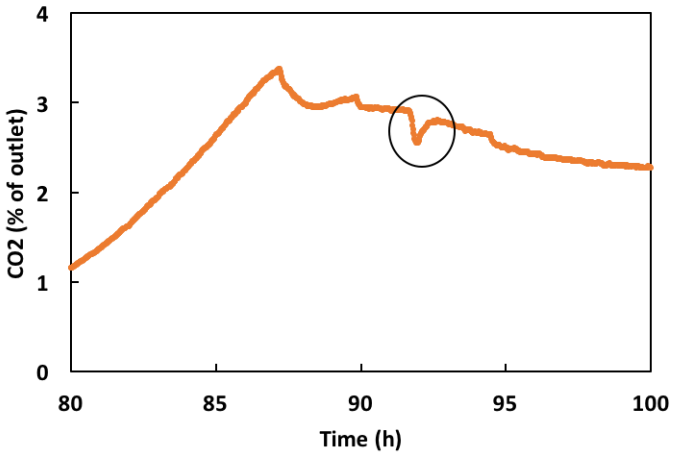


FIGURE 4.2: Carbon evolutionary rate (% of outlet gas) with the characteristic drop in $CO_2$ as a consequence of N-depletion at 92h (black circle). Selected interval of data shown in Figure 4.1.

The dry cell weight (DCW) increased to 8.8 g/l before the N-exhaustion at 92h. The increase of DCW during the lipid accumulation phase is assumed to be solely generation of intracellular lipids. DCW corrected for measured total lipids (3.2.3) was calculated, and is shown in Figure 4.1. DCW corrected for lipid content increases rapidly during the growth phase, before stabilizing at around 8 g/l during the entire lipid accumulation phase. This result demonstrates that the DCW increases because of lipid synthesis after N-depletion.

The oxygen uptake rate (OUR) shown in Figure 4.3, shows the same development as the carbon evolutionary rate in Figure 4.1. The noise associated with sample extraction is not removed, and the OUR values deviate from the general trend at these points.

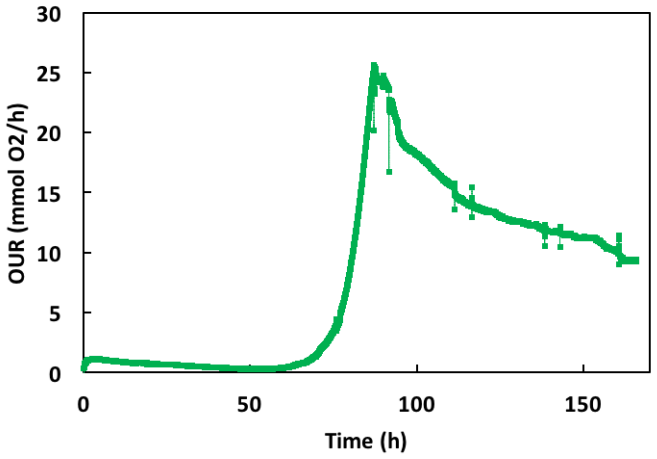


FIGURE 4.3: Oxygen uptake rate (OUR) for the bioreactor culture of *Aurantiochytrium* sp. strain T66, with glucose and glutamate as carbon sources.

The respiratory quotient (RQ) for the bench-top bioreactor is shown in Figure 4.4. The Respiratory quotient fluctuates during the lag phase, increases considerably during the growth phase, and stabilizes in the lipid accumulation phase. Cellular growth demands large amounts of energy - leading to high degree of respiration. RQ increased from 0.6 to 1.1 during the exponential growth phase, and stabilizes around 1.2 after N-exhaustion. The OUR decreases with the same trend as the carbon evolution rate (CER), yielding a stable RQ for the lipid accumulation phase.

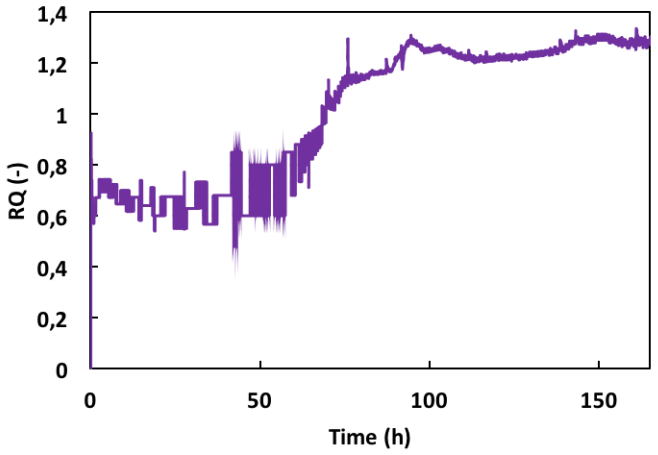


FIGURE 4.4: Respiratory quotient (RQ) for the bioreactor culture of *Aurantiochytrium* sp. strain T66, with glucose and glutamate as carbon sources.

Summarized data from the bioreactor cultivation is listed in Table 4.1. The specific growth rate ($\mu$) develops during the growth phase, starting at 0.12 $h^{-1}$ from 65-77h, reaching $\mu_{max}$ between 77-90h. $\mu_{max}$ reported here was 0.15 $h^{-1}$, and is very similar to previous results on the same strain [16], [22]. The specific growth rate is directly linked to increase in cellular numbers, and is therefore not included for the lipid accumulation phase, where all increase in DCW is assumed to be intracellular lipids.

TABLE 4.1: Selected data from the bioreactor culture of *Aurantiochytrium* sp. T66 grown on glucose (glc) and glutamate (glu) as carbon sources. Glu is also the main N-source. Dry cell weight (DCW), DCW corrected for lipid content (corr. lip., g/l), total lipids (TL, %w/w of DCW), and specific growth rate (μ). Spaces with (-) are not calculated because specific growth rate is associated with cellular division.

| **Sample nr.** | **Time (h)** | **DCW (g/l)** | **DCW corr. lip. (g/l)** | **TL (%w/w)** | μ **($h^{-1}$)** |
|---|---|---|---|---|---|
| 1 | 76.9 | 1.3 | 1.0 | 23 | 0.12 |
| 2 | 87.5 | 6.3 | 4.9 | 22 | 0.15 |
| 3 | 89.9 | 8.8 | 6.8 | 23 | 0.14 |
| 4 | 94.4 | 10.7 | 7.3 | 32 | - |
| 5 | 113.3 | 16.4 | 7.8 | 53 | - |
| 6 | 116.6 | 17.4 | 8.7 | 50 | - |
| 7 | 138.6 | 22.4 | 7.2 | 68 | - |
| 8 | 143.1 | 23.6 | 8.5 | 64 | - |
| 9 | 160.8 | 27.3 | 8.5 | 69 | - |

### 4.1.1 Utilization and consumption of carbon sources during the bioreactor cultivation

Figure 4.5 shows the changes in concentration of carbon sources (glutamate and glucose), evolution of $CO_2$ (% of outlet), and dry cell weight (DCW) for the bioreactor cultivation of *Aurantiochytrium* sp. strain T66. Glutamate contains a carbon backbone and amine groups; providing both N and C. The largest volumetric consumption rate of glucose is displayed during the transition between the growth phase and sole lipid synthesis, from 89.9-94.4h. This could be explained by the need of carbon for increased lipid biosynthesis, carbon for protein-turnover, and substitution of the carbon from limited glutamate resources. A constant decrease of available glucose was observed during the lipid accumulation phase, suggesting that the carbon flow towards lipid synthesis reached the maximal rate and that the enzymatic machinery ran by full capacity.

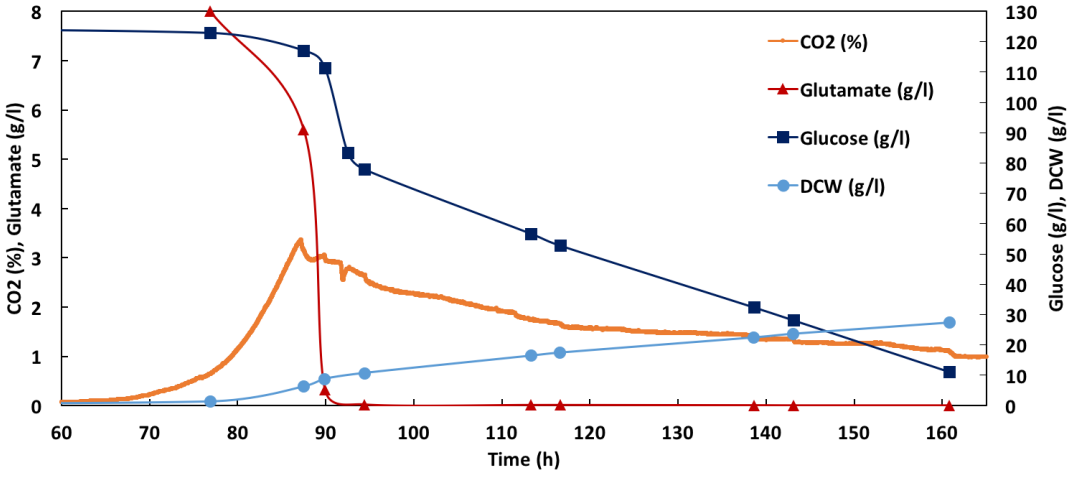


FIGURE 4.5: Change in carbon source content, glucose (dark blue) and glutamate (red), for the bioreactor cultivation of *Aurantiochytrium* sp. strain T66. Dry cell weight (light blue) and $CO_2$ evolution (% of outlet gas) are also shown. The three first measurements of glucose (g/l) is adjusted for addition at 92 hours (shown in Table 3.2).

The large glucose consumption displayed in the transition between growth and the lipid accumulation phase (92-94h), show that the cells have a much larger uptake rate of glucose than observed during the lipid accumulation. This suggests that the lipid synthesis is limited by other factors than glucose uptake. One possible explanation could be the enzymatic conversion rate of acetyl-CoA carboxylase (ACC), producing malonyl-CoA for lipid biosynthesis.

The consumption of glucose and glutamate, with the yield coefficient of biomass from glucose is shown in Table 4.2.

TABLE 4.2: Carbon source consumption of glucose (glc) and glutamate (glu), $r_{glc}$ and $r_{glu}$ with measured dry cell weight (DCW) and measured carbon source concentrations (3.2.2). The yield coefficient ($Y_{xs}$) of gram biomass (x) per gram of carbon source (s). Glucose is the sole carbon source during the lipid accumulation phase (94.4-160.8h). The concentrations of glucose are adjusted to the addition at 92h (shown in Table 3.2).

| **Time (h)** | **DCW (g/l)** | **Glucose (g/l)** | **$r_{glc}$ (g/l·h)** | **Glutamate (g/l)** | **$r_{glu}$ (g/l·h)** | $Y_{xs}$ ($\frac{\text{g DCW}}{\text{g C-source}}$) |
|---|---|---|---|---|---|---|
| 0 | 0.3 | 125 | - | 8.0 | - | - |
| 76.9 | 1.3 | 122.9 | 0.03 | 5.6 | 0.03 | 0.22 |
| 87.5 | 6.3 | 117.1 | 0.55 | 0.33 | 0.50 | 0.45 |
| 89.9 | 8.8 | 111.3 | 2.42 | 0.03 | 0.13 | 0.41 |
| 92 | - | 83.4 | Addition[1] | - | - | |
| 94.4 | 10.7 | 77.9 | 2.89 | 0.01 | 0.00 | 0.25 |
| 113.3 | 16.4 | 56.7 | 1.12 | 0.01 | 0.00 | 0.27 |
| 116.6 | 17.4 | 52.8 | 1.18 | 0.01 | 0.00 | 0.26 |
| 138.6 | 22.4 | 32.4 | 0.93 | 0.00 | 0.00 | 0.25 |
| 143.1 | 23.6 | 28.2 | 0.95 | 0.00 | 0.00 | 0.28 |
| 160.8 | 27.3 | 11.1 | 0.96 | 0.00 | 0.00 | 0.22 |

[1] Addition of more glucose

The largest volumetric consumption rate of glutamate was observed during the exponential growth phase (76.9-87.5h), showing a consumption rate of 0.50 g/l·h. The glutamate concentration ranged from 0.33-0.03 during the late exponential growth phase. The consumption rate of glucose is similar to the glutamate during the lag phase and early growth phase (0-76.9h), as well as during the early exponential growth phase (76.9-87.5h). The glucose consumption rate increased by a fourfold from 87.5-89.9h. $r_{glu}$ remained above 2.5 g/l·h until all N-source is spent ([glutamate] < 0.01). At this point, the lipid accumulation phase is initiated, and the consumption rate of glucose stabilizes around 1 g/l·h.

The biomass yield from carbon source ($Y_{xs}$), is assumed to be all intracellular lipids during the lipid accumulation phase (94.4-160.8h), and was quite steady throughout this phase, ranging from 0.22-0.28 g lipids/g glc. The biomass yield was higher during the exponential growth phase, which could be explained by the considerably higher degree of reduction ($\gamma$) of lipids compared to new biomass.

### 4.1.2 Lipid and fatty acid profile of *Aurantiochytrium* sp. T66 from heterotrophic bioreactor cultivation

The lipid composition changed during the cultivation, showing distinct differences between the growth phase, the lipid accumulation phase, and the transition between them. This section describes several aspects related to the lipid distribution, and fatty acid composition of *Aurantiochytrium* sp. strain T66.

A principal component analysis (PCA) plot was generated with data provided by high-resolution lipid analysis from UPC$^2$-MS. This was performed to establish an understanding of the changes in intracellular lipids as the bioreactor cultivation proceeded. Two parallels, of the nine samples (76.9-160.8h), was analyzed by UPC$^2$-MS. The first and second principal component (PC) for the total lipid data are shown in Figure 4.6. The two PCs collectively make up 75% of the total variance. From the PCA-plot, a trend of change can be observed as the cultivation proceeds. The four first samples (76.6-94.4h) show large degrees of variance, which could be explained by the changes of intracellular lipids from the exponential growth phase, through N-limitation, and into the lipid accumulation phase. A clear time-dependent trend was observed for the last five samples (113.3-160.8h), as they cluster together. The clustering demonstrates little variance between the samples, which indicates similar lipid profiles, suggesting that the production of fatty acids is analogous during this time interval.

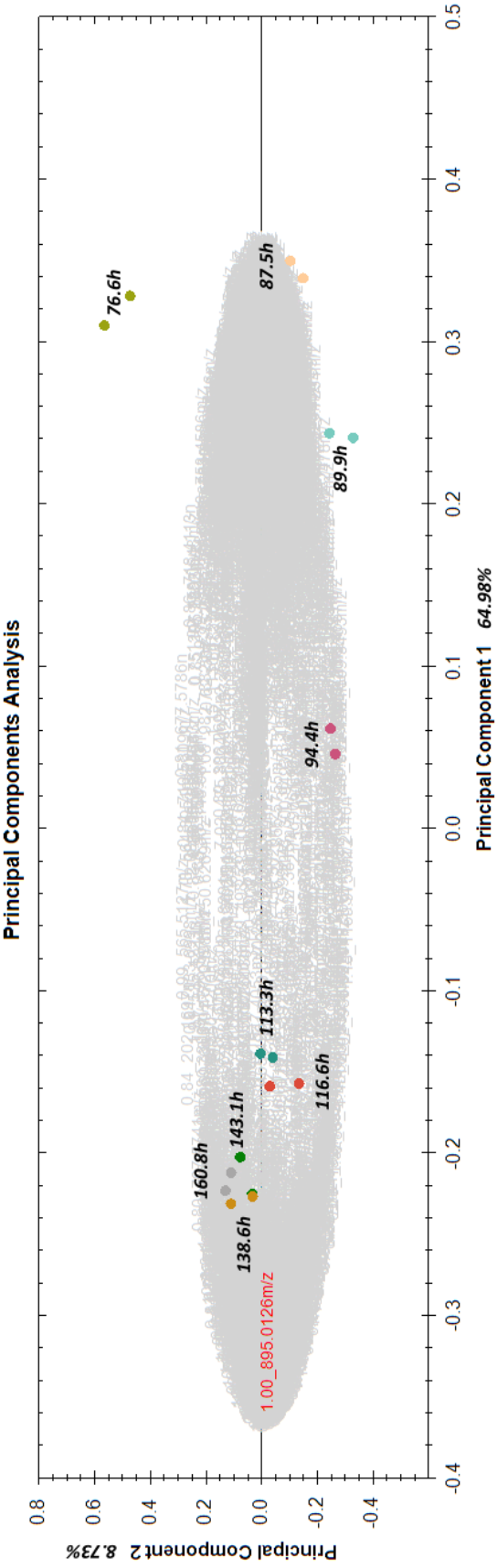


FIGURE 4.6: Principal component analysis (PCA) plot of lipid samples extracted by the Bligh and Dyer method (3.2.3) and analyzed with UPC$^2$-MS based on a lipid profiling method. Two parallels of each sample was tested. List of last five samples (color): 113.3h (turquoise), 116.6h (red), 138.6h (yellowish), 143.1h (green) and 160.8h (grey).

#### 4.1.2.1 Lipid profile and distribution of lipid classes

The total lipids (TL) and total fatty acids (TFA) were measured by Bligh and Dyer (3.2.3) and LC-MS (3.2.4), respectively. Both the TL and the TFA concentration increased with the proceeding cultivation, and they are shown in Figure 4.7. The TL content remained stable during the exponential growth phase (76.9-89.9h), suggesting that the lipid synthesis is regulated to only produce the required lipids for generation of new cells. TL increased rapidly from 20 to 30%w/w after N-limitation, demonstrating that the cells accumulate lipids from excess carbon source during N-starvation. During the lipid accumulation phase, the TL increased from 30-70%w/w. The increase was steady during the this phase, suggesting a constant lipid production rate. TL stabilized at around 70%w/w of DCW, which could suggest that a threshold value for intracellular lipids was reached.

The total fatty acids (TFA) increased steadily throughout the entire cultivation. TFA (of DCW) maintained at around 45% after the lipid accumulation phase was initiated. TFA (g/l) was higher than TL (g/l) during the growth phase, which suggest some analytic error. TFA normally constitute 80-90% of TL [60], whereas TFA decreased from 80% of TL to 65% of TL during the lipid accumulation phase. Systematic errors, from the two analysis methods 3.2.3 and 3.2.4, could explain the deviation. The first data point of TFA (76.9h) is not included, because it showed a content of 145% of DCW.

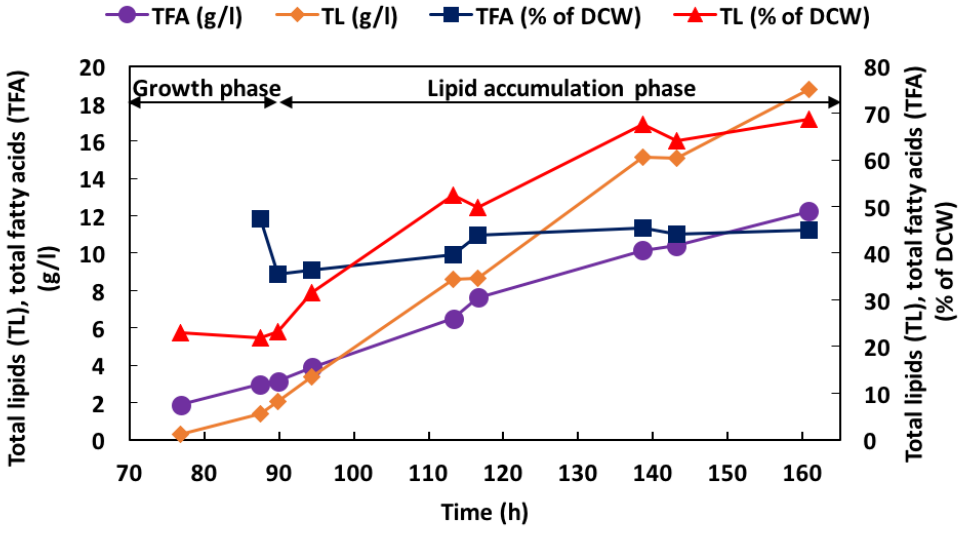


FIGURE 4.7: Change in total lipids (TL) and total fatty acids (TFA) during the bioreactor cultivation, given as (g/l) and % of dry cell weight (DCW). The first data point of TFA (76.9h) is not included (above 100% of DCW).

The TL content, analyzed with UPC$^2$-MS, showed a changing distribution of triacylglycerols (TAGs), diacylglycerols (DGs), monoacylglycerols (MGs), and polar lipids (PL),

during the growth and the lipid accumulation phase. Figure 4.8 shows the distribution of PL, MGs, DGs, and TAGs (% of TL). The TAGs constituted more than 70% of TL during the entire cultivation. The content increased from 80-90% during the late exponential phase. The TAGs stabilized at more than 90% from 113.3h and throughout the lipid accumulation phase, suggesting that the production of lipids was 90% TAGs during this phase. The PL, DGs, and MGs fractions (Figure 4.8 (b)) were higher during the cellular growth phase. The content of these lipids stabilized at 5%, 1% and <1% from 113.3-160.8h, respectively. This suggests that a certain level of these lipid classes is required for maintaining cellular functions, and that newly synthesized lipids were composed of 5%, 1% and 0-1% PL, DGs, and MGs.

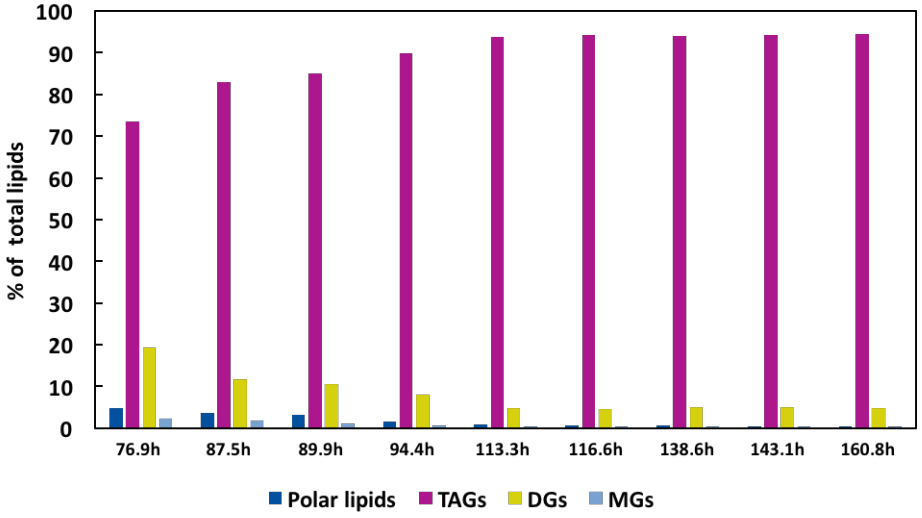


(a)

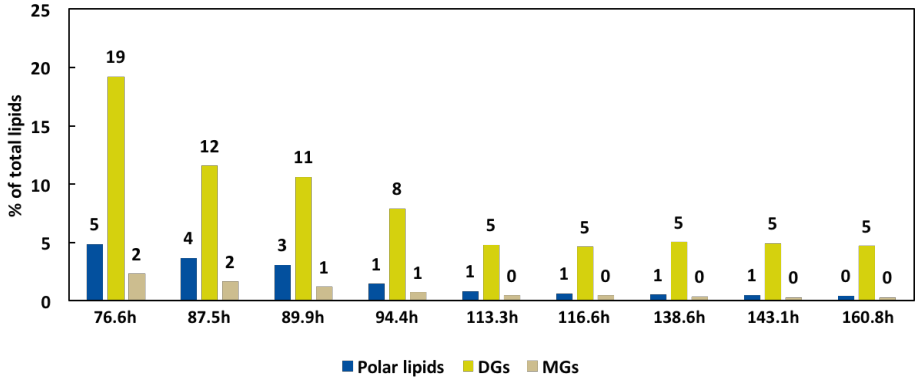


(b)

FIGURE 4.8: (a) Distribution of lipid classes of total lipids (% of TL). (b) is a zoom of (a), and shows distribution of polar lipids (PL), diacylglycerols (DGs), and monoacylglycerols (MGs) of total lipids (%).

Further results from UPC$^2$-MS demonstrated that the two most abundant TAGs were 16:0/22:6/22:6 and 16:0/16:0/22:6. Figure 4.9 shows that the abundance (millions, normalized on lipid content) of DHA-rich TAGs (TGs) was highest at 94.4h, about two hours after N-depletion. The abundance decreased slightly during the lipid accumulation phase. This data suggests that the lipid synthesis produces TAGs containing DHA throughout the cultivation, but distribution of DHA-rich TAGs decreased slightly as the lipid accumulation proceeds toward the proposed threshold value of about 70%w/w of DCW.

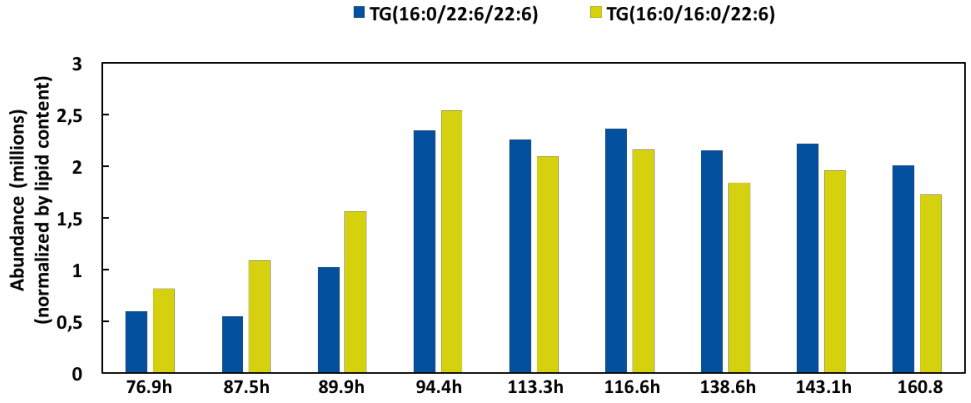


FIGURE 4.9: Relative abundance (millions) of DHA-rich triglycerols (16:0/22:6/22:6) and (16:0/16:0/22:6). DHA (22:6) and palmitic acid (16:0).

Figure 4.10 shows the abundance (thousands, normalized on lipid content) of DHA-rich DG, MG, and glycerolphosphocholine (GPCho).

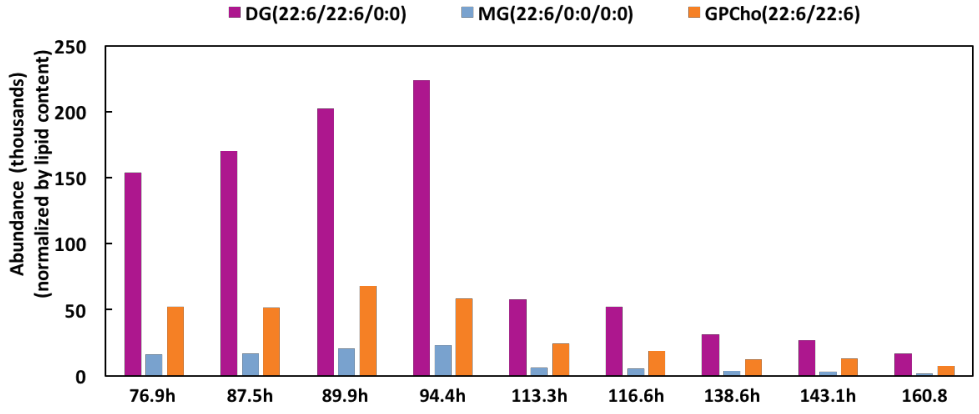


FIGURE 4.10: Relative abundance (thousands) of DHA-rich diglycerol (DG, 22:6/22:6/0:0), monoglycerol (MG, 22:6/0:0/0:0) and glycerophosphocholine (GPCho, 22:6/22:6).

The DHA-rich DGs, MGs and GPCho, increased during the growth phase (76.9-89.9h), before showing a considerable decline from 94.4h to 113.3h. The decline continued until

the cultivation was ended. The increase of DG (22:6/22:6/0:0) after N-limitation (89.9-94.4h), could suggest that some MGs were converted to DGs, by incorporation of newly synthesized DHA (C22:6) or other FAs to create DGs. The large decline of these lipid classes during the lipid accumulation phase, could be explained by conversion to TAGs and reduced biosynthesis of these lipids.

#### 4.1.2.2 Fatty acid profile of the bioreactor culture

The fatty acid profile changed during the cultivation, showing a relative reduction of saturated FA (SFA), and elevated levels of monounsaturated FA (MUFA) and polyunsaturated FA (PUFA). Figure 4.11 shows the fractions of SFA, MUFA and PUFA (% of TFA) changing from growth and through the lipid accumulation phase. MUFAs and PUFAs constituted an increasing portion of the TFA. The MUFA fraction showed the largest relative increase (% of TFA) during the lipid accumulation phase, suggesting that the synthesis of MUFAs increased considerably after N-exhaustion.

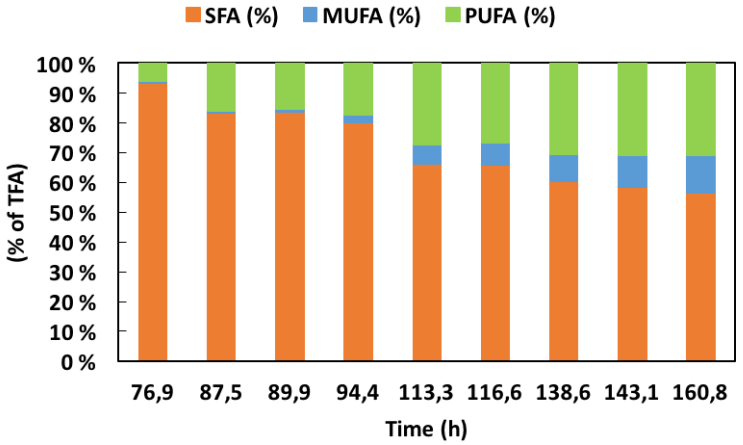


FIGURE 4.11: Fraction of saturated fatty acids (SFAs), monounsaturated fatty acids (MUFAs), and polyunsaturated fatty acids (PUFAs) of bioreactor cultivation of *Aurantiochytrium* sp. T66 with glucose and glutamate as carbon sources. Data from fatty acid analysis with LC-MS (data provided in Appendix B.1.1).

Table 4.3 shows the change in fatty acid concentrations (g/l) throughout the bioreactor cultivation. The data is summarized in Figure 4.12 as % of TFA, where FAs with an abundance lower than 0.5% are not included (all data shown in Table B.2). All FA concentrations, except stearic acid (C18:0), increased from 76.9-160.8h. The stearic acid concentration declined from 1.60 to 1.30 g/l from 138.6-143.1h. This result suggests that stearic acid was consumed during this interval. The fraction of MUFAs with a C18 backbone increased during the same time interval, which could explain the consumption of stearic acid.

TABLE 4.3: Fatty acid (FA) concentrations (g/l) for the bioreactor culture of *Aurantiochytrium* sp. strain T66. Heptadecenoic acid (C17:1) and linoleic acid (C18:2) are not included because the concentrations was measured below 0.002 g/l.

| FA | 76.9h | 87.5h | 89.9h | 94.4h | 113.3h | 116.6h | 138.6h | 143.1h | 160.8h |
|---|---|---|---|---|---|---|---|---|---|
| C14:0 | 0.04 | 0.12 | 0.13 | 0.24 | 0.65 | 0.82 | 1.11 | 1.24 | 1.52 |
| C15:0 | 0.01 | 0.01 | 0.01 | 0.01 | 0.02 | 0.02 | 0.03 | 0.03 | 0.04 |
| C16:0 | 0.71 | 1.06 | 1.08 | 1.37 | 2.20 | 2.67 | 3.36 | 3.50 | 4.02 |
| C16:1 | 0.00 | 0.01 | 0.01 | 0.06 | 0.26 | 0.35 | 0.57 | 0.69 | 0.98 |
| C17:0 | 0.01 | 0.02 | 0.02 | 0.02 | 0.02 | 0.02 | 0.02 | 0.02 | 0.02 |
| C18:0 | 0.97 | 1.28 | 1.38 | 1.47 | 1.40 | 1.50 | 1.60 | 1.29 | 1.32 |
| C18:1 | 0.02 | 0.02 | 0.02 | 0.05 | 0.18 | 0.22 | 0.36 | 0.41 | 0.55 |
| C20:5 | 0.00 | 0.01 | 0.01 | 0.01 | 0.02 | 0.03 | 0.04 | 0.05 | 0.05 |
| C22:5 | 0.03 | 0.11 | 0.10 | 0.18 | 0.48 | 0.61 | 0.87 | 0.95 | 1.11 |
| C22:6 | 0.08 | 0.35 | 0.37 | 0.48 | 1.26 | 1.40 | 2.20 | 2.22 | 2.65 |

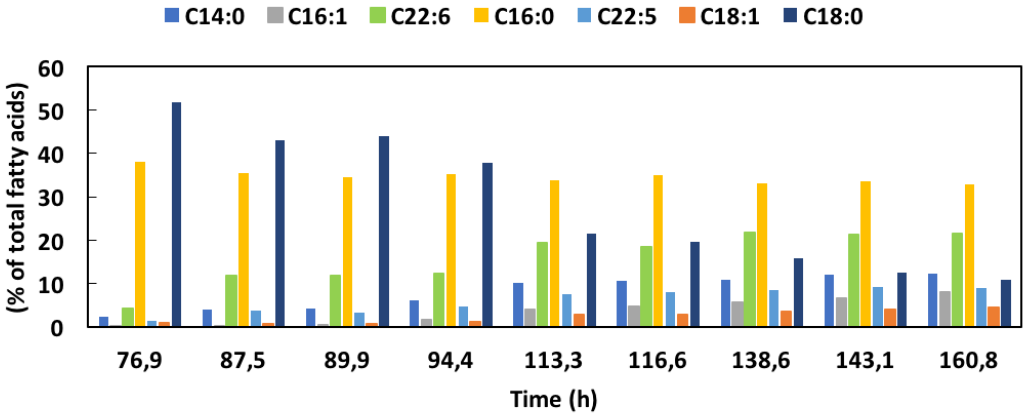


FIGURE 4.12: Fatty acid content (% of total fatty acids) of bioreactor cultivation of *Aurantiochytrium* sp. T66 with glucose and glutamate as C-sources. FAs with abundance lower than about 0.5%w/w of TFA are not included. Fatty acids not included: C15:0, C17:0, C17:1, C18:2, C20:5. Data given in Appendix B.1.1.

The myristic acid (C14:0) constituted a lower fraction of the total fatty acids during growth, compared to the lipid accumulation phase, where the content stabilized at around 10-12% of TFA. Palmitic acid (C16:0) remained quite stable at 1/3 of TFA during the whole cultivation. Stearic acid (C18:0, % of TFA) decreased throughout the entire cultivation, from 52 to 11%. The concentration of C18:0 increased, demonstrating that the synthesis of stearic acid occurred, but the synthesis of other fatty acids reduced the relative amount of C18:0. Increased flow through PKS relative to FAS could also explain the decreasing C18:0 fraction. Jakobsen *et al.* [16] observed a stearic acid (C18:0) level of 1-1.4% of TFA at the end of the cultivation, which suggests that the same trend could be observed for this culture if the cultivation was extended. The content of palmitoleic acid (C16:1) and oleic acid (C18:1), increased from below 1% to 8% and 4.5% of TFA during the lipid accumulation phase. The fractions of DHA (C22:6) and DPA (C22:5), increased from 4-22% and 1-9%w/w of TFA, respectively.

#### 4.1.2.3 DHA content and productivity of the bioreactor cultivation

DHA constituted the largest portion of the PUFAs, and was alone larger than the total concentration of MUFAs. DHA comprised 22% of TFA for the last three measurements, suggesting that PKS assembled at least 22% of newly synthesized FAs during this interval. Jakobsen *et al.* observed a DHA content of 29% of TFA for well-oxygenated *Aurantiochytrium* sp. strain T66, increasing to 50% of TFA for a $O_2$-limited bioreactor cultivation. Only minor fractions of MUFAs were produced during oxygen-limitation, because desaturases are $O_2$-dependent. The developing DHA concentration is shown in Figure 4.13, presenting a steadily increasing concentration.

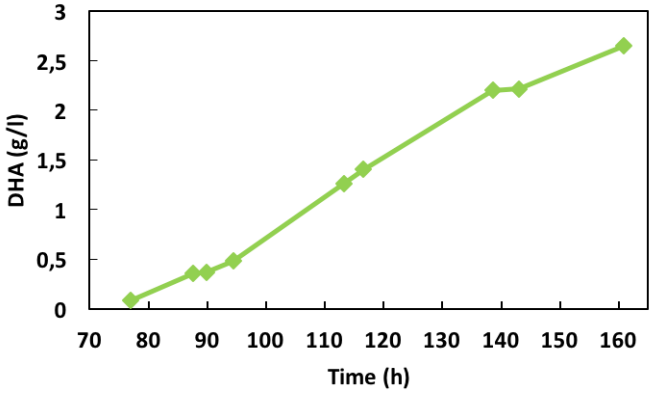


FIGURE 4.13: Docohexaenoic acid (DHA) content (% of total fatty acids) of the bioreactor cultivation of *Aurantiochytrium* sp. strain T66 with glucose and glutamate as carbon sources.

Table 4.4 shows the DHA productivity between the samplings from the bioreactor cultivation. Figure 4.13 demonstrated that the DHA productivity was highest during the lipid accumulation phase after 94.4-138.6h, with a productivity ranging between 24-28 mg/l·h. The productivity of the growth phase, and late lipid accumulation phase, was very similar. The reduced productivity from 143.1-160.8h could be explained by the proposed threshold value of about 70% TL of DCW. By comparing the productivity of the growth phase and the early lipid accumulation phase, it is evident that a two-fold increase of DHA productivity occured once the lipid synthesis phase was initiated.

TABLE 4.4: Volumetric productivity of decahexaenoic acid (DHA), $q_p$, for fermentation with *Aurantiochytrium* sp. T66. The volumetric productivity from inoculation to sample 1 (79.6h) is not listed

| **Time (h)** | **87.5** | **89.9** | **94.4** | **113.3** | **116.6** | **138.6** | **143.1** | **160.8** |
|---|---|---|---|---|---|---|---|---|
| $\mathbf{q_p}$ ($\frac{\mathbf{mg\ DHA}}{\mathbf{l \cdot h}}$) | 15.2 | 3.9 | 26.0 | 26.4 | 28.5 | 24.2 | 2.3 | 16.2 |

Table 4.5 shows reported overall volumetric productivities of DHA for a selection of thraustochytrid strains. Several productivities range well above 100 mg/l·h, with the best productivity of 203 mg/l·h for *Aurantiochytrium* sp. TC20, reported by Chang *et al.* [90]. The production of pigments and squalene of the *Aurantiochytrium* strain investigated here, could explain a lower DHA productivity, but Jakobsen *et al.* [16] investigated the same thraustochytrid strain, showing a possible productivity of 75 mg/l·h under the same conditions as presented during this work. The only difference between the work of Jakobsen *et al.* and this work, was the extended lag phase (from 20h to 60h), which reduced the overall productivity from 22 to 16 mg/l·h.

Table 4.5: Selected DHA producing thraustochytrids from litterature. *TFA equals the the stated % of DCW, because TL was not provided.

| **Thraustochytrids** | *S. limacinum* SR21 | *Aurantiochytrium* sp. T66 | *S. mangrovei* Sk-02 | *Traustochytrium* sp. ONC-T18 | *T. aureum* ATCC28210 | *Aurantiochytrium* sp. TC20 | *Schizochytrium* sp. KH105 | *Aurantiochytrium* sp. T66 |
|---|---|---|---|---|---|---|---|---|
| **Growth parameters** | | | | | | | | |
| Biomass (DCW, g/l) | 48 | 88 | 24 | 26 | 17 | 56 | 29 | 27 |
| TL (% of DCW) | 77 | 58 | 54 | up to 80 | 24 | 52* | 29* | 69 |
| DHA (% of TFA) | 36 | 29 | 40 | 25 | 49 | 48 | 35 | 22 |
| DHA in biomass (mg/g) | 276.5 | 155.7 | 229.2 | 173.1 | 117.0 | 249.6 | 114.8 | 96.3 |
| DHA yield (g/l) | 13.3 | 13.7 | 5.5 | 4.5 | 2.0 | 14.0 | 3.4 | 2.6 |
| DHA productivity (mg/l·h) | 138 | 75 | 115 | 63 | 7 | 203 | 35 | 16 |
| Reference | [39] | [16] | [91] | [59] | [92] | [90] | [93] | This study |

#### 4.1.2.4 Lipid yield on carbon source during the lipid accumulation phase

The maximal theoretical yield of TAGs from glucose, when all glucose is channeled to lipid TAG assembly, is 32%w/w (0.32 g lipid/g glucose) [54]. From the data provided in Table 4.6, an experimental yield during the lipid accumulation phase was calculated to equal 0.23 g lipid/g glucose, or 73% of theoretical lipid yield.

TABLE 4.6: The experimental yield (Exp. yield), lipid yield, $Y_{ls}$, from glucose during the lipid accumulation phase, and selected data for the calculations are shown. The theoretical lipid yield from glucose is 32%w/w (0.32 g lipid/g glucose) [54].

| **Time (h)** | **Glucose (S) (g/l)** | **Lipid (L) (g/l)** | **ΔS (g/l)** | **ΔL (g/l)** | **$Y_{ls}$ (g L/g S)** | **Exp. yield (%)** |
|---|---|---|---|---|---|---|
| 94.4 | 77.9 | 3.4 | 66.8 | 15.4 | 0.23 | 73 |
| 160.8 | 11.1 | 18.8 | | | | |

The theoretical yield of TAGs was computed by Ratledge [54] with the assumption that the fatty acids in the TAGs all have the length of C18:0 (stearic acid). This assumption does not reflect the true situation of thraustochytrids, because their fatty acid profiles show large variations. DHA (C22:6) and palmitic acid (C16:0), were the two most abundant FAs for *Aurantiochytrium* sp. strain T66. Strain T66 contained larger fractions of other SFAs, PUFAs, and MUFAs, as well. The variability in fatty acid composition will change the overall theoretical equation of lipid yield from glucose, because synthesis of shorter FAs, than C18:0, require less NADPH, and the longer FAs demand more NADPH for synthesis. These remarks could explain some of the deviation from the theoretical yield. Furthermore, there is still room for improvement considering the yield of lipids from glucose as carbon source.

### 4.1.3 Carbon balance of growth and lipid accumulation of bioreactor cultivation of *Aurantiochytrium* sp. T66

The carbon balance for the bioreactor cultivation was calculated for the growth phase (76.9-89.9h, Table 4.7) and the lipid accumulation phase (94.5-160.8h, Table 4.8). The cells consume glutamate, glucose, and yeast extract (YE) during the growth phase. YE is assumed to be exhausted during the exponential growth phase, and is therefore only included in the calculations of the growth phase. Furthermore, it is assumed that intracellular lipids are the only produced macromolecules during the lipid accumulation phase.

The recovery rate of carbon was calculated to equal 84% during the growth phase, and 77% during lipid synthesis phase. The results are presented in Table 4.7 and 4.8. Data used to calculate the carbon balances are shown in Appendix D.

TABLE 4.7: The carbon balance of the growth phase (76.9-89.9h) using the Black-Box-model. The carbon from the substrates is converted to carbon for biomass and to $CO_2$ during respiration. Data is listed in Appendix D.1.

**Growth phase**

| **In Glucose (mmol C/l·h)** | **In Glutamate (mmol C/l·h)** | **In Yeast extract (mmol C/l·h)** | **Out $CO_2$ (mmol C/l·h)** | **Out Biomass (mmol C/l·h)** | **Recovery (%)** |
|---|---|---|---|---|---|
| 30 | 15 | 3 | 16 | 24 | 84 |

TABLE 4.8: The carbon balance of the lipid accumulation phase (94.4-160.8h) using the Black-Box-model. Assumed only lipid accumulation, and no cellular division. The carbon from the substrate is converted to carbon in lipids and to $CO_2$ during respiration. Data is listed in Appendix D.2.

**Lipid accumulation phase**

| **In (mmol C/l·h)** | **Out as $CO_2$ (mmol C/l·h)** | **Out as lipid (mmol C/l·h)** | **Recovery (%)** |
|---|---|---|---|
| 34 | 14 | 12 | 77 |

### 4.1.4 Profiling of intracellular metabolites of bioreactor cultivation of *Aurantiochytrium* sp. T66

Several metabolome groups were measured during this MSc thesis. Phosphometabolome, organic acids, amino acids, NADs, and CoAs, were analyzed by different chromatographic and mass spectrometric methods. During earlier work (TBT4505 Specialization Project, Tronsaune [22]), non-optimized sample protocol resulted in energy charges (EC) below 0.2. The energy charges of the bioreactor cultivation of *Aurantiochytrium* sp. T66 performed during the MSc thesis, show a quite different progression (Table 4.9). The energy charge of highly metabolic active cells normally range from 0.8-0.95 [70].

TABLE 4.9: Concentrations of ATP, ADP and AMP for the metabolite samples. The energy charge (EC) is calculated by equation 2.1.

| **Time (h)** | **76.6** | **87.5** | **89.9** | **94.4** | **113.3** | **116.6** | **138.6** | **143.1** | **160.8** |
|---|---|---|---|---|---|---|---|---|---|
| AMP (µM) | 1441 | 514 | 761 | 420 | 648 | 120 | 420 | 143 | 1013 |
| ADP (µM) | 2306 | 740 | 748 | 640 | 478 | 334 | 530 | 381 | 542 |
| ATP (µM) | 2232 | 1849 | 1941 | 1791 | 911 | 1483 | 1418 | 1495 | 683 |
| **EC** | 0.57 | 0.72 | 0.67 | 0.74 | 0.56 | 0.85 | 0.71 | 0.83 | 0.43 |

Several of the measurements lie close to 0.8-0.95, suggesting that the updated sampling protocol provide good results within the experimental margins. The obtained data could therefore be trusted to some extent, mirroring the true situation.

#### 4.1.4.1 Profiling of intracellular phosphometabolites, organic acids and amino acids

All data was normalized on dry cell weight corrected for total lipid content, because the amount of metabolites depend on active biomass [70] (data for normalized dry cell weight corrected for total lipids, was shown in Table 4.1). Selected phosphometabolites, organic acids, and amino acids were quantified by CapIC-MS. Figure 4.14 and Figure 4.15 summarize the metabolic profiles of sampling 3 (89.9h) and 6 (116.6h), compared to sample 1 (76.9h). Sample 9 (160.8h) was similarly compared to sample 3 (89.9h) and sample 6 (116.6h), to investigate the differences between samples of the growth phase and the lipid accumulation phase. Sample 9 compared to sample 3 (89.9h) and sample 6 (116.6h), is shown in Figure 4.16 and 4.17.

All values are represented as log 2 values, where the each metabolite concentration is divided by the same metabolite concentration of the reference sample, and standardized to log 2 values (e.g. the log 2 value of ATP in sample 3 relative to sample 1; divided

ATP concentration of sample 3 by sample 1, and the binary logarithm was used to standardize). The log 2 values were differentiated by color-coding shown below in all figures. Green coloring represents higher concentration, white comparable concentrations, and red coloring lower concentration. Data represented by dark grey coloring was not analyzed, and light grey metabolites had concentrations below detection. The metabolite profiles were generated with OMIX (Omix Visualization GmbH & Co. product).

The first metabolite profile, shown in Figure 4.14, shows the changes of sample 3 (89.9h) to sample 1 (76.9h) of the growth phase. Fructose-1,6-biphosphate (F16BP) and dihydroxyacetone phosphate (DHAP) of the glycolysis was observed with increasing concentrations from sample 1 to sample 3. Glyceraldehyde-3-phosphate (3PG) and glyceraldehyde-2-phosphate (2PG) displayed similar concentrations, while the PEP and pyruvate (Pyr) concentrations were reduced. The concentration of glutamate (nitrogen source) was reduced from 5.6-0.03 g/l from 76.9-89.9h, influencing the metabolic activity of the thraustochytrids, which could explain the reduced amino acid concentrations. Furthermore, the limitation of N reduces cellular division and the generation of energy is weakened, which could explain the decreased flux towards the TCA-cycle (explained by reduced pyr concentration). All nucleic acid phosphates showed similar concentrations, suggesting that the cells had sufficient amount of energy molecules, and equivalent synthesis rates of nucleic acids.

Figure 4.15 compares sample 6 (116.6h) to sample 1 (76.9h). The majority of the metabolites was reduced from the first sampling of the exponential growth phase to sample 6, in the lipid accumulation phase. The reduction of glycolysis, TCA-cycle and 6-phosphogluconate (6PG) of PPP, demonstrates lower metabolic activity (reduced flux) during the lipid accumulation phase. This corresponds well with theory, where generation of new biomass by cellular growth requires high metabolic activity. The lipid accumulation phase is characterized by sole lipid synthesis, where acetyl-CoA is a precursor partly derived from pyruvate, which could explain the concentration of pyr being similar for sample 6 and sample 1. The concentrations of ATP and GTP were similar to the concentration during exponential growth, suggesting that the cells were provided with enough substrate to maintain high levels of energy.

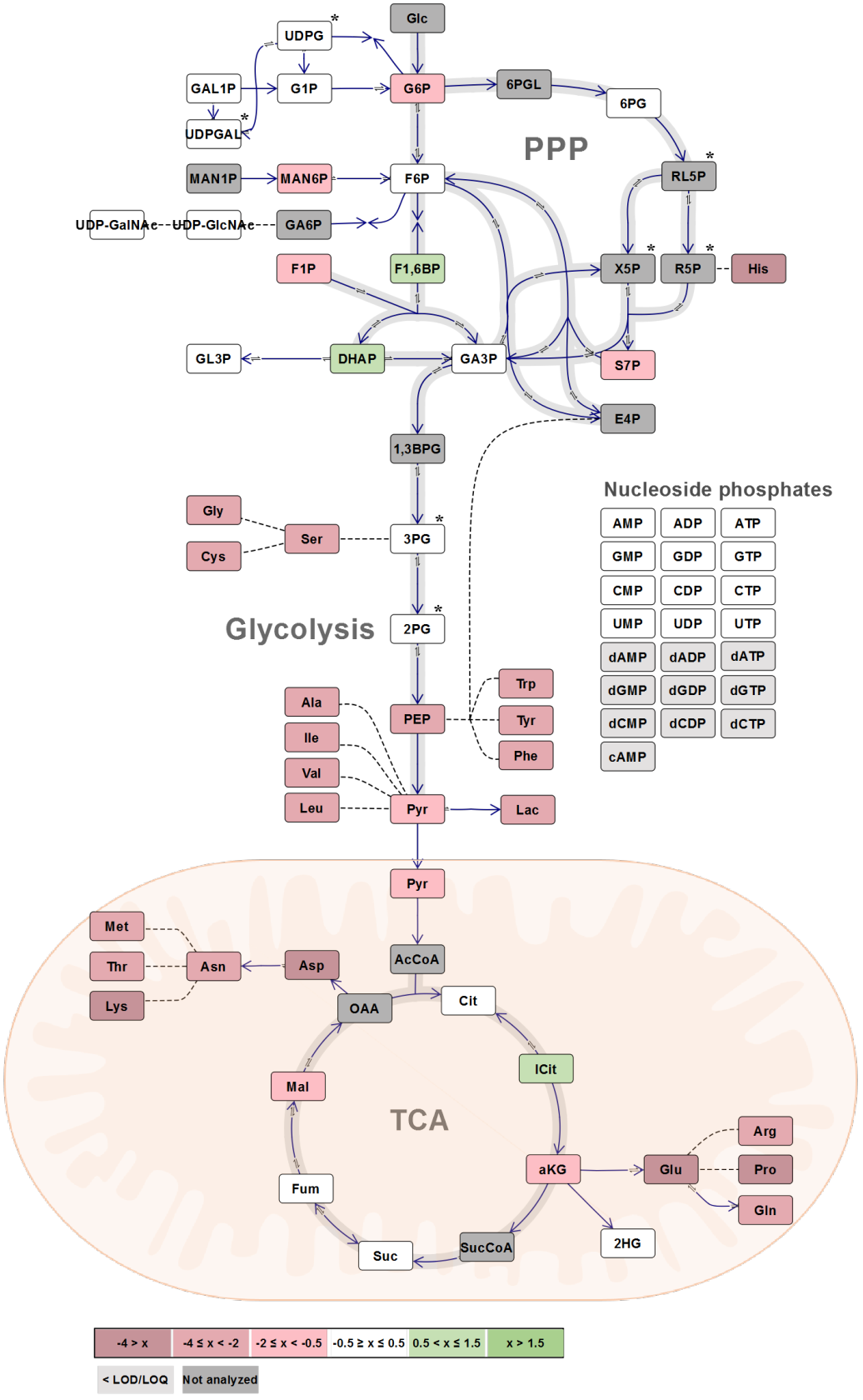


FIGURE 4.14: Intracellular metabolites comparison of sample 3 (89.9h) to sample 1 (76.9h). The coloring explanation is listed in the figure. The values are log 2 (binary logarithm) values of each metabolite divided by the metabolite concentration of sample 1 (76.9h). Positive values correspond to an increase, and negative values to a decrease. Dark grey: not analyzed, light grey: lower concentration than detection, white: similar concentration, red: lower concentration, and green: higher concentration. Generated with OMIX

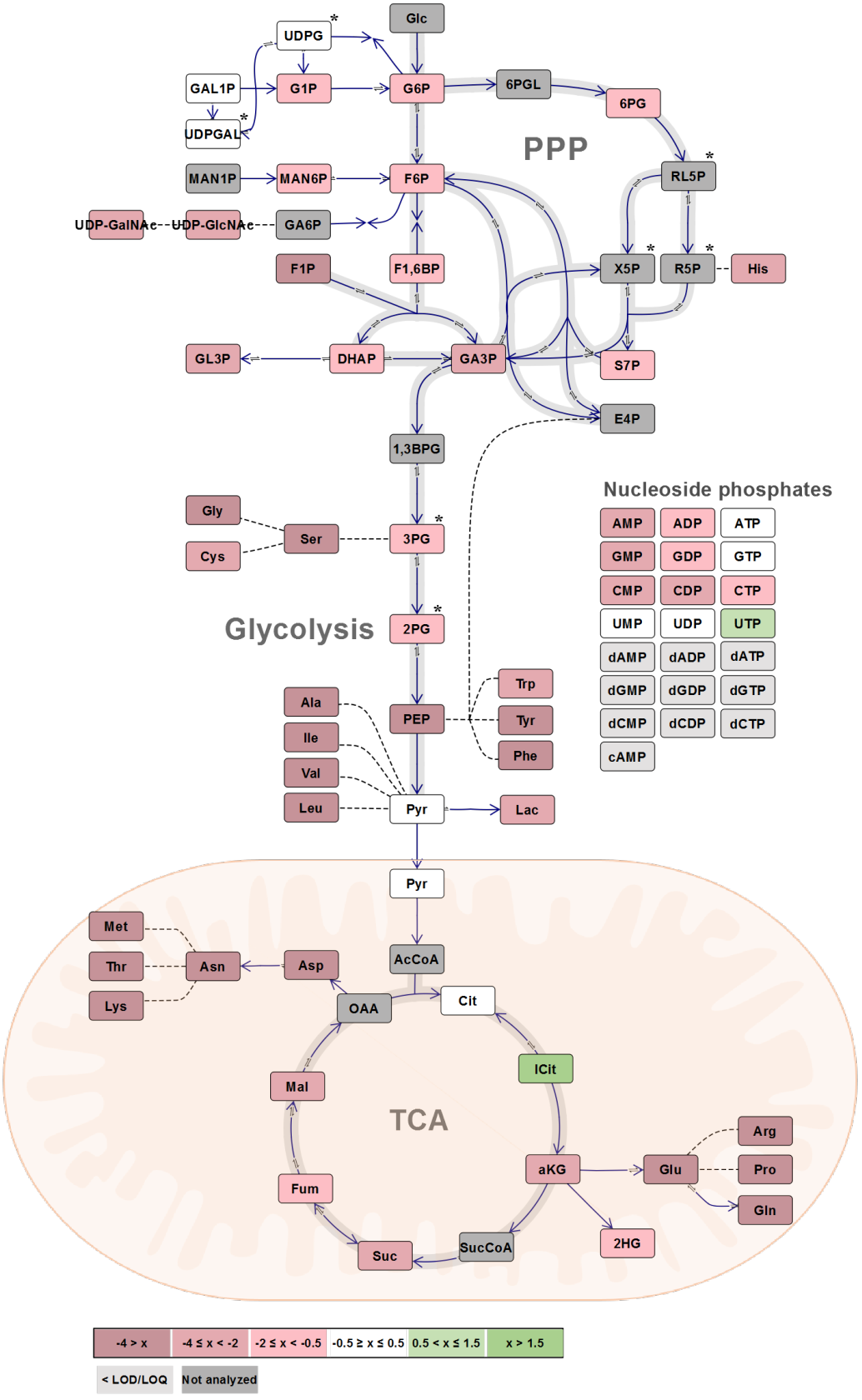


FIGURE 4.15: Intracellular metabolites comparison of sample 6 (116.6h) to sample 1 (76.6h). The coloring explanation is listed in the figure. The values are log 2 (binary logarithm) values of each metabolite divided by the metabolite concentration of sample 1 (76.9h). Positive values correspond to an increase, and negative values to a decrease. Dark grey: not analyzed, light grey: lower concentration than detection, white: similar concentration, red: lower concentration, and green: higher concentration. Generated with OMIX

Figure 4.16 shows decreasing concentrations for more or less all nucleic acids. This points towards lower levels of nucleic acids during late lipid accumulation (sample 9: 160.8h) compared to late growth phase (sample 3: 89.9h). The majority of the glycolysis metabolites showed a lower abundance during late lipid accumulation. The pyruvate and lactic acid content was higher in sample 9, suggesting higher flux towards lipid synthesis from glycolysis, while the lactic acid upturn could be explained by need of more NADH for catabolism. The same was suggested by the increased concentration of 6-phosphogluconate (6PG), channeling more flux through the oxidative PPP.

The last metabolite profile, Figure 4.17, demonstrates an upturn in several metabolites in the glycolysis, the PPP and the TCA-cycle. This could indicate that the overall metabolism was increased from sample 6 to sample 9. The measured lipid content suggested a potential threshold value of storage lipids at about 70%w/w of DCW, which was observed for the last three samples (138.6, 143.6 and 160.8h). The upturn in general metabolism could suggest an increased synthesis of amino acids, nucleotides and other molecules for stimulating cellular growth, as a consequence of reaching the maximum lipid level. The triphosphate concentrations are all decreased compared to the early lipid accumulation phase (sample 6). This points towards limited energy resources, and flux is concentrated towards the TCA-cycle for energy generation. Lactic acid and 6PG are increased, indicating requirements for more NADPH and NADH for anabolic and catabolic reactions.

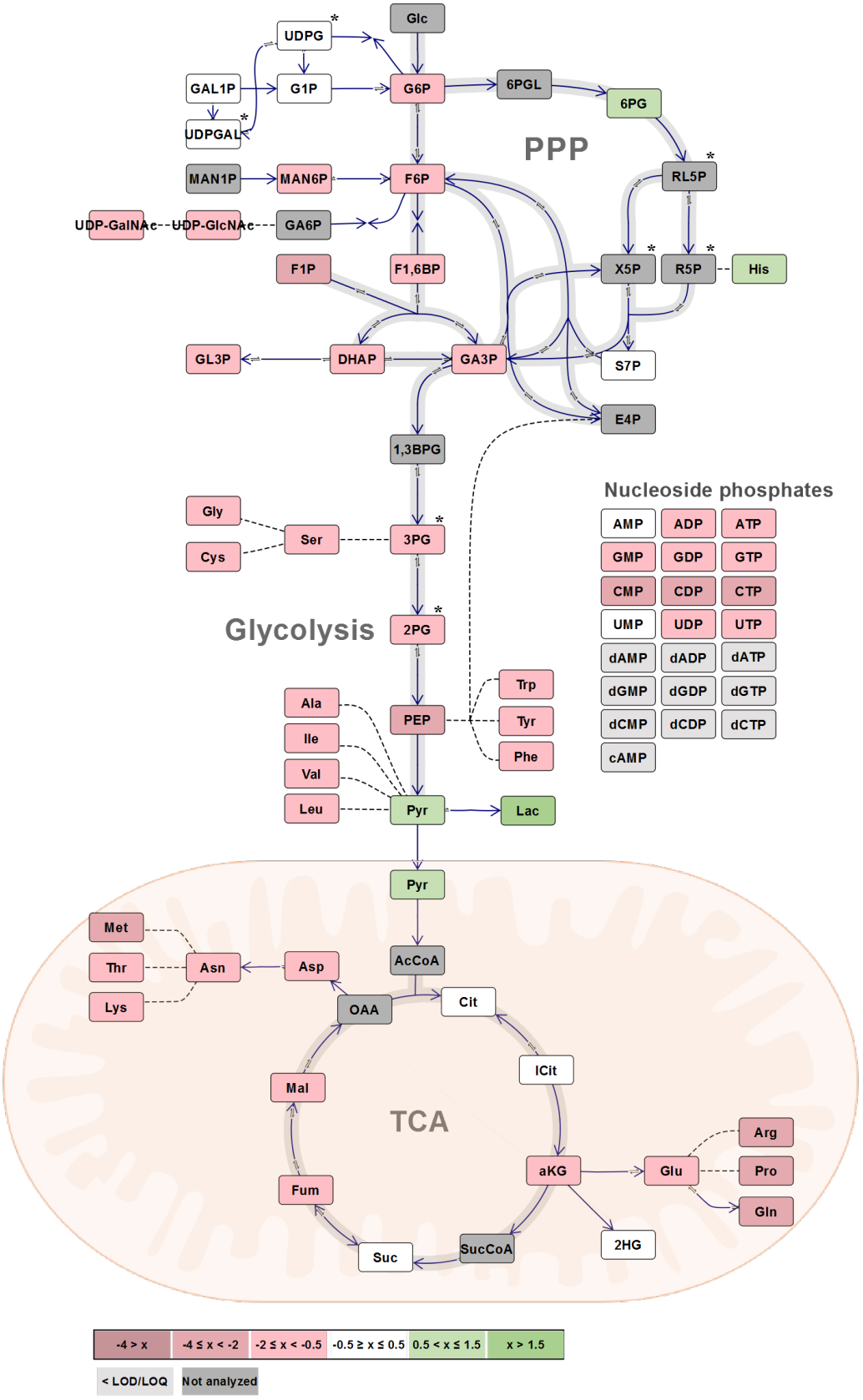


FIGURE 4.16: Intracellular metabolites comparison of sample 9 (160.8h) to sample 3 (89.9h). The coloring explanation is listed in the figure. The values are log 2 (binary logarithm) values of each metabolite divided by the metabolite concentration of sample 3 (89.9h). Positive values correspond to an increase, and negative values to a decrease. Dark grey: not analyzed, light grey: lower concentration than detection, white: similar concentration, red: lower concentration, and green: higher concentration. Generated with OMIX

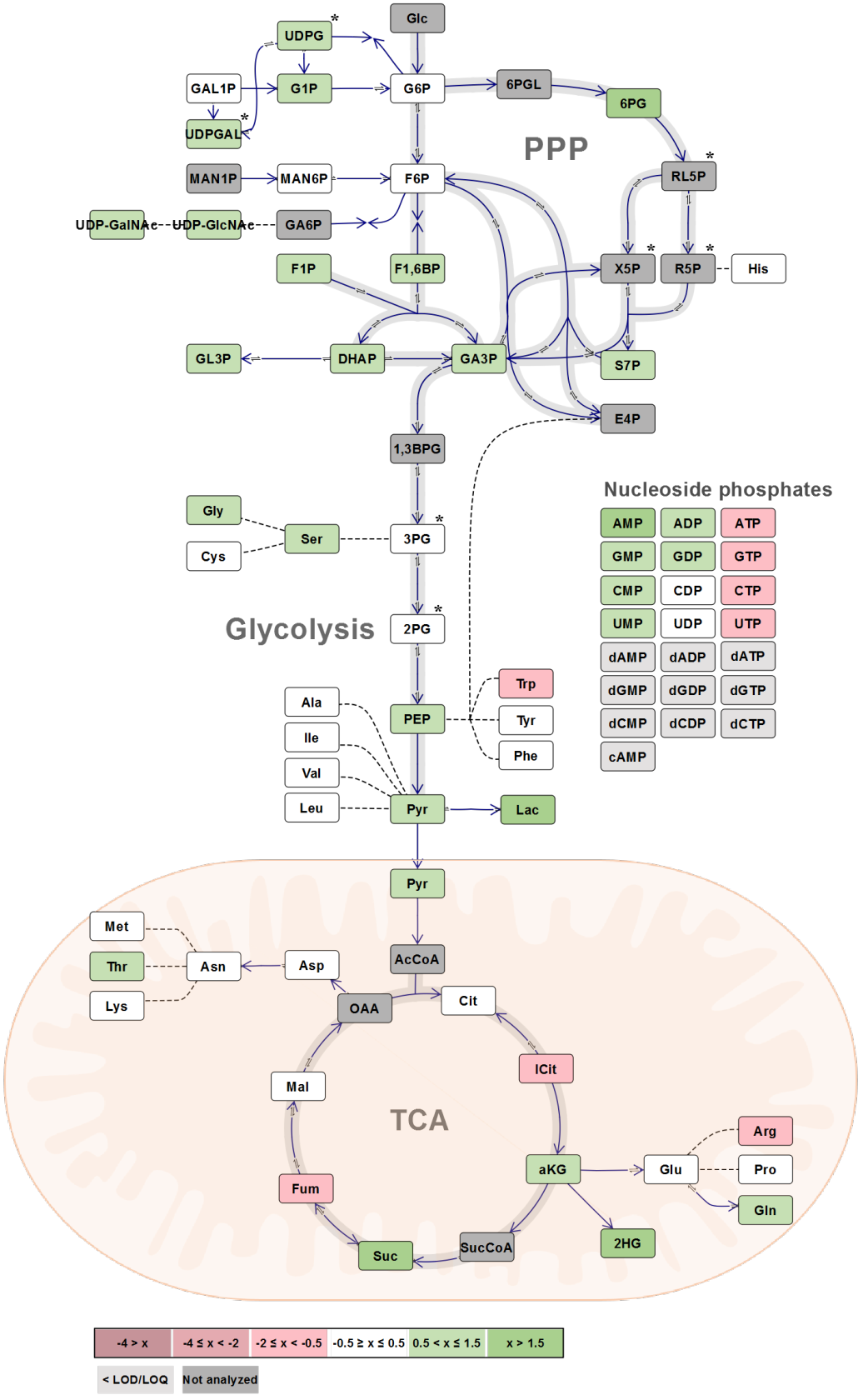


FIGURE 4.17: Intracellular metabolites comparison of sample 9 (160.8h) to sample 6 (116.6h). The coloring explanation is listed in the figure. The values are log 2 (binary logarithm) values of each metabolite divided by the metabolite concentration of sample 6 (116.6h). Positive values correspond to an increase, and negative values to a decrease. Dark grey: not analyzed, light grey: lower concentration than detection, white: similar concentration, red: lower concentration, and green: higher concentration. Generated with OMIX

#### 4.1.4.2 Summarized changes of citrate and gluconate-6-phosphate

The log 2 citrate values (with sample 1: 76.9h, as reference), shown in Table 4.10, were similar throughout the bioreactor cultivation. Citrate is directly involved in lipid synthesis, being both an allosteric activator and a precursor to acetyl-CoA. The stable citrate level indicates sufficient amounts of citrate supplied to cytosol for maximal lipid synthesis.

TABLE 4.10: Relative changes of citrate and 6-phosphogluconate (6PG) during the bioreactor cultivation. The values are log 2 (binary logarithm) values of each metabolite divided by the metabolite concentration of sample 1 (76.9h). Positive values correspond to an increase, and negative values to a decrease.

| **Metabolite** | **Citrate** | **6PG** |
|---|---|---|
| Sample 2 (87.5h) | 0.07 | -0.26 |
| Sample 3 (89.9h) | 0.30 | 0.14 |
| Sample 4 (94.4h) | 0.80 | -0.36 |
| Sample 5 (113.3h) | 0.40 | -0.38 |
| Sample 6 (116.6h) | 0.20 | -1.18 |
| Sample 7 (138.6h) | 0.39 | 0.64 |
| Sample 8 (143.1h) | 0.10 | 0.65 |
| Sample 9 (160.8h) | 0.01 | 0.89 |

The 6-phosphogluconate (6PG) concentration of each sampling compared to sample 1 (76.9h), shows a larger variation. Sample 2 (87.5h) and sample 3 (89.9h) show relatively similar 6PG concentrations as sample 1, showing log 2 values of -0.26, and 0.14, respectively. The raised 6PG concentration was not observed at N-limitation between sample 3 and 4 (89.9-94.4h), showing a reduced 6PG amount during the early lipid accumulation phase (94.4-116.6h). This points towards a lower NADPH demand during the early lipid accumulation phase, compared to the late lipid accumulation between 138.6-160.8h.

#### 4.1.4.3 Summarized changes of selected amino acids

The majority of the amino acid concentrations were roughly constant during the growth phase (sample 1-3, 76.9-89.9h), and decreased during the lipid accumulation phase (94.4-160.8h). Table 4.11 shows the changes of the glutamine, proline, methionine, glutamate and histidine concentrations. All samples are compared by log 2 calculations to sample 2 (87.5h) of the growth phase. The decline is considerably larger for sample 4 (94.4h) compared to sample 3 (89.9h), which could be explained by the depletion of the nitrogen source, reducing the biosynthesis of amino acids. The amino acid levels were relative stable through the whole lipid accumulation phase, displaying similarly low log 2 values.

TABLE 4.11: Relative amounts of selected amino acids measured during the bioreactor cultivation. The values are log 2 (binary logarithm) values of each concentration divided by sample 2 (87.5h) concentration. Positive values correspond to an increase, and negative values to a decrease. Abbreviations: Glutamine (Gln), Proline (Pro), Methionine (Met), Glutamate (Glu), and Histidine (His).

| **Amino acid** | **Gln** | **Pro** | **Met** | **Glu** | **His** |
|---|---|---|---|---|---|
| Sample 3 (89.9h) | -1.67 | -2.31 | -1.35 | -1.43 | 0.20 |
| Sample 4 (94.4h) | -4.44 | -4.67 | -3.55 | -1.76 | 0.76 |
| Sample 5 (113.3h) | -4.59 | -5.01 | -3.61 | -2.95 | 1.17 |
| Sample 6 (116.6h) | -6.09 | -5.25 | -4.56 | -2.48 | 0.82 |
| Sample 7 (138.6h) | -4.43 | -4.88 | -4.23 | -2.54 | 1.35 |
| Sample 8 (143.1h) | -5.49 | -5.44 | -5.01 | -2.65 | 0.92 |
| Sample 9 (160.8h) | -4.66 | -4.73 | -4.65 | -2.93 | 1.00 |

The glutamine (containing two N per molecule) levels became minute after glutamate depletion between sample 3 and sample 4. The large consumption of glutamine during this interval, could be explained by its role as N supplier for essential anabolic reactions, involvement in energy generation, or precursor for purine and protein synthesis.

The glutamate concentration declined greatly from 76.9-89.9h (5.6-0.03 g/l), before depletion initiated N-limitation and the lipid accumulation phase started. Low glutamate concentrations disrupted the contribution of intermediates from glutamate to the TCA-cycle. Furthermore, the limited glutamate level could explain the decreased proline level, which is a derivative of glutamate (NADPH- or NADH-dependent reaction). The transcription and translation are scaled down as a consequence of the limited N resources, which could explain why the methionine concentration is considerably reduced, being the most common start codon for transcription.

Histidine was the only amino acid with increasing concentration during the late growth phase (sample 3, 89.9h) and the lipid accumulation phase (94.4-160.8h). A possible explanation to the increase, is elevated biosynthesis of histidine, which is induced by two meabolic changes; 1) elevated PRPP concentration (product of PPP), and 2) the need of more TCA intermediates, because acetyl-CoA is channeled towards lipid biosynthesis. The histidine biosynthesis consumes glutamine for N incorporation, which could explain the declining glutamine level.

#### 4.1.4.4 Summarized changes of selected organic acids

Table 4.12 shows the measured organic acids by CapIC-MS. The values are log 2 values of each sample (2-9) divided by sample 1 (76.9h). All measurements, except pyruvate (sample 7 and 9), are negative, indicating a decrease of all organic acids from growth through the lipid accumulation phase. The cellular respiration was higher during exponential growth with no nutrient limitation. The decline in organic acids, and central TCA intermediates, demonstrates a lower degree of respiration as a result of lower energy demands during sole lipid biosynthesis.

The TCA-cycle enzymatically oxidizes acetyl-CoA to $CO_2$, with energy conserved as electron carriers NADH and $FADH_2$. The electron carriers are oxidized by reaction with $O_2$ in the respiratory chain, conserving energy as ATP. The OUR decreased after N-depletion, because of reduced energy demands, which corresponds well with the reduced TCA-cycle activity.

TABLE 4.12: Relative amounts of selected organic acids measured during the bioreactor cultivation. The values are log 2 (binary logarithm) values of each concentration divided by sample 1 (76.9h) concentration. Positive values correspond to an increase, and negative values to a decrease. Abbreviations: Pyruvate (Pyr), Fumarate (Fum), Succinate (Suc), Malate (Mal), α-ketoglutarate (aKG), Glx (Glx).

| **Organic acid** | **Pyr** | **Fum** | **Suc** | **Mal** | **aKG** | **Glx** |
|---|---|---|---|---|---|---|
| Sample 2 (87.5h) | -2.42 | -0.46 | 0.47 | -0.63 | -1.48 | -1.69 |
| Sample 3 (89.9h) | -0.57 | -0.91 | -0.10 | -1.07 | -1.03 | -0.54 |
| Sample 4 (94.4h) | -0.30 | -0.78 | -1.27 | -1.27 | -0.72 | -0.16 |
| Sample 5 (113.3h) | -0.80 | -1.34 | -0.73 | -2.20 | -1.56 | -0.74 |
| Sample 6 (116.6h) | -0.44 | -0.94 | -1.58 | -1.76 | -0.35 | -0.66 |
| Sample 7 (138.6h) | 0.51 | -0.75 | -0.86 | -1.70 | -1.12 | -0.69 |
| Sample 8 (143.1h) | -0.57 | -1.01 | -2.20 | -2.81 | -0.93 | -0.69 |
| Sample 9 (160.8h) | 0.23 | -1.13 | -0.19 | -2.09 | -1.16 | -0.54 |

### 4.1.5 NADs and CoAs metabolite profile from shake-flask culture

Shake-flask culture 3 (SF-3) was used for investigation of molecules directly involved in lipid accumulation of *Aurantiochytrium* sp. strain T66. NADP(H), acetyl-CoA, malonyl-CoA, and CoA are of special interest because they are directly linked to generation of reducing power and carbon backbone for FAs synthesis.

This method is currently under development to generate a reproductive protocol. The method was not ready for testing when the bioreactor cultivation was performed, and was therefore completed for a shake-flask culture. Two different sampling volumes and extraction methods were investigated (described in Section 3.2.6.4). Boiling of quick-frozen cells in a ACN:$H_2O$ (90:10, v/v) mix showed scarce extraction of NADs and CoAs metabolites. The homogenization with zirconium oxide beads of 10 ml culture yielded a better extraction, and the results are presented in Table 4.13. The first sample was extracted during the exponential growth phase (about 25h), while the second sample was collected during the lipid accumulation phase (about 46 hours).

Table 4.13 shows the concentrations of NAD, NADP, NADPH, CoA, Acetyl-CoA, Succinyl-CoA, and FAD, from 10 ml culture at the two sampling points. The active biomass is assumed to be unchanged between the two samplings, and that only intracellular storage lipid is responsible for the increasing dry cell weight during the lipid accumulation phase. The concentrations are therefore not adjusted by dry cell weight, and presented as µM in vial from 10 ml culture.

TABLE 4.13: Concentration of NADs and CoAs during exponential growth (exp. growth 25h) and lipid accumulation (lipid acc. 46h) of *Aurantiochytrium* sp. T66 grown on natural glucose and glutamate. The active biomass is assumed to be equal during the two sampling points, the values are therefore not adjusted to dry cell weight, and only presented as µM in vial from 10 ml culture.

| **Compound** | **Exp. growth (µM from 10 ml culture)** | **Lipid acc. (µM from 10 ml culture)** |
|---|---|---|
| NAD | 5.9 | 9.8 |
| NADP | 5.5 | 8.4 |
| NADPH | 9.0 | 17.1 |
| CoA | 8.7 | 9.3 |
| Acetyl-CoA | 2.2 | 2.7 |
| Succinyl-CoA | 2.9 | 3.1 |
| FAD | 2.6 | 4.9 |

The NADPH concentration increased by a two-fold from exponential growth to the lipid accumulation phase. This corresponds well with the increasing need of anabolic reducing power during lipid synthesis. Furthermore, the acetyl-CoA concentration (precursor malonyl-CoA) was quite similar for the two phases. These results suggest that fatty

acid synthesis was not limited by the acetyl-CoA concentration or the availability of NADPH. Results of malonyl-CoA would be of great interest to investigate the activity of acetyl-CoA carboxylase (ACC) converting AcCoA to MalCoA. The extraction of MalCoA was not optimal with the extraction procedure used during this work.

## 4.2 Verification of shake-flask experiments for $^{13}$C-tracer analysis

Initially $^{13}$C-labeling experimentation was outlined to be performed in mini bioreactors, but the experimental set-up was not functioning properly and needed repair. A shake-flask pilot study was therefore established, to verify if shake-flask cultivations were a suitable model-system for $^{13}$C-label experiments, and could provide important information for future $^{13}$C-label experimentation in bioreactors.

Two shaking-flask (SF) cultures (50 ml liquid volume) were investigated to verify that shake-flask cultivations was a relevant model system, and comparable to bioreactor cultivations. The medium used was identical to the one used in the bioreactor cultivation (see Table 3.2 for details). The pH was monitored at each OD measurement, and stayed within 6.8-7.2. The first SF (SF-1) was used for OD, DCW, and glucose and glutamate consumption. The OD measurements are shown in Appendix C.2. The second (SF-2) was used for quantification of a range of intracellular metabolites. Furthermore, three SFs were (with three separate $^{13}$C-labelled glucose substrates) used for profiling of intracellular metabolites and fluxome analysis. These results are presented in Section 4.3. Determination of total lipid content, consumption of glucose and glutamate, and SPE separation of the lipids for fatty acid analysis, were performed for all five shake-flasks.

### 4.2.1 Carbon consumption in shake-flask cultures with $^{13}$C-glucose substrates

Figure 4.18 shows the changes in glucose, glutamate, and DCW for SF-1. The consumption rate of glucose and glutamate was largest during the growth phase. The glutamate and glucose concentration was measured for all five shake-flask cultures at the final sampling point at 73.5h. The results are summarized in Table 4.14.

The final concentrations of glucose and glutamate, were very similar for all shake-flask cultures, suggesting that the consumption rates followed the same trend as for SF-1 shown in Figure 4.18. The glucose consumption was considerably lower during the lipid accumulation phase, demonstrating that the uptake of glucose was not the limiting factor for lipid biosynthesis during this accumulation phase. The same results were observed in the bioreactor cultivation discussed in Section 4.1.1. The consumption rate of glucose and glutamate, of SF-1 and the other shake-flasks, are shown in Table 4.15.

The yield coefficient of biomass from glucose, $Y_{xs}$, was highest from 24.3-44.3h for the shake flask cultivation SF-1. The yield of intracellular lipids from glucose, was higher

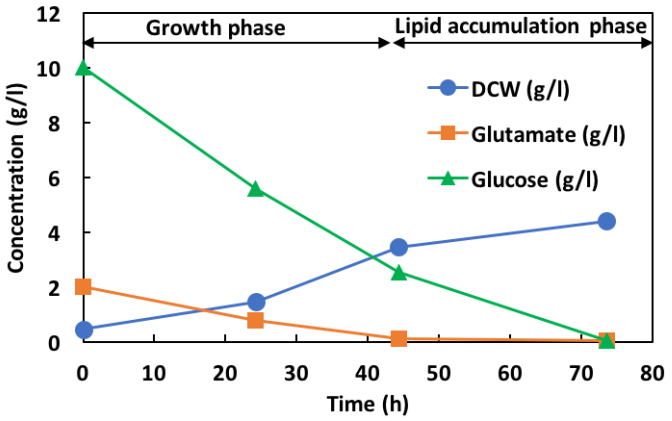


FIGURE 4.18: Changes in glucose (green), glutamate (orange), and dry cellular weight (DCW, blue) during shake flask cultivation (SF-1) of *Aurantiochytrium* sp. T66 grown on natural glucose and glutamate. The four data points are shown with corresponding description of life-stage/phase. Data provided in Table 4.14.

TABLE 4.14: Concentration of glucose and glutamate for the different life-stages of shake flask cultivation of *Aurantiochytrium* sp. T66. The measured concentrations for the other shake-flask cultiure, at the final sampling (during the lipid accumulation phase), are also shown. (-) is shown when glucose was depleted.

| **Shake flask (time)** | **Phase** | **Glucose (g/l)** | **Glutamate (g/l)** |
|---|---|---|---|
| SF-1 (0h) | start | 10.0 | 2.0 |
| SF-1 (24.3h) | exponential growth | 5.6 | 0.8 |
| SF-1 (44.3h) | N-source limitation | 2.6 | 0.1 |
| SF-1 (73.5h) | lipid accumulation | 0.03 | 0.06 |
| SF-2 (73.5h) | end lipid accumulation | - | 0.08 |
| SF-1-$^{13}C_1$ (73.5h) | lipid accumulation | - | 0.08 |
| SF-1,2-$^{13}C_2$ (73.5h) | lipid accumulation | - | 0.06 |
| SF-U-$^{13}C_6$ (73.5h) | lipid accumulation | - | 0.01 |

TABLE 4.15: Change in specific growth rate ($\mu$), consumption rate of glucose ($r_{glucose}$), consumption rate of glutamate ($r_{glutamate}$), and yield coefficient of biomass (x) from carbon source (s) ($Y_{xs}$) of shake-flask cultivation SF-1 of *Aurantiochytrium* sp. T66. Glutamate and glucose are carbon sources for the two first samplings, while only glucose is consumed during the lipid accumulation phase (44.3-73.5h).

| **Shake flask (time)** | $\mu$ **($h^{-1}$)** | $r_{glucose}$ **(g/l·h)** | $r_{glutamate}$ **(g/l·h)** | $Y_{xs}$ **(g/g C-source)** |
|---|---|---|---|---|
| SF-1 (24.3h) | 0.05 | 0.18 | 0.05 | 0.18 |
| SF-1 (44.3h) | 0.04 | 0.15 | 0.03 | 0.54 |
| SF-1 (73.5h) | - | 0.09 | 0.00 | 0.38 |

during lipid accumulation phase of SF-1, compared to the bioreactor culture. The specific growth rate ($\mu$) is considerably lower in the shake-flask culture compared to the bioreactor cultivation, showing 0.05 versus 0.15 $h^{-1}$, respectively. Limited aeration of

the shake-flask culture could explain the reduced growth rate. This could indicate that shake-flask cultivations is not suitable for $^{13}$C-tracer analysis, and that $^{13}$C-analysis should be performed in bioreactors.

### 4.2.2 Total lipids of shake-flask cultures with $^{13}$C-glucose substrates

The total lipid content was calculated for all shake-flasks, ranging from 61-65% w/w of DCW for shake-flask culture SF-1, SF-2, and the three $^{13}$C-glucose labeled SFs , as shown in Figure 4.19. These results indicate that the lipid biosynthesis rate was similar for all shake-flask cultures.

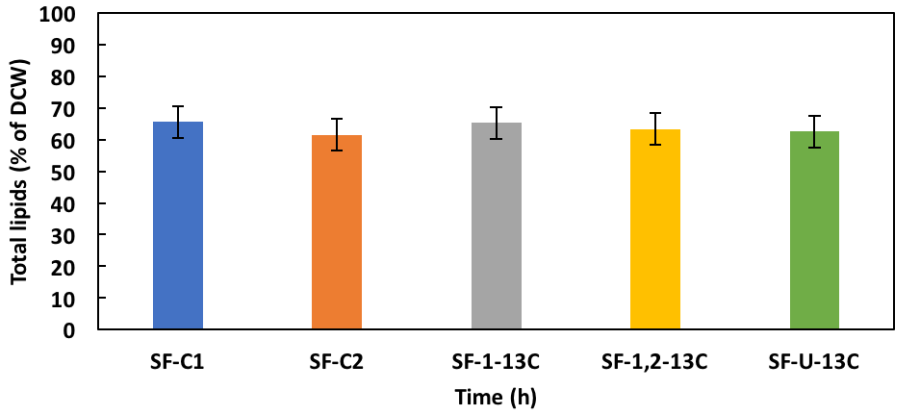


FIGURE 4.19: Total lipid content of shake-flask (SF) cultures of the $^{13}$C-labeled glucose substrate experiments with *Aurantiochytrium* sp. strain T66. SF-1 and SF-2 are control flasks with natural glucose. The other three are differently $^{13}$-C labeled.

### 4.2.3 Fatty acid profiling of shake-flask culture SF-1 and SF-2

Extracted lipids (by Bligh and Dyer 3.2.3), were hydrolyzed, by the fatty acid (FA) analysis method 3.2.4, to establish FAs profiles of the two shake-flasks. Solid phase extraction was used to separate the lipids into a neutral (NL) and a polar lipid (PL) fraction (SPE separation - 3.2.5). This was performed for all shake-flask cultures, but this section describe only SF-1 and SF-2.

The two fractions, containing NL (frac A) and PL (Frac B) separately, were hydrolyzed before FA profiles were established. The FA profiles of TL were matched against the FA profiles of the NL and PL, to investigate the variation between the two lipid groups. Table 4.16 shows the similar fatty acid profiles of shake-flask culture SF-1 and SF-2.

TABLE 4.16: Fatty acid distribution of the control shake flask cultures (SF-1 and SF-2). All values are % of total fatty acids in each shake flask.

| **Fatty acid** | **C14:0** | **C16:0** | **C16:1** | **C18:0** | **C18:1** | **C22:5** | **C22:6** |
|---|---|---|---|---|---|---|---|
| SF-1 | 4.5 | 48.0 | 2.7 | 21.5 | 2.7 | 7.2 | 13.4 |
| SF-2 | 5.0 | 48.0 | 2.7 | 23.0 | 2.4 | 6.6 | 12.2 |

The FA profile of the shake-flask cultures was different from the FA profile reported for the lipid accumulation phase of the bioreactor culture. The myristic acid (C14:0) fraction of TFA ranged between 10-12%, being considerably lower in the shake-flask cultures; 4.5-5% of TFA. Palmitic acid (C16:0) constituted about 1/3 of TFA for the bioreactor culture, and almost 50% of TFA for the shake-flask cultures. Stearic acid (C18:0) comprised 22-23% of TFA for the shake-flask cultures, the same relative amount was observed for C18:0 at 113.3h (early in the lipid accumulation phase) for the bioreactor cultivation. The C18:0 amount decreased to 10.8% from 113.3-160.8h for the bioreactor culture. The fractions of MUFAs were lower for the shake-flasks, which could support the proposed $O_2$-limitation that yielded the reduced growth rate. The PUFA fractions were also reduced for the shake-flasks compared to the bioreactor, with a DHA fraction of 12-13% to 22%, for the shake-flasks and bioreactor, respectively.

#### 4.2.3.1 Fatty acid profile of neutral and polar lipids

The fatty acid profiles of the NL and PL, for fraction A and B (frac A, frac B), of the shake-flask cultures SF-1 and SF-2, are shown in Table 4.17.

TABLE 4.17: Fatty acid distribution in the neutral lipids (NL) (=fraction A) and polar lipids (PL) (=fraction B) for shake flask culture SF-1 and SF-2. All values are % of total fatty acids in each shake flask or in each fraction. NQ: not quantified in the lipid class (fraction).

| **Fatty acid** | **C14:0** | **C16:0** | **C16:1** | **C18:0** | **C18:1** | **C22:5** | **C22:6** |
|---|---|---|---|---|---|---|---|
| **SF-1:** | | | | | | | |
| NL (Frac A) | 10.6 | 41.5 | NQ | 25.2 | 4.0 | 6.8 | 11.9 |
| PL (Frac B) | NQ | 32.2 | NQ | 60.5 | 0.4 | 2.8 | 4.0 |
| **SF-2:** | | | | | | | |
| NL (Frac A) | 12.6 | 41.5 | NQ | 23.6 | 3.9 | 6.6 | 11.7 |
| PL (Frac B) | NQ | 32.4 | NQ | 60.0 | 0.4 | 2.8 | 4.4 |

The fatty acid profiles were quite similar for the two shake-flask cultures, with the same variations between the NL and PL. The myristic acid (C14:0) constitutes 11-13% of the NL, in contrast to being undetectable in the PL. The portion of palmitic acid (C16:0) constituted more than 1/3 for both NL and PL, showing a higher C16:0 content in NL. The MUFA of palmitic acid, palmitoleic acid (C16:1), was not detected for any of the

lipid classes, but was measured to 2.7% of the TFA in SF-1 and SF-2, shown in Table 4.16. Stearic acid (C18:0) was the most abundant FA in PL, constituting 60% of TFA. The C18:0 content ranged 24-25% of the NL.

The PUFAs, DPA (22:5) and DHA (22:6), showed higher fractions in NL compared to the PL. DPA constituted 6-7% of NL, and about 3% of the PL. The DHA content was considerably higher in the NL, demonstrating a three-fold abundance in NL relative to the PL. This result is contrasting to earlier reported results, observing a higher abundance of DHA in the PL compared to the NL [48], [46], [47].

## 4.3 Investigation of $^{13}$C-labeling pattern in shake-flask cultures

$^{13}$C-labeled glucose substrates were used to investigate the intracellular metabolic flux distribution in *Aurantiochytrium* sp. T66 cells grown in shake-flasks. Three different $^{13}$C-labeled glucose substrates were used; 1-$^{13}C_1$-glucose, 1,2-$^{13}C_2$-glucose, and U-$^{13}C_6$-glucose. The different substrates were used for investigation of carbon flux distribution through central metabolism, and into fatty acids biosynthesis. Branch points of the carbon flux distribution between glycolysis, pentose phosphate pathway (PPP), the tricarboxylic acid cycle (TCA-cycle), and the fatty acid (FA) synthesis, are significant for developing an increased DHA bioprocess in strain T66.

### 4.3.1 Isotopologue analysis and sum fractional labeling of shake-flask cultures with $^{13}$C-glucose substrates

Qualitative MS-analysis of all fatty acid isotopologues from hydrolyzed lipids (3.2.4) in $^{13}$C-tracer glucose shake-flasks, was performed to determine the labeling patterns. All isotopologoues were summarized, and the sum fractional labeling (SFL) was calculated, and the data is provided in Table 4.18.

TABLE 4.18: Sum fractional label (SFL) of selected fatty acids of the shake-flask cultures, with natural glucose (SF-1, SF-2) and $^{13}$C-labeled glucose substrates. Samples were collected at 73.5 hours. Isotopologue data is given in Appendix B.2.

| **Fatty acid** | **C14:0 SFL (%)** | **C16:0 SFL (%)** | **C16:1 SFL (%)** | **C18:0 SFL (%)** | **C22:6 SFL (%)** |
|---|---|---|---|---|---|
| SF-1 | 2.9 | 0.9 | 0.2 | 1.7 | 3.3 |
| SF-2 | 2.6 | 0.9 | 0.2 | 1.6 | 3.2 |
| SF-1-$^{13}C_1$ | 20.6 | 7.5 | 17.6 | 4.3 | 20.1 |
| SF-1,2-$^{13}C_2$ | 49.9 | 15.3 | 40.5 | 5.5 | 46.4 |
| SF-U-$^{13}C_6$ | 83.2 | 27.7 | 97.4 | 11.7 | 90.3 |

The natural $^{13}$C-labeling of natural glucose is very similar for the two control shake-flask cultures (SF-1 and SF-2). The SFL fractions of C14:0, C16:1, and C22:6, are close to the theoretically predicted values of 25%, 50% and 100%, for 1-$^{13}C_1$-, 1,2-$^{13}C_2$-, and U-$^{13}C_6$-glucose, respectively. These results indicate that the labeling pattern follow theory. The SFL for full-labeled glucose of C16:1 is very close to the theoretical value, indicating that fully labeled glucose was the only precursor for FA synthesis of C16:1, and potentially other MUFAs. This support the observations from the bioreactor culture, where the fraction of MUFAs increased considerably after glutamate depletion.

The SFL for C16:0 and C18:0 was considerably lower, showing large deviations from the proposed labeling pattern. This could suggest that glutamate supply the main C portion for C16:0/C18:0 biosynthesis by FAS pathway during the growth phase. The FAS pathway activity declined during N-starvation, and only a small portion of C16:0 and C18:0 was synthesized during the lipid accumulation phase, yielding low SFL fractions. The $^{13}$C-labeling of C18:0 was very low for all shake-flask cultures, and the samples were therefore re-run by an alternative method, which confirmed the low $^{13}$C-labeling of stearic acid. As for now, this result is not fully understood, and further investigations are needed.

### 4.3.2 Profiling of $^{13}$C-incorporation of intracellular metabolites of shake-flask cultures

A selection of central intracellular metabolites were analyzed by CapIC-MS, programmed for isotopologue determination and not qualitative metabolite profiling. Amino acids were not analyzed because of time-limitation, but the samples were prepared, and they will be analyzed during the fall of 2018 as a part of the ongoing AurOmega project [4]. Table 4.19 and 4.20 show the sum fractional labels (SFL) of selected metabolites. SF-2 with natural glucose and the three $^{13}$C-glucose labeled shake flask cultures, were sampled during exponential growth (about 25h) and the lipid accumulation phase (about 46h). Figure 4.20 shows the measured metabolites, as blue boxes in their intracellular metabolic position.

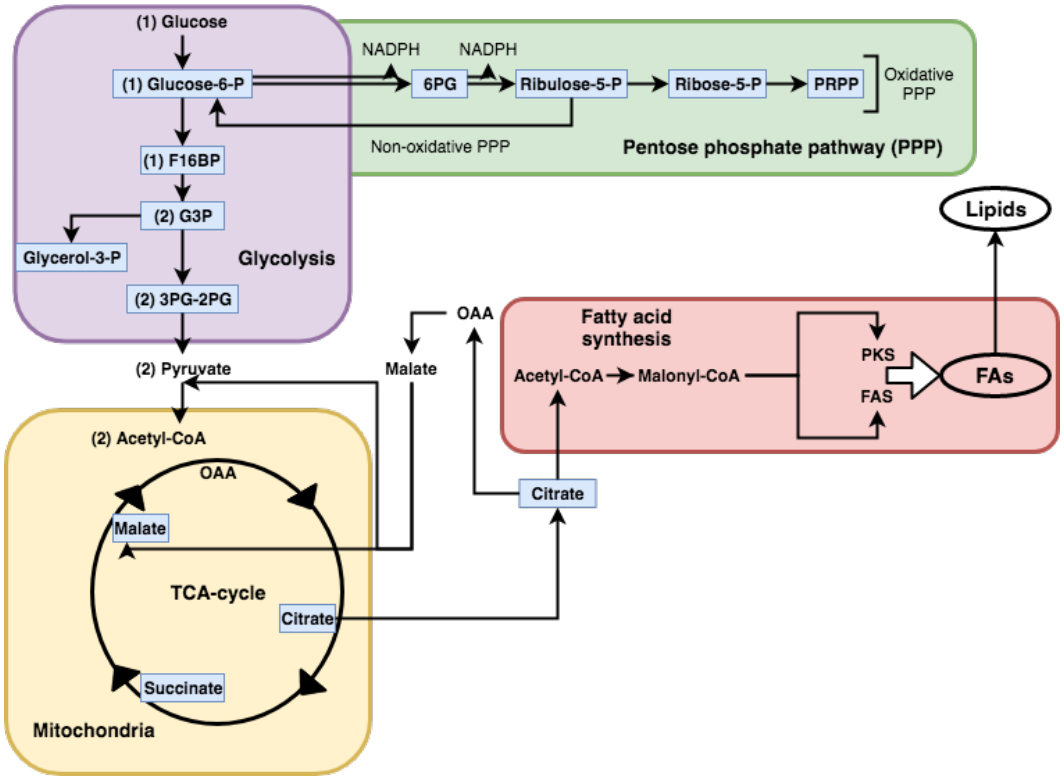


FIGURE 4.20: Overview of selected intracellular metabolites of glycolysis, pentose phosphate pathway (PPP), TCA-cycle and fatty acid synthesis. The blue squared metabolites were analyzed by CapIC-MS, programmed for isotopologue determination, and the sum fractional labels are listed in Table 4.19.

TABLE 4.19: Sum fractional label (SFL) of selected metabolites measured during exponential growth (exp growth) and lipid accumulation (lipid acc.) phase of shake flask cultures of *Aurantiochytrium* sp. T66.

| **Metabolite** | **Glucose labeling** | **Exp. growth SFL (%)** | **Lipid acc. SFL (%)** |
|---|---|---|---|
| **Glycolysis:** | | | |
| HexP | Natural | 1.4 | 1.3 |
| HexP | 1-$^{13}C_1$ | 16.1 | 15.1 |
| HexP | 1,2-$^{13}C_2$ | 36.1 | 35.3 |
| HexP | U-$^{13}C_6$ | 98.2 | 98.4 |
| F16BP | Natural | 1.9 | 1.8 |
| F16BP | 1-$^{13}C_1$ | 14.5 | 13.9 |
| F16BP | 1,2-$^{13}C_2$ | 33.7 | 33.5 |
| F16BP | U-$^{13}C_6$ | 97.5 | 98.2 |
| G3P | Natural | 0.6 | 0.6 |
| G3P | 1-$^{13}C_1$ | 11.5 | 10.5 |
| G3P | 1,2-$^{13}C_2$ | 33.4 | 36.1 |
| G3P | U-$^{13}C_6$ | 86.6 | 97.1 |
| Gly3P | Natural | 2.0 | 1.4 |
| Gly3P | 1-$^{13}C_1$ | 13.6 | 12.3 |
| Gly3P | 1,2-$^{13}C_2$ | 30.9 | 29.5 |
| Gly3P | U-$^{13}C_6$ | 95.7 | 95.3 |
| 3PG-2PG | Natural | 1.7 | 1.9 |
| 3PG-2PG | 1-$^{13}C_1$ | 13.2 | 14.0 |
| 3PG-2PG | 1,2-$^{13}C_2$ | 30.0 | 31.9 |
| 3PG-2PG | U-$^{13}C_6$ | 91.7 | 96.8 |
| **PPP:** | | | |
| PentP | Natural | 0.6 | 0.8 |
| PentP | 1-$^{13}C_1$ | 7.2 | 5.8 |
| PentP | 1,2-$^{13}C_2$ | 29.0 | 27.9 |
| PentP | U-$^{13}C_6$ | 98.9 | 99.6 |
| PRPP | Natural | 1.4 | 1.3 |
| PRPP | 1-$^{13}C_1$ | 10.1 | 8.7 |
| PRPP | 1,2-$^{13}C_2$ | 32.0 | 29.8 |
| PRPP | U-$^{13}C_6$ | 98.2 | 98.8 |
| 6PG | Natural | 1.6 | 1.5 |
| 6PG | 1-$^{13}C_1$ | 15.3 | 14.1 |
| 6PG | 1,2-$^{13}C_2$ | 34.9 | 34.1 |
| 6PG | U-$^{13}C_6$ | 97.5 | 97.6 |
| **TCA-cycle:** | | | |
| Mal | Natural | - | 2.2 |
| Mal | 1-$^{13}C_1$ | 12.4 | 18.5 |
| Mal | 1,2-$^{13}C_2$ | 22.1 | 32.6 |
| Mal | U-$^{13}C_6$ | 57.0 | 87.0 |
| Succ | Natural | - | 6.6 |
| Succ | 1-$^{13}C_1$ | 16.4 | 20.1 |
| Succ | 1,2-$^{13}C_2$ | 14.1 | 26.4 |
| Succ | U-$^{13}C_6$ | 50.8 | 68.1 |
| Cit | Natural | 1.8 | 1.6 |
| Cit | 1-$^{13}C_1$ | 13.7 | 17.6 |
| Cit | 1,2-$^{13}C_2$ | 25.9 | 35.1 |
| Cit | U-$^{13}C_6$ | 62.9 | 89.5 |

TABLE 4.20: Sum fractional label (SFL) of GTP and CDP measured during exponential growth (exp growth) and lipid accumulation (lipid acc.) phase of shake flask cultures of *Aurantiochytrium* sp. T66. Abbreviations: guanosin triphosphate (GTP) and cytidine diphosphate (CDP).

| **Metabolite** | **Glucose labeling** | **Exp. growth SFL (%)** | **Lipid acc. SFL (%)** |
|---|---|---|---|
| **All:** | | | |
| GTP | Natural | 1.7 | 1.7 |
| GTP | 1-$^{13}C_1$ | 12.4 | 11.9 |
| GTP | 1,2-$^{13}C_2$ | 28.0 | 27.9 |
| GTP | U-$^{13}C_6$ | 28.9 | 51.4 |
| CDP | Natural | 1.6 | 1.4 |
| CDP | 1-$^{13}C_1$ | 10.1 | 10.4 |
| CDP | 1,2-$^{13}C_2$ | 25.6 | 27.1 |
| CDP | U-$^{13}C_6$ | 74.3 | 79.4 |

The natural glucose containing shake-flasks showed SFLs ranging between 1-2% for most of the metabolites. SFL for 1-$^{13}C_1$-glucose and 1,2-$^{13}C_2$-glucose should by theory constitute around 17 and 33% of all carbon, respectively. The SFLs for 1- and 1,2-labeled reported here, point towards a sum of labeling ranging close to theoretical predicted values. The fully labeled glucose, U-$^{13}C_6$, shows SFLs ranging between 95-99% (within the uncertainty of the analysis method) for the metabolites of the glycolysis and PPP.

The upper glycolysis and pentose phosphate pathway showed no change between the growth phase and the lipid accumulation phase. This demonstrates that the glutamate carbon did not enter those pathways via anaplerotic reactions. The SFL of PentP, for 1-$^{13}C_1$, was reduced from 7.2 to 5.8%. This indicates that the non-oxidative PPP was operated reversibly.

The SFL of the TCA-cycle intermediates increased after glutamate depletion, which was expected, but the SFLs did not increase above 95% for fully labeled $^{13}$C-glucose during the lipid accumulation phase.

## 4.4 Investigation of cellular life-cycle of *Aurantiochytrium* sp. strain T66

The reason to study the cellular life-cycle of *Aurantiochytrium* sp. strain T66 was that several inoculated bioreactor cultures failed to initiate growth, and a side-project with shake-flask cultures was undertaken to characterize and understand more about cell development stages. The motivation was to improve the inoculum preparation stages for more robust and reproductive bioreactor cultivations.

Observations from shake flask cultivations and the bioreactor cultivation of *Aurantiochytrium* sp. T66, suggested that the two cell modes can co-exist within the same culture, as observed by Bongiorni *et al.* [45]. No binary cell division was observed, but the common rosette structures of 4-8 cells enclosed by both separate and a shared membrane indicate that cellular division took place. Formation of zoospores was observed in shake-flask cultivations, as well as during the lag phase of the bioreactor cultivation. Figure 4.21 shows zoospores and normal cells after release of zoospores from a zoosporangium.

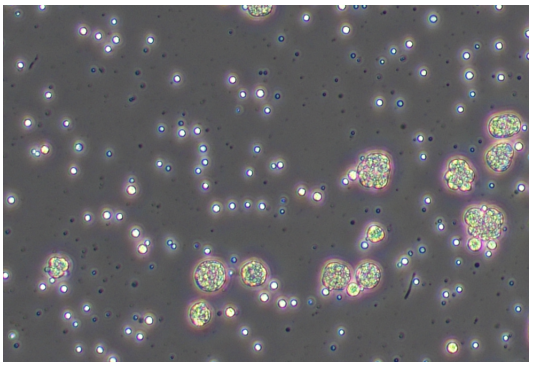

FIGURE 4.21: Zoospore content after release of zoospores from several zoosporangium. The larger cells are vegetative *Aurantiochytrium* sp. T66 cells

Prior to the liberation of zoospores, rapid movements of zoospores inside the zoosporangium was observed. This lasted for a short time; about 5 seconds, before the sporangium became rigid. The same result was observed by Bongiorni *et al.* [45] with their study of *Thraustochytrium gaertnerium*. The release of zoospores from the zoosporangium was observed during microscopic investigation, and was caught on video. The initial release occurred through a small tear in the cell wall, followed by total disintegration after two-three minutes.

Three shake-flasks were inoculated with three ampules, where two ampules originated from the same ampule stock, and the last ampule was prepared during the work by Tronsaune [22]. The shake-flask cultures were kept for several weeks, up to 1 month (28°C and 200 rpm), to investigate zoospore formation. Zoospores were present from

the fist microscopic investigation of the two shake-flasks from the same ampule-stock. The presence of zoospores was absolute, and did not change, indicating that it can be quite difficult to convert zoospores to vegetative cells. The third shake-flask did not develop zoospores, suggesting that the ampules was the source of the zoospores.

The bioreactor inoculum contained large amounts of zoospores, resulting in a longer lag phase than reported by earlier work with *Aurantiochytrium* sp. T66 ([60], [16], [22]). The lag-phase lasted for about 60h to the normal 20h. The amount of zoospores declined considerably during the fermentation, but minute numbers were present until the termination.

Marchan *et al.* [41] describe the *Aurantiochytrium* genus with a characteristic that vegetative cells are generally dispersed as single cells. The observations during this work showed differently. Figure 4.22 shows the high cluster (a) content, but single cells (b) were also present. Both aggregates, single cells, and the rosette structures of 4-8 cells sharing a outer membrane, existed in the different cellular phases (growth and lipid accumulation). This could suggest that some extracellular signaling induce aggregation. The stored lipids were visible as small lipid droplets inside the cells. Once the lipid content increased towards the suggested threshold of 70%w/w, the ratio of aggregates inclined.

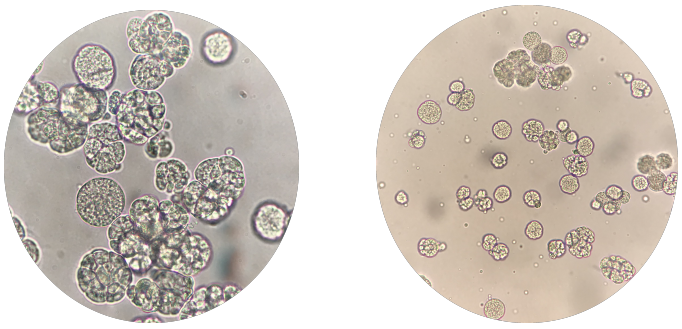

(a) (b)

FIGURE 4.22: *Aurantiochytrium* sp. strain T66. Microscope: Motic BA310, NTNU

Further studies of the cellular life cycles are needed to fully understand the development of *Aurationchytrium* sp. T66.

### 4.4.1 Staining of *Aurantiochytrium* sp. T66

Staining with Live/Dead Assay L7012 (Live/Dead BacLight Bacterial Viability Kits [84]) was completed to observe differences between cultures with and without zoospores. The fluorescent coloring showed high metabolic activity (as a direct consequence of ATP levels) for both vegetative cells and zoosporangium. Figure 4.23 shows staining

of a shake-flask culture with no observed zoospores, collected during the early lipid accumulation phase. The capture shows presence of both red and green coloring. This could suggest that there are cells with both high and low metabolic activity present, or that the protocol is not well-suited for eukaryotic cells.

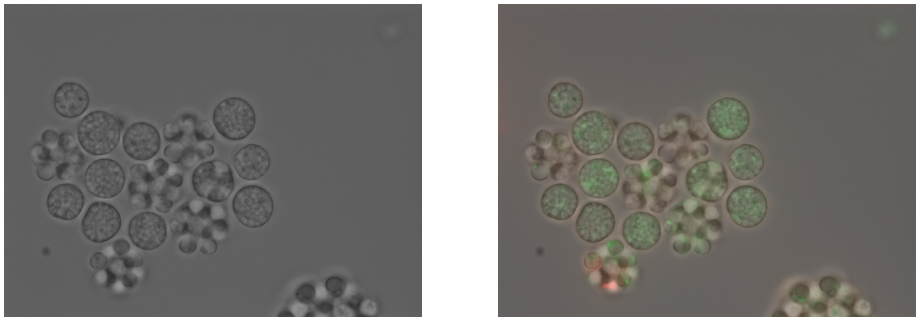

(a) (b)

FIGURE 4.23: Microscope pictures of *Aurantiochytrium* sp. T66. (a) and (b) show the same capture, where (b) is added fluorescent coloring (Live/Dead Assay L7012 [84]) to investigate the metabolic activity. Green indicates metabolic activity, while red coloring indicates low degree of metabolic activity. Microscope: Zeiss Apotome Imager.Z2 with AxioCam ERc5s

Figure 4.24 shows several zoosporangium from a shake-flask culture left in the stationary phase for several weeks, before 1 ml was added to 100 ml fresh medium (creating a 1% inoculum). The capture was taken during the early growth phase of the new shake flask cultivation. The zoosporangium shows high metabolic activity, and considerable amounts of zoospores are visible as the small circular formations inside the zoosporangium.

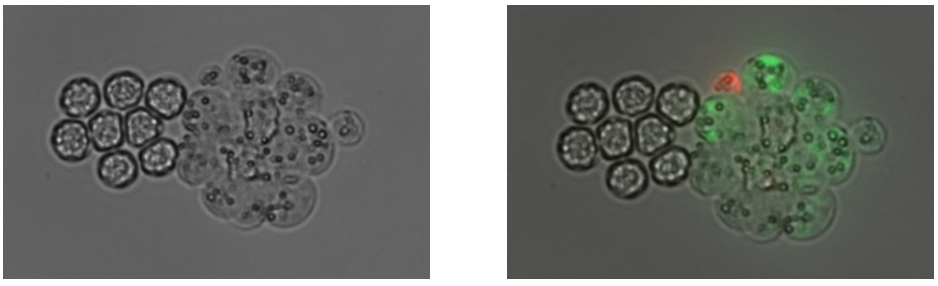

(a) (b)

FIGURE 4.24: Microscope pictures of *Aurantiochytrium* sp. T66 zoosporangium. (a) and (b) show the same capture, where (b) is added fluorescent coloring (Live/Dead Assay L7012 [84]) to investigate the metabolic activity. Green indicates metabolic activity, while red coloring indicates low degree of metabolic activity. Microscope: Zeiss Apotome Imager.Z2 with AxioCam ERc5s

# 5

# Concluding remarks

*Aurantiochytrium* sp. strain T66 was investigated as a potential production host for high lipid-containing biomass, rich in DHA. T66 was cultivated in a top-bench bioreactor and shake-flask cultures, using a glucose-glutamate containing growth medium. Analysis of intracellular lipids, central metabolites, in combination with $^{13}$C-glucose tracers, provided information about the variations between the growth phase, the lipid accumulation phase, and the transition between these phases.

Investigation of the *Aurantiochytrium* sp. strain T66 life-cycle was performed as a consequence of several inoculated bioreactor cultures failing to initiate growth, and a side-project with shake-flask cultures was established to characterize and develop the understanding of the life-cycle stages. A co-existence between vegetative cells and bi-flaggelated zoospores was reported, and the inoculum preparations were improved to introduce more robust and reproducible bioreactor cultivations. Further studies of the life-cycle of strain T66 will be significant for developing DHA producing cell factories.

Establishing robust and reproducible sampling protocols for quantification of intracellular metabolites in thraustochytrids, was a central part of this work. The intracellular metabolites were determined by CapIC-MS for the bioreactor culture and the shake-flask cultures. The metabolic changes emerging from the transition between growth and sole lipid accumulation, as well as the two distinct phases, were investigated to map possible

limiting steps for synthesis of DHA and other fatty acids. Visual comparison between different samples of the bioreactor culture was performed with Omix, and demonstrated that the cytosolic citrate concentration was relatively constant throughout the cultivation. The concentrations of amino acids and nucleic acids decreased considerably from growth to lipid accumulation, and a potential decrease in carbon flow through glycolysis was observed. The latter corresponds well with the observed decrease in glucose uptake from growth to the lipid accumulation phase.

The bioreactor cultivation was operated for 161 hours, with a maximal growth rate of 0.15 $h^{-1}$ during the exponential growth rate. The final biomass concentration was 27 g/l dry cell weight, with a total lipid content of 69%w/w, and DHA (C22:6) constituting 22% of the total fatty acids. The total lipid content increased from 20% to 30% during the exponential growth phase (65-92h), and from 30% to 69% during the lipid accumulation phase. The lipid synthesis rate was constant during the lipid accumulation phase. The lipid productivity of the lipid accumulation phase (92-161h), and the overall productivity, was calculated to 0.263 g lipid/l·h and 0.116 g lipids/l·h, respectively. The lipid yield on glucose, the sole carbon source after glutamate exhaustion, was determined to 73% of the theoretical yield. An overall carbon mass balance was applied to the bioreactor system, with a carbon recovery rate of 84% and 77%, during the exponential growth phase (77-90h) and the lipid accumulation phase (94-161h), respectively. The final concentration of DHA was determined to 2.6 g/l, resulting in an overall productivity of 16 mg DHA/l·h.

Experimental observations suggested that the glucose uptake capacity was not fully utilized during the lipid accumulation phase, which could indicate other limiting mechanisms. Further investigation of potential limiting causes, like enzyme conversion rates and assembly of proteins for the protein-rich membrane surrounding the intracellular lipid reserves, could yield important information for improving the production rate of lipids and DHA. The NADPH and acetyl-CoA concentrations in the growth phase and lipid accumulation phase were measured for a shake-flask culture. The concentration of NADPH increased by a two-fold, while the acetyl-CoA concentration was stable. These results indicate that the fatty acid synthesis was not limited by the availability of NADPH or acetyl-CoA.

The lipid composition changed as the cultivation proceeded from growth, through N-limitation, and into the lipid accumulation phase. Two lipid classes were observed in T66: neutral and polar lipids, with neutral lipids being the largest group. Composition of TAGs, DGs, MGs and polar lipids was determined for the two lipid classes, and TAGs constituted more than 90% of total lipids during the lipid accumulation phase. DGs and MGs comprised around 1% during the same phase. The polar lipids decreased

from about 20% of total lipids, to 5% after N-exhaustion, remaining at 5% throughout the cultivation, demonstrating that polar lipids were synthesized during the lipid accumulation phase.

The absolute amounts (g/l) of all fatty acids, except stearic acid for the two last samplings (143-161h), increased in the bioreactor cultivation. The relative fatty acid contents (% of TFA), changed with the advancing bioreactor cultivation, showing increased levels of PUFAs and MUFAs of total fatty acids. The increase of these fatty acid classes continued throughout the cultivation, comprising 31% and 13% of total fatty acids, for PUFAs and MUFAs, respectively. Palmitic acid (C16:0) was relatively stable at about 35% for the entire cultivation, and the fraction of C16:0 of TFA did not decrease like the other saturated fatty acids after N-limitation. The stearic acid (C18:0) content decreased from 50% to 11% of TFA, in connection with the saturated fatty acids decreasing from 93% to 56% during the same interval. The fatty acid profiles of the shake-flask cultures was compared to the fatty acid profile of the bioreactor culture, showing large variations. Lower fractions of MUFAs and PUFAs, and higher fraction of SFA, in the fatty acids profiles of the shake-flask cultures, was observed. Palmitic acid constituted about 50% of TFA in the shake-flask cultures, and the DHA content was 12-13% of TFA.

Shake-flask cultures with $^{13}$C-labeled glucose substrates, were investigated and compared to shake-flask cultures with only natural glucose. The investigated glucose substrates were 1-$^{13}C_1$-, 1,2-$^{13}C_2$-, and U-$^{13}C_6$-glucose. The labeling patterns were used to distinguish the distribution, and potential branch points, for C-flux towards fatty acid synthesis and DHA production. The $^{13}$C-tracer experiments were analyzed by CapIC programmed to detect isotopologues, which were used for sum fractional labeling (SFL) calculations. The SFL values were used to compare the labeling patterns of the growth phase, the lipid accumulation phase, and synthesis of fatty acids from acetyl-CoA. The results suggested no change between growth and lipid accumulation for the upper glycolysis and pentose phosphate pathway, showing that the glutamate carbon is not incorporated into these pathways. The SFL of selected fatty acids showed that the labeling pattern of myristic acid (C14:0), palmitoleic acid (C16:1), and DHA (C22:6), followed theory. Stearic acid (C18:0) and palmitic acid (C16:0) deviated from theoretically labeling patterns, pointing towards a decreased synthesis after glutamate depletion. However, this result is not fully understood, and further investigations are needed.

The shake-flask cultures containing only natural glucose was used to verify the use of shake-flask cultivations as a model-system for $^{13}$C-experiments of *Aurantiochytrium* sp. strain T66 and their lipid accumulation. The total lipids ranged from 61-65% of dry cell weight, and the consumption of carbon sources, fatty acid profiles, and growth rates, were similar for both shake-flasks containing labeled and natural glucose. Furthermore,

the distribution of fatty acids of the neutral and polar lipids were analyzed by UPC$^2$-MS. The growth rate of the shake-flask cultures were reduced by a three-fold compared to the bioreactor culture. This could be explained by limited aeration, reducing the validity of the experimental data from the $^{13}$C-labeling experiments in shake-flasks. Bioreactor cultivations, where the oxygen supply is strictly monitored, was therefore selected as the optimal experimental procedure for $^{13}$C-tracer analysis of *Aurantiochytrium* sp. strain T66.

# 6

# Future work

Several important aspects regarding the potential high lipid-containing biomass production from *Aurantiochytrium* sp. strain T66 were reported during this MSc Thesis. However, further investigations are vital for increasing the basic knowledge of cell life-cycle, optimal cultivation conditions, and understanding the complex production pattern of lipid biosynthesis. The following bullet-points are important elements for developing thraustochytrids and their DHA production:

- The transition between the growth phase and the lipid accumulation phase is of special interest, because metabolism changes from cellular division to sole lipid accumulation. Furthermore, this transition showed the highest glucose uptake rate; a 2.5 times higher than during lipid accumulation. A more dense time-series of sampling points, and feeding of $^{13}$C-labeled glucose substrates, during this transition, could yield important information expanding the understanding of thraustochytrid metabolism. This combination of metabolome and fluxome analysis, could generate an adamant map of metabolic flux.
- The metabolic flux changes in upper glycolysis and the pentose phosphate pathway was stable from growth through lipid accumulation, suggesting that glutamate carbon is not entering these pathways via anaplerotic reactions. Label experiments with labeled glutamate would therefore be of high interest to validate the fate

of glutamate. This could provide information about glutamate flux through the TCA-cycle, incorporation to fatty acid biosynthesis, or other central metabolites.

- The labeling pattern of palmitic acid (C16:0) and stearic acid (C18:0) is not understood, and further investigations of the labeling pattern of these saturated fatty acids, could provide very important information about the regulation of the PKS and FAS pathways during N-starvation.

- The results provided here indicated that shake-flask cultivations are limited compared to bioreactors, and future $^{13}$C-experiments should therefore be performed in bioreactors to control the aeration. Furthermore, could bioreactor cultivations provide overall carbon balance of the system, which is an important feature of bioreactor cultivations.

# Bibliography


[1] Food and Agriculture Organization of the United Nations. Food outlook - biannual report on global food markets. Technical report, Food and Agriculture Organization Project Department, 2014.

[2] Ana Maria de Oliveira Finco, Luis Daniel Goyzueta Mamani, Júlio Cesar de Carvalho, Gilberto Vinícius de Melo Pereira, Vanete Thomaz-Soccol, and Carlos Ricardo Soccol. Technological trends and market perspectives for production of microbial oils rich in omega-3. *Critical Reviews in Biotechnology*, 37(5):656–671, 2017. PMID: 27653190.

[3] Statistisk sentralbyrå. Jord, skog, jakt og fiskeri - akvakultur, 2016.

[4] Per Bruheim. Microbial production of omega-3 fatty acids - a model based approach, 2017-2021.

[5] Chen F. Fan K. *Bioprocessing for Value-Added Products from Renewable Resources.* Elsevier, 2007.

[6] Adarsha Gupta, Colin J. Barrow, and Munish Puri. Omega-3 biotechnology: Thraustochytrids as a novel source of omega-3 oils. *Biotechnology Advances*, 30(6):1733 – 1745, 2012. Special issue on ACB 2011.

[7] A.P. Simopoulos. Evolutionary aspects of diet, the omega-6/omega-3 ratio and genetic variation: nutritional implications for chronic diseases. *Biomedicine and Pharmacotherapy*, 60(9):502 – 507, 2006. Special Issue for the 50è anniversary of the journal.

[8] Gian Luigi Russo. Dietary n-6 and n-3 polyunsaturated fatty acids: From biochemistry to clinical implications in cardiovascular prevention. *Biochemical Pharmacology*, 77(6):937 – 946, 2009.

[9] Eileen E. Birch, Sharon Garfield, Yolanda Castañeda, Dianna Hughbanks-Wheaton, Ricardo Uauy, and Dennis Hoffman. Visual acuity and cognitive outcomes at 4 years

of age in a double-blind, randomized trial of long-chain polyunsaturated fatty acid-supplemented infant formula. *Early Human Development*, 83(5):279 – 284, 2007.

[10] Barbara J. Meyer, Neil J. Mann, Janine L. Lewis, Greg C. Milligan, Andrew J. Sinclair, and Peter R. C. Howe. Dietary intakes and food sources of omega-6 and omega-3 polyunsaturated fatty acids. *Lipids*, 38(4):391–398, Apr 2003.

[11] L. Sijtsma and M. E. de Swaaf. Biotechnological production and applications of the $\omega$-3 polyunsaturated fatty acid docosahexaenoic acid. *Applied Microbiology and Biotechnology*, 64(2):146–153, Apr 2004.

[12] Inga Marie Aasen, Helga Ertesvåg, Tonje Marita Bjerkan Heggeset, Bin Liu, Trygve Brautaset, Olav Vadstein, and Trond E. Ellingsen. Thraustochytrids as production organisms for docosahexaenoic acid (dha), squalene, and carotenoids. *Applied Microbiology and Biotechnology*, 100(10):4309–4321, May 2016.

[13] Ratledge C. *Single cell oils for the 21th century.* Lipid Research Center UK, 2005.

[14] Stylianos Fakas, Seraphim Papanikolaou, Athanasios Batsos, Maria Galiotou-Panayotou, Athanasios Mallouchos, and George Aggelis. Evaluating renewable carbon sources as substrates for single cell oil production by cunninghamella echinulata and mortierella isabellina. *Biomass and Bioenergy*, 33(4):573 – 580, 2009.

[15] Denver J. Pyle, Rafael A. Garcia, and Zhiyou Wen. Producing docosahexaenoic acid (dha)-rich algae from biodiesel-derived crude glycerol: Effects of impurities on dha production and algal biomass composition. *Journal of Agricultural and Food Chemistry*, 56(11):3933–3939, 2008. PMID: 18465872.

[16] Anita N. Jakobsen, Inga M. Aasen, Kjell D. Josefsen, and Arne R. Strøm. Accumulation of docosahexaenoic acid-rich lipid in thraustochytrid aurantiochytrium sp. strain t66: effects of n and p starvation and o2 limitation. *Applied Microbiology and Biotechnology*, 80(2):297, Jun 2008.

[17] I. Voss and A. Steinbüchel. High cell density cultivation of rhodococcus opacus for lipid production at a pilot-plant scale. *Applied Microbiology and Biotechnology*, 55(5):547–555, May 2001.

[18] Ana Mendes, Alberto Reis, Rita Vasconcelos, Pedro Guerra, and Teresa Lopes da Silva. Crypthecodinium cohnii with emphasis on dha production: a review. *Journal of Applied Phycology*, 21(2):199–214, Apr 2009.

[19] T. Yokochi, D. Honda, T. Higashihara, and T. Nakahara. Optimization of docosahexaenoic acid production by schizochytrium limacinum sr21. *Applied Microbiology and Biotechnology*, 49(1):72–76, Jan 1998.

[20] C Shene, A Leyton, Y. Esparza, L Flores, B QuilodrÃ¡n, I Hinzpeter, and M Rubilar. Microbial oils and fatty acids: Effect of carbon source on docosahexaenoic acid (c22:6 n-3, dha) production by thraustochytrid strains. *Journal of soil science and plant nutrition*, 10:207 – 216, 07 2010.

[21] P. K. Bajpai, P. Bajpai, and O. P. Ward. Optimization of production of docosahexaenoic acid (dha) bythraustochytrium aureum atcc 34304. *Journal of the American Oil Chemists' Society*, 68(7):509–514, Jul 1991.

[22] Simen Liberg Tronsaune. Comparison of glucose and glycerol as carbon source for omega-3 production in *Aurantiochytrium* sp. t66. *TBT4505 - Specialization Project*, 2017.

[23] M. Sprague, J. Walton, P.J. Campbell, F. Strachan, J.R. Dick, and J.G. Bell. Replacement of fish oil with a dha-rich algal meal derived from schizochytrium sp. on the fatty acid and persistent organic pollutant levels in diets and flesh of atlantic salmon (salmo salar, l.) post-smolts. *Food Chemistry*, 185:413 – 421, 2015.

[24] Ming-Hua Liang and Jian-Guo Jiang. Advancing oleaginous microorganisms to produce lipid via metabolic engineering technology. *Progress in Lipid Research*, 52(4):395 – 408, 2013.

[25] Royal Dutch State Mines (DSM). Global nutrient and health supplier, former martek biosciences corporation.

[26] Chih-Hung Hsieh and Wen-Teng Wu. Cultivation of microalgae for oil production with a cultivation strategy of urea limitation. *Bioresource Technology*, 100(17):3921 – 3926, 2009.

[27] Yonghong Li, Zongbao (Kent) Zhao, and Fengwu Bai. High-density cultivation of oleaginous yeast rhodosporidium toruloides y4 in fed-batch culture. *Enzyme and Microbial Technology*, 41(3):312 – 317, 2007.

[28] Kazuhiko Kurosawa, Paolo Boccazzi, Naomi M. de Almeida, and Anthony J. Sinskey. High-cell-density batch fermentation of rhodococcus opacus pd630 using a high glucose concentration for triacylglycerol production. *Journal of Biotechnology*, 147(3):212 – 218, 2010.

[29] Ana Arabolaza, Eduardo Rodriguez, Silvia Altabe, Hector Alvarez, and Hugo Gramajo. Multiple pathways for triacylglycerol biosynthesis in streptomyces coelicolor. *Applied and environmental microbiology*, 74(9):2573—2582, May 2008.

[30] Kavita P. Patil and Parag R. Gogate. Improved synthesis of docosahexaenoic acid (dha) using schizochytrium limacinum sr21 and sustainable media. *Chemical Engineering Journal*, 268:187 – 196, 2015.

[31] Lina Sun, Lujing Ren, Xiaoyan Zhuang, Xiaojun Ji, Jiacheng Yan, and He Huang. Differential effects of nutrient limitations on biochemical constituents and docosahexaenoic acid production of schizochytrium sp. *Bioresource Technology*, 159:199 – 206, 2014.

[32] Jonathan A. Foley Jason Hill Eric Larson Lee Lynd Stephen Pacala John Reilly Tim Searchinger Chris Somerville David Tilman, Robert Socolow and Robert Williams. Beneficial biofuels - the food, energy, and environment trilemma. *Science*, 325:270–271, 2009.

[33] Pauline Spolaore, Claire Joannis-Cassan, Elie Duran, and Arsène Isambert. Commercial applications of microalgae. *Journal of Bioscience and Bioengineering*, 101(2):87 – 96, 2006.

[34] Svetlana V. Khotimchenko and Irina M. Yakovleva. Lipid composition of the red alga tichocarpus crinitus exposed to different levels of photon irradiance. *Phytochemistry*, 66(1):73 – 79, 2005.

[35] Susan M Renaud, Luong-Van Thinh, George Lambrinidis, and David L Parry. Effect of temperature on growth, chemical composition and fatty acid composition of tropical australian microalgae grown in batch cultures. *Aquaculture*, 211(1):195 – 214, 2002.

[36] A.M Illman, A.H Scragg, and S.W Shales. Increase in chlorella strains calorific values when grown in low nitrogen medium. *Enzyme and Microbial Technology*, 27(8):631 – 635, 2000.

[37] Mutsumi Takagi, Karseno, and Toshiomi Yoshida. Effect of salt concentration on intracellular accumulation of lipids and triacylglyceride in marine microalgae dunaliella cells. *Journal of Bioscience and Bioengineering*, 101(3):223 – 226, 2006.

[38] King-Wai Fan, Yue Jiang, Lok-Tang Ho, and Feng Chen. Differentiation in fatty acid profiles of pigmented and nonpigmented aurantiochytrium isolated from hong kong mangroves. *Journal of Agricultural and Food Chemistry*, 57(14):6334–6341, 2009. PMID: 19534536.

[39] T. Yaguchi, S. Tanaka, T. Yokochi, T. Nakahara, and T. Higashihara. Production of high yields of docosahexaenoic acid by schizochytrium sp. strain sr21. *Journal of the American Oil Chemists' Society*, 74(11):1431–1434, Nov 1997.

[40] Zu yi Li and O. P. Ward. Production of docosahexaenoic acid bythraustochytrium roseum. *Journal of Industrial Microbiology*, 13(4):238–241, Jul 1994.

[41] Loris Fossier Marchan. Screening fatty acid composition of british heterotrophic microalgae thraustochytrids for production of omega-3 oils and biodiesel. *New Biotechnology*, 33:S91, 2016. Abstracts of the 17th European Congress on Biotechnology.

[42] R. M. Bennett, D. Honda, G. W. Beakes, and M. Thines. *Labyrinthulomycota*, pages 1–36. Springer International Publishing, Cham, 2017.

[43] Izumi Iwata, Kei Kimura, Yuji Tomaru, Taizo Motomura, Kanae Koike, Kazuhiko Koike, and Daiske Honda. Bothrosome formation in schizochytrium aggregatum (labyrinthulomycetes, stramenopiles) during zoospore settlement. *Protist*, 168(2):206 – 219, 2017.

[44] Michael W. Dick. *Systematics*, pages 267–432. Springer Netherlands, Dordrecht, 2001.

[45] Lucia Bongiorni, Ruchi Jain, Seshagiri Raghukumar, and Ramesh Kumar Aggarwal. Thraustochytrium gaertnerium sp. nov.: a new thraustochytrid stramenopilan protist from mangroves of goa, india. *Protist*, 156(3):303 – 315, 2005.

[46] A. Ashford, W. R. Barclay, C. A. Weaver, T. H. Giddings, and S. Zeller. Electron microscopy may reveal structure of docosahexaenoic acid-rich oil within schizochytrium sp. *Lipids*, 35(12):1377–1387, Dec 2000.

[47] Kendrick Andrew and Ratledge Colin. Lipids of selected molds grown for production of n3 and n6 polyunsaturated fatty acids. *Lipids*, 27(1):15–20, 1992.

[48] Jianzhong Huang, Tsunehiro Aki, Kazutaka Hachida, Toshihiro Yokochi, Seiji Kawamoto, Seiko Shigeta, Kazuhisa Ono, and Osamu Suzuki. Profile of polyunsaturated fatty acids produced by thraustochytrium sp. kk17-3. *Journal of the American Oil Chemists' Society*, 78(6):605–610, Jun 2001.

[49] T. Nakahara, T. Yokochi, T. Higashihara, S. Tanaka, T. Yaguchi, and D. Honda. Production of docosahexaenoic and docosapentaenoic acids byschizochytrium sp. isolated from yap islands. *Journal of the American Oil Chemists' Society*, 73(11):1421–1426, Nov 1996.

[50] Colin Ratledge. Fatty acid biosynthesis in microorganisms being used for single cell oil production. *Biochimie*, 86(11):807 – 815, 2004. Recent advances in lipid metabolism and related disorders.

[51] James G. Metz, Paul Roessler, Daniel Facciotti, Charlene Levering, Franziska Dittrich, Michael Lassner, Ray Valentine, Kathryn Lardizabal, Frederic Domergue, Akiko Yamada, Kazunaga Yazawa, Vic Knauf, and John Browse. Production of

polyunsaturated fatty acids by polyketide synthases in both prokaryotes and eukaryotes. *Science*, 293(5528):290–293, 2001.

[52] J. Casey Lippmeier, Kristine S. Crawford, Carole B. Owen, Angie A. Rivas, James G. Metz, and Kirk E. Apt. Characterization of both polyunsaturated fatty acid biosynthetic pathways in schizochytrium sp. *Lipids*, 44(7):621–630, Jul 2009.

[53] Colin Ratledge and Casey Lippmeier. Chapter 7 - microbial production of fatty acids. In Moghis U. Ahmad, editor, *Fatty Acids*, pages 237 – 278. AOCS Press, 2017.

[54] Colin Ratledge. The role of malic enzyme as the provider of nadph in oleaginous microorganisms: a reappraisal and unsolved problems. *Biotechnology Letters*, 36(8):1557–1568, Aug 2014.

[55] David L. Nelson and Michael M. Cox. *Principles of Biochemistry*. W.H. Freeman and Company, 2013.

[56] Jiancai Wang, Ronghua Xu, Ruling Wang, Mohammad Enamul Haque, and Aizhong Liu. Overexpression of acc gene from oleaginous yeast lipomyces starkeyi enhanced the lipid accumulation in saccharomyces cerevisiae with increased levels of glycerol 3-phosphate substrates. *Bioscience, Biotechnology, and Biochemistry*, 80(6):1214–1222, 2016. PMID: 26865376.

[57] Ruchi Jain, Seshagiri Raghukumar, Kari Sambaiah, Yasuyuki Kumon, and Toro Nakahara. Docosahexaenoic acid accumulation in thraustochytrids: search for the rationale. *Marine Biology*, 151(5):1657–1664, Jun 2007.

[58] Nielsen J. Kerkhoven E., Lathvee P. Applications of computational modeling in metabolic engineering of yeast. *FEMS Yeast Research*, 2014.

[59] Adam M. Burja, Helia Radianingtyas, Anthony Windust, and Colin J. Barrow. Isolation and characterization of polyunsaturated fatty acid producing thraustochytrium species: screening of strains and optimization of omega-3 production. *Applied Microbiology and Biotechnology*, 72(6):1161, Apr 2006.

[60] Inga Marie Aasen. Supervisor, SINTEF Materials and Chemistry - Biotechnology and Nanomedisin.

[61] Lucchini S *et. al* Rolfe MD, Rice CJ. Lag phase is a distinct growth phase that prepares bacteria for exponential growth and involves transient metal accumulation. *Journal of Bacteriology*, 194(3):686–701, 2012.

[62] Martin D.S. The oxygen consumption of escherichia coli during the lag and logarithmic phases of growth. *The Journal of General Physiology*, 15(6):691–708, 1932.

[63] Violeta Ugalde, Roberto E. Armenta, Azadeh Kermanshahi-pour, Zhiyong Sun, Kevin T. Berryman, and Marianne S. Brooks. Improvement of culture conditions for cell biomass and fatty acid production by marine thraustochytrid f24-2. *Journal of Applied Phycology*, 30(1):329–339, Feb 2018.

[64] Andrew Kendrick and Colin Ratledge. Lipids of selected molds grown for production of n-3 and n-6 polyunsaturated fatty acids. *Lipids*, 27(1):15–20, Jan 1992.

[65] Benita Quilodrán, Ivonne Hinzpeter, Emilio Hormazabal, Andrés Quiroz, and Carolina Shene. Docosahexaenoic acid (c22:6n-3, dha) and astaxanthin production by thraustochytriidae sp. as4-a1 a native strain with high similitude to ulkenia sp.: Evaluation of liquid residues from food industry as nutrient sources. *Enzyme and Microbial Technology*, 47(1):24 – 30, 2010.

[66] Arief Budiyanto, Nazim U. Ahmed, An Wu, Toshinori Bito, Osamu Nikaido, Toshihiko Osawa, Masato Ueda, and Masamitsu Ichihashi. Protective effect of topically applied olive oil against photocarcinogenesis following uvb exposure of mice. *Carcinogenesis*, 21(11):2085–2090, 2000.

[67] Hans F. N. Kvitvang, Trygve Andreassen, Tomas Adam, Silas G. Villas-Bôas, and Per Bruheim. Highly sensitive gc/ms/ms method for quantitation of amino and nonamino organic acids. *Analytical Chemistry*, 83(7):2705–2711, 2011. PMID: 21388201.

[68] Hans F.N. Kvitvang, Kåre A. Kristiansen, and Per Bruheim. Assessment of capillary anion exchange ion chromatography tandem mass spectrometry for the quantitative profiling of the phosphometabolome and organic acids in biological extracts. *Journal of Chromatography A*, 1370:70 – 79, 2014.

[69] Marit H. Stafsnes, Lisa M. Røst, and Per Bruheim. Improved phosphometabolome profiling applying isotope dilution strategy and capillary ion chromatography-tandem mass spectrometry. *Journal of Chromatography B*, 1083:278 – 283, 2018.

[70] Per Bruheim. Supervisor, NTNU Institute of Biotechnology and Food Science.

[71] Pauline M. Doran. *Bioprocess Engineering Principles*. Elsevier, 2013.

[72] Kelly Bender Daniel Buckley Michael Madigan, John Martinko and David Stahl. *Brock Biology of Microorganisms*. Pearson, 2015.

[73] Eiko Morita, Yasuyuki Kumon, Toro Nakahara, Satoshi Kagiwada, and Tetsuko Noguchi. Docosahexaenoic acid production and lipid-body formation in schizochytrium limacinum sr21. *Marine Biotechnology*, 8(3):319–327, Jun 2006.

[74] Sabine Cohen, Lars P. Jordheim, Mehdi Megherbi, Charles Dumontet, and Jérôme Guitton. Liquid chromatographic methods for the determination of endogenous nucleotides and nucleotide analogs used in cancer therapy: A review. *Journal of Chromatography B*, 878(22):1912 – 1928, 2010.

[75] Silas Granato Villas-Boas and Per Bruheim. The potential of metabolomics tools in bioremediation studies. *Omics - J. Intgr. Biol.*, 11:305–313, 2007.

[76] Daniel E. Atkinson. Energy charge of the adenylate pool as a regulatory parameter. interaction with feedback modifiers. *Biochemistry*, 7(11):4030–4034, 1968. PMID: 4972613.

[77] Maciek R. Antoniewicz, Joanne K. Kelleher, and Gregory Stephanopoulos. Elementary metabolite units (emu): A novel framework for modeling isotopic distributions. *Metabolic Engineering*, 9(1):68 – 86, 2007.

[78] Woo Suk Ahn and Maciek R. Antoniewicz. Parallel labeling experiments with [1,2-13c]glucose and [u-13c]glutamine provide new insights into cho cell metabolism. *Metabolic Engineering*, 15:34 – 47, 2013.

[79] Christensen Bjarke, Karoly Gombert Andreas, and Nielsen Jens. Analysis of flux estimates based on 13c-labelling experiments. *European Journal of Biochemistry*, 269(11):2795–2800, 2002.

[80] Boros LG et al. Buescher JM, Antoniewicz MR. A roadmap for interpreting 13c metabolite labeling patterns from cells. *Current opinion in biotechnology.*, 34:189–201, 2015.

[81] Scott B. Crown, Woo Suk Ahn, and Maciek R. Antoniewicz. Rational design of 13c-labeling experiments for metabolic flux analysis in mammalian cells. *BMC Systems Biology*, 6(1):43, May 2012.

[82] Christopher T. Evans and Colin Ratledge. Effect of nitrogen source on lipid accumulation in oleaginous yeasts. *Microbiology*, 130(7):1693–1704, 1984.

[83] Svante Wold, Kim Esbensen, and Paul Geladi. Principal component analysis. *Chemometrics and Intelligent Laboratory Systems*, 2(1):37 – 52, 1987. Proceedings of the Multivariate Statistical Workshop for Geologists and Geochemists.

[84] Molecular Probes. Live/dead baclight viability kits. 2004.

[85] E.G. Bligh and W.J. Dyer. A rapid method of total lipid extraction and purification. *Canadian Journal of Biochemistry and Physiology*, 37:911–917, 1959.

[86] Fabrice Pernet, Claude J. Pelletier, and Joyce Milley. Comparison of three solid-phase extraction methods for fatty acid analysis of lipid fractions in tissues of marine bivalves. *Journal of Chromatography A*, 1137(2):127 – 137, 2006.

[87] Silje Malene Olsen. Researcher at NTNU Institute of Biotechnology and Food Science.

[88] Bo Tan, Zhaohai Lu, Sucai Dong, Genshi Zhao, and Ming-Shang Kuo. Derivatization of the tricarboxylic acid intermediates with o-benzylhydroxylamine for liquid chromatography–tandem mass spectrometry detection. *Analytical Biochemistry*, 465:134 – 147, 2014.

[89] Lisa Marie Røst. Ph.d candidate at NTNU Institute of Biotechnology and Food Science.

[90] Kim Jye Lee Chang, Geoff Dumsday, Peter D. Nichols, Graeme A. Dunstan, Susan I. Blackburn, and Anthony Koutoulis. High cell density cultivation of a novel aurantiochytrium sp. strain tc 20 in a fed-batch system using glycerol to produce feedstock for biodiesel and omega-3 oils. *Applied Microbiology and Biotechnology*, 97(15):6907–6918, Aug 2013.

[91] Panida Unagul, Caetharin Assantachai, Saranya Phadungruengluij, Manop Suphantharika, Morakot Tanticharoen, and Cornelis Verduyn. Coconut water as a medium additive for the production of docosahexaenoic acid (c22:6 n3) by schizochytrium mangrovei sk-02. *Bioresource Technology*, 98(2):281 – 287, 2007.

[92] A. Singh and O. P. Ward. Production of high yields of docosahexaenoic acid bythraustochytrium roseum atcc 28210. *Journal of Industrial Microbiology*, 16(6):370–373, Jun 1996.

[93] Takashi Yamasaki, Tsunehiro Aki, Masami Shinozaki, Masahiro Taguchi, Seiji Kawamoto, and Kazuhisa Ono. Utilization of shochu distillery wastewater for production of polyunsaturated fatty acids and xanthophylls using thraustochytrid. *Journal of Bioscience and Bioengineering*, 102(4):323 – 327, 2006.

# A

# Additional Medium Components

## A.1 Vitamin mix

The vitamin mix was prepared by dissolving the listed components (Table A.1) in deionized water to a total volume of 500 ml. The solution was separated into smaller volumes and stored at -20 °C. The vitamin mix was sterile filtered prior to addition.

Table A.1: Vitamin mix used during cultivation and fermentation of T66

| **Vitamin** | **(mg/l)** |
|---|---|
| Biotin | 5 |
| B12 (cobalamine) | 5 |
| Folic acid | 100 |
| Calcium-panthotenat | 100 |
| Thiamin-HCl | 200 |

## A.2 TMS-6

TMS-6 is a mixture of trace minerals and some components which are necessary for the thraustochytrids during the fermentation. The solution was prepared by SINTEF Materials and Chemistry. The components of TMS-6 is shown in Table A.2 below.

TABLE A.2: Components of TMS-6 with corresponding concentration. 50 ml of 37 % HCl was added to the solution. All components were dissolved in deionized water.

| **Chemical component** | **(mg/l)** |
|---|---|
| $FeSO_4 \cdot 7H_2O$ | 50 000 |
| $CuSO_4 \cdot 5H_2O$ | 3900 |
| $ZnSO_4 \cdot 7H_2O$ | 4400 |
| $MnSO_4 \cdot H_2O$ | 1500 |
| $Na_2MoO_4 \cdot 2H_2O$ | 100 |
| $CoCl_2 \cdot 6H_2O$ | 200 |
| HCl | 50 ml |

# B

# Primary Data

All primary data is not listed here, but stored electronically, and accessible upon request. Please contact Professor Per Bruheim at per.bruheim@ntnu.no for access.

Some primary data is included here, as supplementary information to the data provided in Section Results and Discussion 4.

## B.1 Supplementary bioreactor culture data

Table B.1 shows optical density (OD), dry cell weight (g/l), lipid content (TL, % of DCW), and fatty acid content (TFA, g/l), measured for the bioreactor cultivation of *Aurantiochytrium* sp. strain T66, as described in section Materials and Methods 3.

TABLE B.1: Total fatty acids (TFA), lipid content (TL) and DHA, with corresponding DCW for fermentation with glucose.

| **Time (h)** | **DCW (g/l)** | **TFA (g/l)** | **TL (g/l)** | **DHA (g/l)** | **TFA (%w/w)**[1] | **TL (%w/w)**[1] | **DHA (%w/w)**[2] |
|---|---|---|---|---|---|---|---|
| 76.9 | 1.3 | 1.9 | 0.4 | 0.01 | 146 | 23 | 4 |
| 87.5 | 6.3 | 3.0 | 1.4 | 0.3 | 48 | 22 | 12 |
| 89.9 | 8.8 | 3.1 | 2.0 | 0.4 | 35 | 23 | 12 |
| 94.4 | 10.7 | 3.9 | 3.4 | 0.5 | 36 | 32 | 12 |
| 113.3 | 16.4 | 6.5 | 8.6 | 1.3 | 40 | 53 | 19 |
| 116.6 | 17.4 | 7.6 | 8.7 | 1.4 | 44 | 50 | 18 |
| 138.6 | 22.4 | 10.1 | 15.2 | 2.2 | 45 | 68 | 22 |
| 143.1 | 23.6 | 10.4 | 15.1 | 2.2 | 44 | 64 | 21 |
| 160.8 | 27.3 | 12.2 | 18.8 | 2.6 | 45 | 69 | 22 |

[1] Weight fraction of dry cell weight (DCW)
[2] Weight fraction of total fatty acids (TFA)

### B.1.1 Fatty acid data from the bioreactor culture

TABLE B.2: Fatty acid (FA) fractions of total fatty acids (% of TFA) for *Aurantiochytrium* sp. strain T66 from a top-bench bioreactor culture.

| **FA** | **76.9h** | **87.5h** | **89.9h** | **94.4h** | **113.3h** | **116.6h** | **138.6h** | **143.1h** | **160.8h** |
|---|---|---|---|---|---|---|---|---|---|
| C14:0 | 2.3 | 4.0 | 4.2 | 6.2 | 10.1 | 10.7 | 10.9 | 11.9 | 12.4 |
| C15:0 | 0.2 | 0.3 | 0.2 | 0.2 | 0.3 | 0.3 | 0.3 | 0.3 | 0.3 |
| C16:0 | 38.1 | 35.4 | 34.6 | 35.3 | 33.9 | 34.9 | 33.1 | 33.7 | 32.8 |
| C16:1 | 0.1 | 0.2 | 0.3 | 1.5 | 4.0 | 4.6 | 5.6 | 6.7 | 8.0 |
| C17:0 | 0.7 | 0.5 | 0.5 | 0.5 | 0.3 | 0.3 | 0.2 | 0.2 | 0.2 |
| C17:1 | 0.0 | 0.0 | 0.0 | 0.0 | 0.0 | 0.0 | 0.0 | 0.0 | 0.0 |
| C18:0 | 51.8 | 43.0 | 44.0 | 37.8 | 21.5 | 19.6 | 15.7 | 12.4 | 10.8 |
| C18:1 | 0.8 | 0.6 | 0.7 | 1.2 | 2.7 | 2.8 | 3.6 | 3.9 | 4.5 |
| C18:2 | 0.1 | 0.1 | 0.1 | 0.1 | 0.0 | 0.0 | 0.0 | 0.0 | 0.0 |
| C20:5 | 0.1 | 0.3 | 0.3 | 0.3 | 0.4 | 0.4 | 0.4 | 0.5 | 0.4 |
| C22:5 | 1.4 | 3.7 | 3.3 | 4.6 | 7.4 | 8.0 | 8.5 | 9.1 | 9.0 |
| C22:6 | 4.3 | 11.9 | 11.7 | 12.3 | 19.4 | 18.4 | 21.7 | 21.3 | 21.6 |

TABLE B.3: Isotopologues of myristic acid (C14:0) for each of the shake-flask cultures. All values are shown as relative values, and the sum of 12C (M) and all corresponding isotopologues (M+n, n=1-14) is shown in the last row. (-) is equal to not detected.

| **Fatty acids** | **SF-C1** | **SF-C2** | **SF-1-13C** | **SF-1,2-13C** | **SF-U-13C** |
|---|---|---|---|---|---|
| 12C (M) | 2.84 | 3.42 | 0.42 | 0.25 | 0.24 |
| M+1 | 0.28 | 0.36 | 0.54 | 0.05 | - |
| M+2 | - | - | 1.1 | 0.2 | - |
| M+3 | - | - | 1.0 | 0.3 | - |
| M+4 | - | - | 0.6 | 0.6 | - |
| M+5 | - | - | 0.2 | 0.5 | - |
| M+6 | - | - | - | 0.6 | - |
| M+7 | - | - | - | 0.4 | - |
| M+8 | - | - | - | 0.3 | - |
| M+9 | - | - | - | 0.2 | - |
| M+10 | - | - | - | 0.1 | 0.1 |
| M+11 | - | - | - | - | 0.1 |
| M+12 | - | - | - | - | 0.6 |
| M+13 | - | - | - | - | 0.6 |
| M+14 | - | - | - | - | 2.6 |
| **Sum** | 3.1 | 3.8 | 4.0 | 3.5 | 4.3 |

## B.2 Isotopologue data from shake-flask cultures grown on $^{13}$C-glucose substrates

The data provided in Table B.3-B.7 is relative concentrations, of $^{12}$C (M) and all isotopologues M+n, n=1 to number of carbons in fatty acid acyl-chain, for myristic acid (C14:0), palmitic acid (C16:0), palmitoleic acid (C16:1), stearic acid (C18:0), and docohecxaenoic acid (DHA, C22:6).

TABLE B.4: Isotopologues of palmitic acid (C16:0) for each of the shake-flask cultures. All values are shown as relative values, and the sum of 12C (M) and all corresponding isotopologues (M+n, n=1-16) is shown in the last row. (-) is equal to not detected.

| **Fatty acids** | **SF-C1** | **SF-C2** | **SF-1-13C** | **SF-1,2-13C** | **SF-U-13C** |
|---|---|---|---|---|---|
| 12C (M) | 23.2 | 27.3 | 15.4 | 12.9 | 15.7 |
| M+1 | 3.4 | 4.2 | 3.9 | 2.1 | 2.3 |
| M+2 | 0.2 | 0.2 | 2.6 | 0.6 | 0.1 |
| M+3 | - | - | 2.7 | 0.7 | - |
| M+4 | - | - | 2.4 | 1.3 | - |
| M+5 | - | - | 1.1 | 1.5 | - |
| M+6 | - | - | 0.3 | 1.5 | - |
| M+7 | - | - | - | 1.4 | - |
| M+8 | - | - | - | 1.3 | - |
| M+9 | - | - | - | 0.5 | - |
| M+10 | - | - | - | 0.6 | 0.2 |
| M+11 | - | - | - | 0.2 | 0.1 |
| M+12 | - | - | - | 0.1 | 0.6 |
| M+13 | - | - | - | - | 0.6 |
| M+14 | - | - | - | - | 2.1 |
| M+15 | - | - | - | - | 1.4 |
| M+16 | - | - | - | - | 2.6 |
| **Sum** | 26.7 | 31.7 | 28.4 | 24.4 | 25.8 |

TABLE B.5: Isotopologues of palmitoleic acid (C16:1) for each of the shake-flask cultures. All values are shown as relative values, and the sum of 12C (M) and all corresponding isotopologues (M+n, n=1-16) is shown in the last row. (-) is equal to not detected.

| **Fatty acids** | **SF-C1** | **SF-C2** | **SF-1-13C** | **SF-1,2-13C** | **SF-U-13C** |
|---|---|---|---|---|---|
| 12C (M) | 1.3 | 1.5 | - | - | - |
| M+1 | - | - | - | - | - |
| M+2 | - | - | - | - | - |
| M+3 | - | - | - | - | - |
| M+4 | - | - | 0.1 | - | - |
| M+5 | - | - | - | 0.1 | - |
| M+6 | - | - | - | - | - |
| M+7 | - | - | - | - | - |
| M+8 | - | - | - | 0.1 | - |
| M+9 | - | - | - | - | - |
| M+10 | - | - | - | - | - |
| M+11 | - | - | - | - | - |
| M+12 | - | - | - | - | - |
| M+13 | - | - | - | - | - |
| M+14 | - | - | - | - | 0.1 |
| M+15 | - | - | - | - | 0.1 |
| M+16 | - | - | - | - | 0.7 |
| **Sum** | 1.3 | 1.6 | 0.2 | 0.3 | 1.0 |

TABLE B.6: Isotopologues of stearic acid (C18:0) for each of the shake-flask cultures. All values are shown as relative values, and the sum of 12C (M) and all corresponding isotopologues (M+n, n=1-18) is shown in the last row. (-) is equal to not detected.

| **Fatty acids** | **SF-C1** | **SF-C2** | **SF-1-13C** | **SF-1,2-13C** | **SF-U-13C** |
|---|---|---|---|---|---|
| 12C (M) | 10.1 | 12.8 | 10.6 | 8.9 | 10.6 |
| M+1 | 1.6 | 2.1 | 2.1 | 1.7 | 2.0 |
| M+2 | 0.1 | 0.2 | 0.2 | 0.1 | 0.2 |
| M+3 | - | - | - | - | - |
| M+4 | - | - | - | 0.3 | - |
| M+5 | - | - | - | - | - |
| M+6 | - | - | 0.2 | 0.4 | - |
| M+7 | - | - | 0.1 | 0.3 | - |
| M+8 | - | - | - | - | - |
| M+9 | - | - | - | - | - |
| M+10 | - | - | - | - | - |
| M+11 | - | - | - | - | - |
| M+12 | - | - | - | - | - |
| M+13 | - | - | - | - | - |
| M+14 | - | - | - | - | 0.3 |
| M+15 | - | - | - | - | 0.3 |
| M+16 | - | - | - | - | 1.0 |
| M+17 | - | - | - | - | - |
| M+18 | - | - | - | - | - |
| **Sum** | 11.8 | 15.0 | 13.2 | 11.5 | 14.3 |

TABLE B.7: Isotopologues of docohexaenoic acid (DHA,C22:6) for each of the shake-flask cultures. All values are shown as relative values, and the sum of 12C (M) and all corresponding isotopologues (M+n, n=1-22) is shown in the last row. (-) is equal to not detected.

| **Fatty acids** | **SF-C1** | **SF-C2** | **SF-1-13C** | **SF-1,2-13C** | **SF-U-13C** |
|---|---|---|---|---|---|
| 12C (M) | 6.4 | 7.0 | - | - | - |
| M+1 | 1.3 | 1.4 | 0.2 | - | - |
| M+2 | 2.4 | 2.5 | 0.8 | - | - |
| M+3 | 0.4 | 0.5 | 1.5 | - | - |
| M+4 | - | - | 2.2 | 0.1 | - |
| M+5 | - | - | 1.9 | 0.2 | - |
| M+6 | - | - | 2.2 | 0.9 | - |
| M+7 | - | - | 0.9 | 0.9 | - |
| M+8 | - | - | 0.1 | 1.0 | - |
| M+9 | - | - | - | 0.6 | - |
| M+10 | - | - | - | 1.2 | - |
| M+11 | - | - | - | 0.8 | - |
| M+12 | - | - | - | 1.0 | - |
| M+13 | - | - | - | 0.5 | - |
| M+14 | - | - | - | 0.2 | - |
| M+15 | - | - | - | - | - |
| M+16 | - | - | - | - | 0.1 |
| M+17 | - | - | - | - | - |
| M+18 | - | - | - | - | 0.4 |
| M+19 | - | - | - | - | 0.5 |
| M+20 | - | - | - | - | 1.5 |
| M+21 | - | - | - | - | 1.7 |
| M+22 | - | - | - | - | 3.7 |
| **Sum** | 10.6 | 11.4 | 9.9 | 7.3 | 7.9 |

# C

# Optical Density

The optical density (OD) was measured throughout the cultivation of the bioreactor culture and the shake-flask cultures. OD was measured at 660 nm, and was used for establishing a correlation between OD and dry cell weight (DCW) for later use to monitor growth.

## C.1 Optical density of the bioreactor culture

Table C.1 shows OD and DCW measured for each sample. Figure C.1 show OD plotted versus DCW and time.

TABLE C.1: Optical density measurements at 660 nm for the bioreactor culture.

| **Sample time (h)** | **Optical density (OD, 660 nm)** |
|---|---|
| 76.9 | 1.4 |
| 87.5 | 12.8 |
| 89.9 | 9.3 |
| 94.4 | 11.9 |
| 113.3 | 26.7 |
| 116.6 | 29.3 |
| 138.6 | 34.5 |
| 143.1 | 30.2 |
| 160.8 | 40.4 |

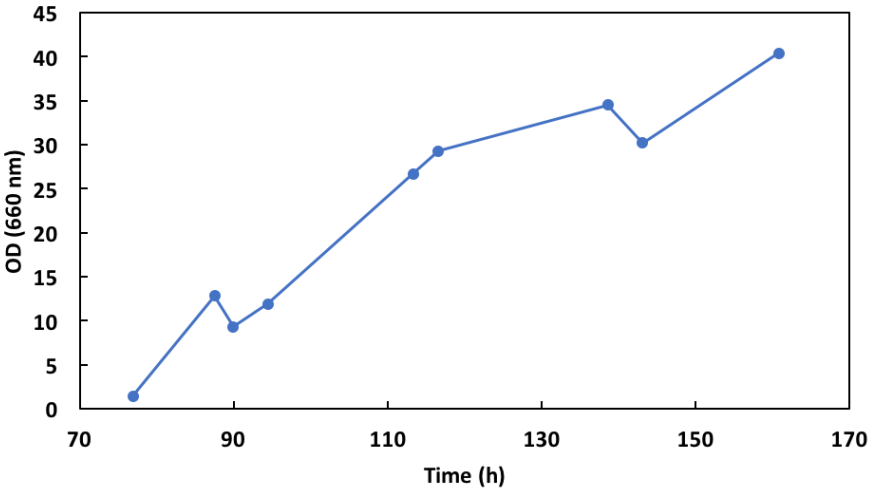


(a) OD versus time

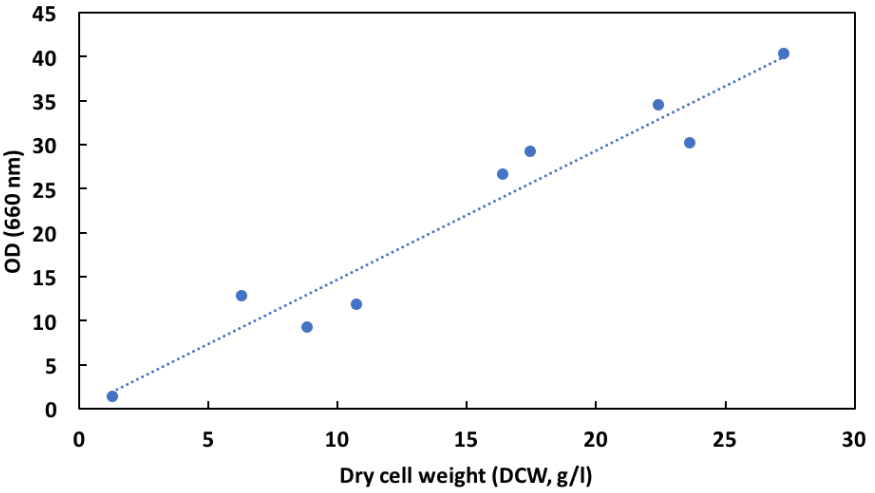


(b) OD versus dry cellular weight

FIGURE C.1: Optical density versus time and dry cellular weight (DCW) for the bioreactor culture. Trend line C.1b) of OD vs. DCW: y = 1.47x, $R^2$ = 0.94.

## C.2 Optical density of $^{13}C$ shake-flask cultures

SF-C3 was used for establishing a optical density curve, which can be used to monitor the growth of the investigated cellular system is shake-flask cultivations. Table C.2 below shows the measured OD throughout the fermentation of SF-C3. The resulting Figure is shown in C.2.

TABLE C.2: Development of optical density (OD, 660 nm) for shake-flask culture of control 3 (SF-C3).

| **Time (h)** | **OD (660 nm)** |
|---|---|
| 0 | 0.3 |
| 20.5 | 1.4 |
| 22.8 | 1.8 |
| 24.3 | 2.1 |
| 20.8 | 3.3 |
| 43.1 | 5.8 |
| 44.3 | 6.1 |
| 67.0 | 8.1 |
| 73.5 | 7.8 |

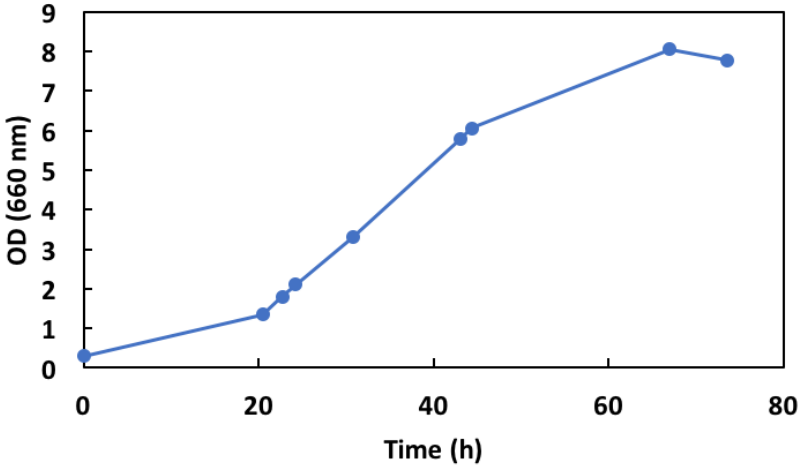


FIGURE C.2: Development of optical density (OD, 660 nm) versus time (h) of shake flask control 3 (SF-C3).

# D

# Carbon Balance of the Bioreactor Culture

This calculations are based on the assumption of the *Aurantiochytrium* sp. T66 cells being Black-boxes, as discussed in 2.5.1. The carbon balance is divided between the growth phase and the lipid accumulation phase. The growth phase is assumed to range from 76.6-89.9h, and the lipid accumulation phase from 94.4-160.8h. The summarized result is shown in Table 4.8 and Table 4.7 in Section 4.1.2.4.

## D.1 Carbon balance of the exponential growth phase

The average molecular weight during the growth phase was calculated by discussions with Inga Marie Aasen [60] and Per Bruheim [70]. Average elemental formula was selected as $CH_{1.8}O_{0.5}N_{0.2}$ $M_W$, equal to 24.5 g/mol. Table D.1, D.2 and D.3 below show the data used to calculate the carbon balance for the exponential growth phase shown in Table D.4.

The carbon balance is summarized in the Table below, and is also shown in 4.7.

TABLE D.1: Calculated change in carbon source, glucose: $S_1$ glutamate: $S_2$, and change in biomass. The consumption of yeast extract is assumed to be constant from 76.9h to 89.9h, and is depleted before N-limitation. Carbon content in YE is assumed to be 48%w/w with the average molecular formula of 17.9 g/mol of YE (Sigma-Aldrich).

| **Time (h)** | **Glucose ($S_1$) (g/l)** | **Glutamate ($S_2$) (g/l)** | **Yeast extract (g/l)** | **Biomass (X) (g/l)** |
|---|---|---|---|---|
| 76.9 | 122.9 | 5.6 | 1.0 | 1.3 |
| 89.9 | 111.3 | 0.0 | 0.0 | 8.8 |
| $\Delta t$=13 | $\Delta S_1$=11.6 | $\Delta S_2$=5.6 | $\Delta$YE = 1.0 | $\Delta$X=7.5 |

TABLE D.2: Calculated data of carbon flow **into** the system. Molecular weights, $M_W$: glucose (glc, 6 carbon) 180 g/mol, and glutamate (glu, 5 carbon) 147 g/mol. Yeast extract (1.0 g/l), with 48%w/w carbon (C), equals 0.48 g C/l.

| **C-source** | $\Delta S_1/\Delta M_W$ **(mol glc/l)** | $n_C$ **(mol C/l)** | $n_C/\Delta t$ **(mol C/l·h)** | **C in glc (mmol C/l·h)** |
|---|---|---|---|---|
| Glc | 0.064 | 0.39 | 0.030 | 30 |
| Glu | 0.038 | 0.19 | 0.015 | 15 |
| YE | 0.060 | 0.040 | 0.0030 | 3 |

TABLE D.3: Calculated carbon flow **out** of the system. The molecular weight, $M_w$, for average molecular weight: 24.5 g/mol was used for the growth phase. Entries marked with Biomass and $CO_2$ are connected to the calculations of these carbon flows.

| **Biomass** $\Delta X/M_w$ $(\frac{\text{mol C}}{\text{l·h}})$ | **Biomass C to lipid** $(\frac{\text{mmol C}}{\text{l·h}})$ | **$CO_2$ Av. Flow** $(\frac{\text{l air}}{\text{h}})$ | **$CO_2$ Av. $CO_2$** (%) | **$CO_2$ C til $CO_2$** $(\frac{\text{mmol CO2}}{\text{l·h}})$ |
|---|---|---|---|---|
| 0.024 | 24 | 29.3 | 2.1 | 16 |

TABLE D.4: The carbon balance of the growth phase (76.9-89.9h) using the Black-Box-model.

**Carbon balance growth phase**

| **In Glucose (mmol C/l·h)** | **In Glutamate (mmol C/l·h)** | **In Yeast extract (mmol C/l·h)** | **Out $CO_2$ (mmol C/l·h)** | **Out Biomass (mmol C/l·h)** | **Recovery (%)** |
|---|---|---|---|---|---|
| 30 | 15 | 3 | 16 | 24 | 84 |

## D.2 Carbon balance of the lipid accumulation phase

The molecular weight on average during the lipid accumulation phase was selected by discussions with Inga Marie Aasen [60] and Per Bruheim [70]. The $M_W$ equals 17.9 g/mol. The molecular weight was used to calculate the molar flow of carbon to lipids during the lipid accumulation phase. Table D.5, D.6 and D.7 below show the data used to calculate the carbon balance for the lipid accumulation phase shown in Table D.8.

TABLE D.5: Calculated change in of glucose: $S_1$, and change in biomass during the lipid accumulation phase.

| **Time (h)** | **Glucose ($S_1$) (g/l)** | **Biomass (X) (g/l)** |
|---|---|---|
| 94.4 | 77.9 | 10.7 |
| 160.8 | 11.1 | 27.3 |
| $\Delta t$=66.4 | $\Delta S_1$=66.8 | $\Delta X$=16.6 |

TABLE D.6: Calculated data of carbon flow **into** the system. Molecular weight, $M_W$: glucose (glc, 6 carbon) 180 g/mol.

| $\mathbf{\Delta S_1/\Delta M_W}$ **(mol glc/l)** | $\mathbf{n_C}$ **(mol C/l)** | $\mathbf{n_C/\Delta t}$ **(mol C/l·h)** | **C in glc (mmol C/l·h)** |
|---|---|---|---|
| 0.37 | 2.225 | 0.034 | 34 |

TABLE D.7: Calculated carbon flow **out** of the system for the lipid accumulation phase. $M_W$ for the lipid accumulation phase was assumed to equal 17.9 g/mol.

| **Lipid** $\mathbf{\Delta X/M_w}$ $(\frac{\text{mol C}}{\text{l·h}})$ | **Lipid C to lipid** $(\frac{\text{mmol C}}{\text{l·h}})$ | **$CO_2$ Av. Flow** $(\frac{\text{l air}}{\text{h}})$ | **$CO_2$ Av. $CO_2$ (%)** | **$CO_2$ C til $CO_2$** $(\frac{\text{mmol CO2}}{\text{l·h}})$ |
|---|---|---|---|---|
| 0.014 | 14 | 29.3 | 1.6 | 12 |

TABLE D.8: The carbon balance of the lipid accumulation phase (94.4-160.8h). Assumed only lipid accumulation, and no cellular division.

**Carbon balance of the lipid accumulation phase**

| **In (mmol C/l·h)** | **Out as $CO_2$ (mmol C/l·h)** | **Out as lipid (mmol C/l·h)** | **Recovery (%)** |
|---|---|---|---|
| 34 | 14 | 12 | 77 |

# E

# Materials and Methods

## E.1 Sugars with HPLC

Method for analysis of sugars, organic acids, and ethanol: Column: Agilent Hi-Plex H, 7.7·300 mm, 8 µm (p/n PL1170-6830). Mobile phase: 0.05M $H_2SO_4$. Storage solution: 5% MeOH. Flow rate: 0.6 ml/min (0-6.5 min, 20.5-30 min), 0.4 ml/min (7-20 min). Temperature: 20°C. Wash vial - P2-A1. A standard curve was developed for each run, and used to quantify the glucose concentration in each sample.

One standard of concentrated (as listed in Table E.1), 0.75 std, 0.5 std and 0.25 std was prepared from the concentrated sample. All samples were filtered with 0.2 µm membrane filter.

TABLE E.1: Standard solution for HPLC analysis of supernatant samples. *Volatiles are freshly prepared.

| **Stock Compound** | **Volume ml** | **Stock conc. (g/l)** | **Final conc. (g/l)** |
|---|---|---|---|
| Fructose | 1 | 50 | 5 |
| Glucose | 1 | 50 | 5 |
| Sucrose | 1 | 50 | 5 |
| Maltose | 1 | 50 | 5 |
| Glycerol | 1 | 25 | 2.5 |
| Ethanol* | 2 | 50 | 10 |
| Acetic acid* | 0.375 | 16 | 0.6 |
| Succinic acid | 0.3 | 50 | 1.5 |
| Citric acid | 0.12 | 50 | 0.6 |
| Lactic acid | 0.3 | 50 | 1.5 |

## E.2 Glutamate with UPLC-MS

Reverse phase-protocol for chromatographic separation of PITC-Glutamic acid Column: Waters AQUITY UPLC BEH C18 1.7 µm, 2.1·50 mm. Column temperature: 40°C. Flow rate: 0.6 ml/min. Injection volume: 2 µl. Mobile phase A: H2O added 0.2% formic acid. Mobile phase B: acetonitrile (ACN) added 0.2% formic acid.
Mobile phase gradient (%v/v):

- 0.00-0.50 min: 1% B
- 0.50-2.00 min: 1-100% B
- 2.00-2.50 min: 100% B
- 2.60-3.10 min: 1% B
- 3.10 min: end

## E.3 LC-MS settings

LC-MS analysis were performed on a Waters AQUITY I-Class UPLC/Waters Xevo TQ-MS system operated in positive electrospray mode, for amino acid and organic acid analysis. The setting used for fatty acid analysis is described below, and was performed in collaboration with SINTEF. MS-settings including MRM-transitions can be obtained from supervisor Per Bruheim [70] upon request.

### E.3.1 Amino acid analysis with LC-MS

**Reverse phase-protocol for chromatographic separation of PITC-amino acids**: Column: Waters AQUITY UPLC BEH C18 1.7 µm, 2.1·75 mm, Column temperature: 50°C, Flow rate: 0.6 ml/min, Injection volume: 2 µl, Mobile phase A: H2O added 0.2% formic acid, Mobile phase B: Acetonitrile added 0.2% formic acid, and Mobile phase gradient (%v/v):

- 0.00-0.45 min: 0% B
- 0.45-3.30 min: 0-15% B
- 3.30-5.90 min: 15-70% B
- 5.90-6.05 min: 70-100% B
- 6.05-6.52 min: 100% B
- 6.52-7.30 min: 0% B
- 7.30 min: end

**ESTD stock solution (2.5mM):** Ala, Arg, Asp, Cys, Glu, Gly, His, Ileu, Leu, Lys, Met, Phe, Pro, Ser, Thr, Tyr, Val. **Supplementary ESTD (10 mM):** Glu, Asp, Cys, Try.

**$^{13}$C$^{15}$N ISTD-mix (100 µM):** Ala, Arg, Asp, Cys, Glu, Gly, His, Ileu, Leu, Lys, Met, Phe, Pro, Ser, Thr, Tyr, Val. **Supplementary $^{13}$C$^{15}$N ISTD-mix (100 µM):** Glu, Asp, Cys.

### E.3.2 Organic acid analysis with LC-MS

**Reverse phase-protocol for chromatographic separation of o-BHA-organic acids** Column: Waters AQUITY UPLC BEH C18 1.7 µm, 2.1·100 mm, Column temperature: 40°C, Flow rate: 0.25 ml/min, Injection volume: 10 µl, Mobile phase A: H2O added 0.1% formic acid, Mobile phase B: Methanol, Mobile phase gradient (%v/v):

- 0.00 - 0.50 min: 55% B
- 0.50 - 5.00 min: 55-85% B
- 5.00 - 5.10 min: 85-99% B
- 5.10-5.50 min: 99% B

- 5.50-5.60 min: 99-55% B
- 5.60-8.00 min: 55% B
- 8.00 min: end

### E.3.3 Fatty acid analysis with LC-MS

The LC-MS method: 1 µl sample injection onto a C18 RP non-polar LC column (Ascentis Express, 15cm x 2.1 mm, 2.7 µm particle). Temperature was 15°C and a flow rate of 0.5 mL/min. The mobile phase solvent A: 25 mM ammonium formate (AmFA) in water, and mobile phase solvent B: pure acetonitrile (ACN). The separation was performed starting at 75% B for 0.5 min, then increased with a linear gradient to 100% B over 8.5 min, and the 100% B was kept isocratic for 1 min to ensure complete washout. The gradient was then lowered to 75% B for 2 min.

The LC column effluent was introduced into a QqQ/MS (Agilent 6490) and operated in –ESI mode. The ion source parameters were as followed: The nebulizer was set at 45 psi and operated at 3.0 kV. Nitrogen gas ($N_2$) was used as the nebulizer gas. $N_2$ was set at 250°C and gas flow was 12 l/min. Sheath gas temperature was set at 400°C and gas flow was 11 l/min, while the nozzle voltage was set at 1500 V. The fragmentor was fixed at 380 V. Analysis were performed in single ion monitoring (SIM) mode, where each SIM was monitored for 50 ms (dwell time). Fatty acids detected by MS were confirmed based on a comparison with known standards.

## E.4 Metabolite analysis with CapIC-MS

CapIC-MS settings[69]: A Thermo Scientific Dionex ICS-4000 capillary IC was operated in external mode with DI-water delivered by an external AXP pump at a flow rate of 30 µl/min. To assist desolvation for better electrospray, a makeup solvent of 90% ACN in DI-water containing 0.01% ammonium hydroxide ($NH_4OH$) was delivered by an external AXP-MS pump at 30 µl/min, combined with the eluent via a low dead volume mixing tee and passed through a grounding union before entering the MS. A minimized length of peak tubing (0.08 mm/0.003 in. ID) (P/N 049715) was used for the capIC-MS interphase. The capIC analysis was performed with a IonPac AS11HC-4µm, 0.4·250 mm column (2000 Å) and a IonPac AG11-HC 4 µm 0.4·50 mm guard column. IC flow rate was 16 µl/min at 40°C. The gradient conditions were as follows: an initial 4 mM KOH was held for 1 min, increased to 12 mM at 5 min, to 20 mM at 13 min, and 70 mM at 22 min, held at 70 mM for 7.5 min, followed by a rapid increase to 100 mM at 31 min,

held 100 mM for 5 min and decreased to 4 mM in 4 min, and finally held for 10 min to re-equilibrate the column. The total run time was 50 min.

A Waters Xevo TQ-S triple-quadrupole MS was operated in negative electrospray ionization (ESI) mode with a capillary voltage of 2.5 kV and ion-source temperature of 150°C. The desolvation gas was nitrogen, and the flow was set to 800 l/h at a temperature of 300°C. The collision energy for each MRM transition was optimized for each compound both manually and using the Intellistart-function in MassLynx 4.1. The MS was run in dynamic MRM mode, and the retention time (RT) window for each compound was set to ±2 min of the expected RT. Downstream data processing was performed in MassLynx V4.1.

### E.4.1 Original protocol intracellular metabolites

The original protocol was developed by Kvitvang *et al.* [68]. Vacuum filtration was used to separate cell mass from the sample.

**Vacuum:** Set the vacuum as little as possible, but be careful not to disrupt the cells (*Eshcerichia coli* is normally vacuum-filtered at 600 Pa, and *Saccharomyces cerevisae* at 800 Pa. The T66 cells were not possible to vacuum filter at high cell concentrations, even though the pressure was lowered to about 120 Pa).

**Filtration and washing:**

1. A filter (0.8 µm was used in this protocol) was placed in the filtration manifold and about 1 ml of deionized $H_2O$ was added to moist the filter.
2. Primarily 5 ml of sample (reduced to 1 ml) was added to the filter.
3. 10 ml cold saline water (15 g/l NaCl, kept on ice) was used to wash the cells (added right before the filter paper went dry).
4. 10 ml cold deionized $H_2O$ (kept on ice) was used to wash the cells (added right before the filter paper went dry).

**Quenching:**

1. The filter was removed from the vacuum manifold, and placed in a 50 ml falcon tube with 13 ml 55:45 ACN-$H_2O$ (kept on ice).
2. The samples were stored at -80°C.

3. Three freeze-thaw cycles (a and b) were preformed to disrupt the cells, and release the metabolites to the solvent:
   (a) 1 min in liquid $N_2$.
   (b) Place in EtOH bath at 0°C for about 20 min.
4. The centrifuge was set to 0°C and 5000 rpm for 5 min.
5. The largest filter parts were removed, and the samples centrifuged.
6. Three 15 ml falcon tubes from each sample was prepared.
7. The falcon tubes were stored at -80°C (horizontally to maximize the surface area).
8. The samples were freeze-dried at -150°C and about 20 Pa.

**CapIC-MS analysis**:

1. Re-suspended the samples in 500 µl cold $H_2O$.
2. The samples were centrifuged at 5000 rpm for 4 min at 4°C.
3. 450 µl was transferred to 3000 kD spinfilters.
4. Centrifuged at 5000 rpm for 10 min at 4°C.
5. 2·100 µl was transferred to two HPLC vials for CapIC.

## E.5 Sigmol analysis by UPLC-TQS

Addition of 5 µl sample to a Agilent AdvanceBio MS Spent Media column (2.1·100 mm) at 30°C. The flow rate was set to 0.4 ml/min. The mobile phase was A: 10% 100 mM ammonium acetate in water pH 9, 90% water, and B: 10% 100 mM ammonium acetate in water, 90% acetonitrile (ACN). The separation was performed starting at 100% solvent B for 15 min, decreased to to 80% of B for 0.5 min. After 15.5 min, the fraction of solvent B was increased back to 100%, and run until the 20 min cycle was completed.

A Waters Xevo TQ-S was operated in negative electrospray ionization (ESI) mode with a capillary voltage of 2.2 kV and ion-source temperatyre of 150°C. The desolvation gas was nitrogen, and the flow set to 1000 l/h at a temperature of 500°C. The collision energy of each multiple reaction minitoring (MRM) and transition was optimized both manually and sing the infusion function in MassLynx V4.1. Downstream data processing was performed in MassLynx V4.1.